Quantification of Morphological Characteristics of Aggregates at Multiple Scales

Wenjuan Sun

Dissertation submitted to the faculty of
the Virginia Polytechnic Institute and State University
in partial fulfillment of the requirements for the degree of
Doctor of Philosophy

In

Civil Engineering

Linbing Wang, Chair
Joseph E. Dove
Russel A. Green
Anbo Wang

October 29, 2014

Blacksburg, Virginia

Keywords: Morphological Characteristics, Aggregate Image Analysis, Two-dimensional Fourier Transform Method, Atomic-scale Roughness

Quantification of Morphological Characteristics of Aggregates at Multiple Scales

Wenjuan Sun

Abstract

Properties of aggregates are affected by their morphological characteristics, including shape factors, angularity and texture. These morphological characteristics influence the aggregate's mutual interactions and strengths of bonds between the aggregates and the binder. The interactions between aggregates and bond strengths between the aggregate and the binder are vital to rheological properties, related to workability and friction resistance of mixtures. As a consequence, quantification of the aggregate's morphological characteristics is essential for better quality control and performance improvement of aggregates. With advancement of hardware and software, the computation capability has reached the stage to rapidly quantify morphological characteristics at multiple scales using digital imaging techniques. Various computational algorithms have been developed, including Hough transform, Fourier transform, and wavelet analysis, etc. Among the aforementioned computational algorithms, Fourier transform has been implemented in various areas by representing the original image/signal in the spatial domain as a summation of representing functions of varying magnitudes, frequencies and phases in the frequency domain. This dissertation is dedicated to developing the two-dimensional Fourier transform (FFT2) method using the Fourier Transform Interferometry (FTI) system that is capable to quantify aggregate morphological characteristics at different scales. In this dissertation, FFT2 method is adopted to quantify angularity and texture of aggregates based on surface coordinates acquired from digital images in the FTI system. This is followed by a

comprehensive review on prevalent aggregate imaging techniques for the quantification of aggregate morphological characteristics, including the second generation of Aggregate Image Measurement System (AIMS II), University of Illinois Aggregate Image Analyzer (UIAIA), the FTI system, etc. Recommendations are made on the usage of aggregate imaging system in the measurements of morphological parameters that are interested. After that, the influence of parent rock, crushing, and abrasion/polishing on aggregate morphological characteristics are evaluated. Atomic-scale roughness is calculated for crystal structures of five representative minerals in four types of minerals (i.e., α-quartz for quartzite/granite/gravel/aplite, dolomite for dolomite, calcite for limestone, haematite and magnetite for iron ore); roughness ranking at atomic-scale is further compared with surface texture ranking at macroscale based on measurement results using the FTI system and AIMS II. Morphological characteristics of aggregates before and after crushing test and micro-deval test are measured to quantitatively evaluate the influences of the crushing process and the abrasion/polishing process on morphological characteristics of aggregates, respectively.

Acknowledgements

The research reported in this dissertation was financially supported by a National Cooperative Highway Research Project (NCHRP) 4-34, “Application of LADAR in the Analysis of Aggregate Characteristics” and a Federal Highway Administration (FWHA) project (DTFH61-10-C-00019), “Mechanical and Structure Nanoscale Modeling of Hydrated cement Concrete”. The NCHRP project was conducted by Virginia Polytechnic Institute and State University (Virginia Tech) with participation of the University of Illinois at Urbana-Champaign; the FHWA project was conducted by Virginia Tech, in cooperation with California Institute Technology (CalTech) and Western Research Institute (WRI). These financial supports are gratefully acknowledged. The inspiring comments and suggestions from both project panels are greatly appreciated, and the generous help from all the partners are sincerely appreciated.

It would not have been possible for me to complete this PhD research work and to write this dissertation without help and support of all the kind people around me, to only some of whom it is possible to give particular gratitude hereby. First of all, I wish to express my deepest gratitude and respect to my advisor, Dr. Linbing Wang, for having accepted me as his PhD student and for the guidance, trust, encouragement, support, scientific training and freedom he has offered during the course of my doctoral research. I am particularly grateful for many stimulating discussions we have had in the analysis of aggregate morphological characteristics at multiple scales. Working with him was a great pleasure.

In the meantime, I would like to sincerely thank my committee members, i.e. Dr. Joseph E. Dove, Dr. Russell A. Green, and Dr. Anbo Wang, for serving on my committee, and for their valuable guidance on my research and the improvement on my dissertation. Particularly, I am in debt to Dr. Dove for the advice on establishing possible multiscale models to analyze mechanical performances of engineering materials before my preliminary exam.

This work involves a huge amount of computer implementation of numerical methods and laboratory work; both the computational theories and laboratory work would not have been as easy without the constant help from our partners and my colleagues. I deeply appreciate the support of Dr. Evan M. Lally and Ashley Stanford for their inspiring discussions and encouragements in the development of Fourier Transform Interferometry (FTI) system and the two-dimensional Fourier transform (FFT2) method. I also wish to acknowledge the generous help and strong support from Richard C. Meininger for coordinating the use of the AIMS II at FHWA. Sincere thanks are also extended to Yuanjie Xiao for scanning aggregate particles for the NCHRP4-34 project using the first generation of University of Illinois Aggregate Image Analyzer (UIAIA), and to Ed Harrigan and Alan Robords for their assistance in collecting information of aggregates analyzed in the NCHRP 4-34 project.

In addition, I have been fortunate to work with very nice colleagues to whom I would like to express my gratitude from the deepest of my heart. I would like to say thank you to Dong Wang and Wenjing Xue for stimulating discussions and generous help in my research and graduate life. Special thank goes to Haocheng Xiong, Yinning Zhang, and Ying Li for many inspiring talks,

warm encouragements, and home-like dinners together. I would also like to express my grateful thanks to Xinfei Wang for his generous help on the C++ program compilation in LAMMPS in the Linux operating system. My sincere gratitude also goes to Yue Hou for his great help on the establishment of multiscale failure model and to Bo Peng for her kind help on modifying C++ codes in LAMMPS. I also want to thank my other former and current colleagues including Cristian Druta, Fotini Vasilikou, Yucheng Huang, Wei Zhang, and Yufeng Liu for their encouragements during my graduate study. Living abroad far away from my family would be much harder without the company of good friends to whom I particularly give thanks for the valuable friendship and strong support of years, and for the great time we have spent together. I will definitely miss many dinners, hikes, and travels, as well as the other good times that we had together in the past few years.

Last but not least, I would like to thank my families for their unconditional love, unequivocal support, and great patience, as well as continuous encouragement at all times.

W. Sun

Blacksburg, VA

October 2014

Table of Content

List of Figures

List of Tables

List of Abbreviations

AIMS II	= second generation of aggregate image measurement system
ANOVA	= analysis of variance between groups
BFS	= blast furnace slag
Bulk dry SpGr	= bulk dry specific gravity
CO	= copper ore
DLT	= dolomite
FFT2	= two-dimensional Fourier transform
FTI	= Fourier transform interferometry
GGC/CGG	= glacial gravel crushed
GGR/RGG	= glacial gravel rounded
HMA	= hot mix asphalt
IO	= iron ore
LAA	= Los Angeles abrasion
LST	= limestone
MD	= micro-deval
PSDA	= micrometric optimizer particle size distribution analyzer
SMA	= stone matrix asphalt
UIAIA	= University of Illinois aggregate image analyzer
VIS	= video image system

Preface / Attribution

This dissertation is ultimately based on the experimental apparatus and data analysis of aggregate digital images of the Fourier Transform Interferometry (FTI) system. The equipment of the FTI system that was designed and installed by Dr. Evan M. Lally is described in the third chapter; experimental data of aggregates measured in both the FTI system and the second generation of Aggregate Image Measurement System (AIMS II) were performed by me and Ashley Stanford; the corresponding analysis method, i.e. two-dimensional Fourier transform method, developed by both me and Ashley is described in the third chapter. Experimental data from the University of Illinois Aggregate Image Analyzer (UIAIA) were performed by Yuanjie Xiao. The data analysis in this chapter was my original work. The evaluation of aggregate imaging techniques for quantification of aggregate morphological characteristics in the fourth chapter was my original work. The initial idea to contemplate the influence of parent rock, crushing, and abrasion/polishing on aggregate morphological characteristics in the fifth chapter was originated from Dr. Linbing Wang. The experimental data of micro-deval test and aggregate morphological characteristics measured before and after the micro-deval test were all from VTRC 10-cr7 final report that was prepared by Dr. Cristian Druta. The surface roughness analysis of mineral crystal structures in five representative minerals in four types of aggregates and the measurement and analysis of both rounded and crushed glacial gravel aggregates using the FTI system and AIMS II were all my original work, and the imaging analysis results of Stone-Matrix Asphalt (SMA) aggregates using the updated FTI system were performed by Yufeng Liu.

Introduction

1.1 Research Background

Aggregates are an important component in asphalt concrete, cement concrete, and granular bases. The morphological characteristics, including shape, angularity and surface texture, of aggregates have a significant influence on their mechanical performances and serviceability. These morphological characteristics influence aggregate mutual interactions and strengths of bonds between the aggregate and the binder (Al-Rousan et al. 2006). The interactions between aggregates and bond strengths between the aggregate and the binder are vital to rheological properties, related to workability and friction resistance of mixtures. As a consequence, quantification of aggregate morphological characteristics is essential for better quality control of aggregates and performance improvement of both asphalt concrete and cement concrete.

In the past decades, tremendous efforts have been made to measure the morphological characteristics of both coarse and fine aggregates for better mix design. These measurement methods can be discretized into two categories: direct and indirect methods. In direct methods, aggregates are measured by either visual inspection according to the Krumbein roundness chart, manual measurement of the dimensions using calipers (ASTM D3398), or by computation algorithms from digital image analyses. Conversely, indirect methods measure the shear strength of specimens composed of graded aggregates or air void content of uncompacted specimens (ASTM D4792, ASTM D5821), based on the assumption that uncompacted void content and

shear strength are related to shape, angularity, and surface texture of aggregates. There is a concern that direct methods with visual inspection using a caliper or the Krumbein roundness chart are time consuming, laborious and subjective, whereas indirect methods cannot separate the contributions to strength and deformation resulting from different mechanisms.

With the advancement of computer hardware and cost-effective software packages, direct methods using digital image analysis techniques become popular due to that advantage of rapidly quantifying aggregate morphological characteristics with objective results. Some image analysis techniques analyze aggregates by using two-dimensional (2-D) shape analysis, and that is not accurately enough to represent three-dimensional (3-D) aggregate surfaces. Furthermore, current imaging techniques use different image acquisition methods and different definitions of shape, angularity, and surface texture; there is no standard morphological parameter that can be used to objectively compare measurement results from different aggregate imaging analysis techniques. This dissertation starts with an introduction of a new digital image analysis technique named the Fourier Transfer Interferometry (FTI) system that is capable to quantify morphological characteristics of both coarse and fine aggregates (in the third chapter), and then compares prevalent aggregate imaging techniques with recommendations on the usage of aggregate imaging techniques for measurements of morphological parameters in measurements that we are interested in (the fourth chapter). After that, further evaluations on the influence of parent rock, crushing, and abrasion/polishing on aggregate morphological characteristics are performed (the fifth chapter).

1.2 RESEARCH MOTIVATION

Aggregate morphological characteristics significantly affect the mutual interactions and bond strengths between the aggregate and the binder (Al-Rousan et al. 2006). They greatly influence durability, workability, tensile strength, stiffness, shear resistance, friction resistance and fatigue resistance of concrete. To promote quality assurance and quality control of concrete mixtures, there are requirements or limitations on aggregate morphological characteristics in specifications and standards of mix design. For example, elongated and flat aggregate particles are limited by the quantity in hot mix asphalt concrete in Superpave specifications. Consequently, there is an increasing need to rapidly and accurately measure morphological characteristics of aggregates in the following areas: (*i*) quality assurance and quality control in the production of high-quality construction materials, (*ii*) mix design of concrete with desired engineering properties, and (*iii*) investigations on relationships between morphological characteristics of aggregates and mechanical performances of concrete.

It is difficult to timely and accurately measure morphological characteristics through either direct manual measurement methods or indirect methods according to standards. Digital imaging techniques offer an alternative solution for this problem. Digital imaging techniques have been widely used for aggregate morphology evaluation by using various computational algorithms to analyze digital images of aggregates. Computational theories for quantification of morphological characteristics from digital images mainly include the following methods: Hough transform (Wilson and Klotz 1996), Fourier analysis (Wang et al. 1997), interpolation from projections (Rao and Tutumluer 2000), spherical harmonics (Garboczi 2002), wavelet transform (Kim et al. 2003), fast Fourier transform (Penumadu and Wettimuny 2002), unified Fourier transform

(Wang et al. 2005), etc. These aggregate imaging techniques use different imaging methods and incompatible computation theories to quantify shape, angularity and surface texture from digital images, sometimes resulting in incomparable values of morphological characteristics. Some of these imaging techniques analyze morphological characteristics based on 2D or semi-3D coordinates of aggregate surfaces calculated from digital images. These methods are limited in accuracy, as 2D or semi-3D aggregate coordinates cannot accurately represent actual 3D surface of real aggregates. Therefore, it is vital to develop a more accurate imaging technique that is capable to rapidly and reliably capture aggregate morphological characteristics based on actual 3D coordinates of aggregate surfaces from high resolution images. Furthermore, this evaluates prevalent aggregate imaging techniques so that both researchers and engineers can select an aggregate imaging technique ain to the measurement of morphological property that they are interested in.

Conversely, the resistance to crushing and abrasion/polishing is an important ability of aggregates to resist crushing and skidding, with a significant influence on mechanical performances of concrete. Manufactured aggregates are crushed from parent rocks into coarse and fine aggregates, and then exposed to degradation (including abrasion/polishing and breakage) during production, transportation and construction. The degradation process may alter aggregate morphological characteristics, resulting in aggregate particles with less angular and smoother textured surfaces, ultimately influencing mechanical performances of aggregates. On the other hand, mineralogy and petrographic properties are inherently crucial factors that influence aggregate resistance to crushing and abrasion/polishing. Previous studies focused on characterization of aggregate degradation and its influence on the bearing capacity of unbounded

layers, such as decreases in aggregate size, changes in aggregate size distribution (Pintner et al. 1987; Lynn et al. 2007), andthe evolution of surface texture throughout the abrasion/polishing process (Masad et al. 2009; Mahmond et al. 2014; Ortiz et al. 2014; Wang et al. 2010). However, very few research studies have been conducted on quantifying the influence of crushing and abrasion/polishing on aggregate morphological characteristics, not to mention the fundamental reasons why some aggregates would turn into crack failures following certain crack paths due to mineral compositions and inherent defects.

1.3 DISSERTATION OUTLINE

Figure 1-1 plots the flowchart of this dissertation. There are six chapters and two appendices. The first chapter introduces the research background for this dissertation, indicating the importance and necessity of quantification of aggregate morphological characteristics at multiple scales. Later, research motivations and objectives are outlined.

The second chapter gives a literature review on prevalent digital image analysis methods for quantifying aggregate morphological characteristics. There are three categories of imaging techniques, including early imaging method, dynamic digital image method, and static digital image method. The equipment for capturing aggregate images and the corresponding analysis methods for quantifying aggregate morphological characteristics from digital images are summarized.

The third chapter presents a new image analysis technique – Fourier Transform Interferometry (FTI) system for quantification of morphological characteristics of both coarse and fine

aggregates with the size ranging from ¾-inch (19.05 mm) to No. 50 (0.3 mm). Computational algorithms for analyzing digital images are developed based on the two-dimensional Fourier transform (FFT2) method. The FFT2 results are analyzed based on 3D coordinates of the top surface of the ¾-inch aggregates (passing 1-inch sieve and retaining on ¾-inch sieve) in MATLAB. Further validations are made with comparisons to measurement results from the second generation of Aggregate Image Measurement System (AIMS II) and the University of Illinois Aggregate Image Analyzer (UIAIA).

The fourth chapter evaluates prevalent aggregate imaging techniques for quantification of morphological characteristics. After that, measurement results of ½-inch aggregates (passing ¾'' sieve and retaining on ½'' sieve) from three aggregate imaging techniques (including AIMS II, UIAIA, and the FTI system) are compared with each other. Recommendations are made at the end of this chapter for the measurement of different morphological characteristics.

The fifth chapter investigates the influence of parent rock, crushing, and abrasion/polishing on aggregate morphological characteristics. Five crystal structures are established to quantify atomic-scale roughness as representative minerals for granite/aplite/quartzite/glacial gravel (α-quartz), dolomite (dolomite), limestone (calcite), and iron ore (hematite and magnetite). Crushing effects on morphological characteristics are performed on glacial gravel by comparing morphological parameters of rounded glacial gravel aggregates and crushed glacial gravel aggregates from the same origin in Michigan. Further evaluations on the influence of abrasion/polishing on aggregate morphological characteristics are performed on four types of aggregates in Virginia, including granite, quartzite, dolomite and limestone.

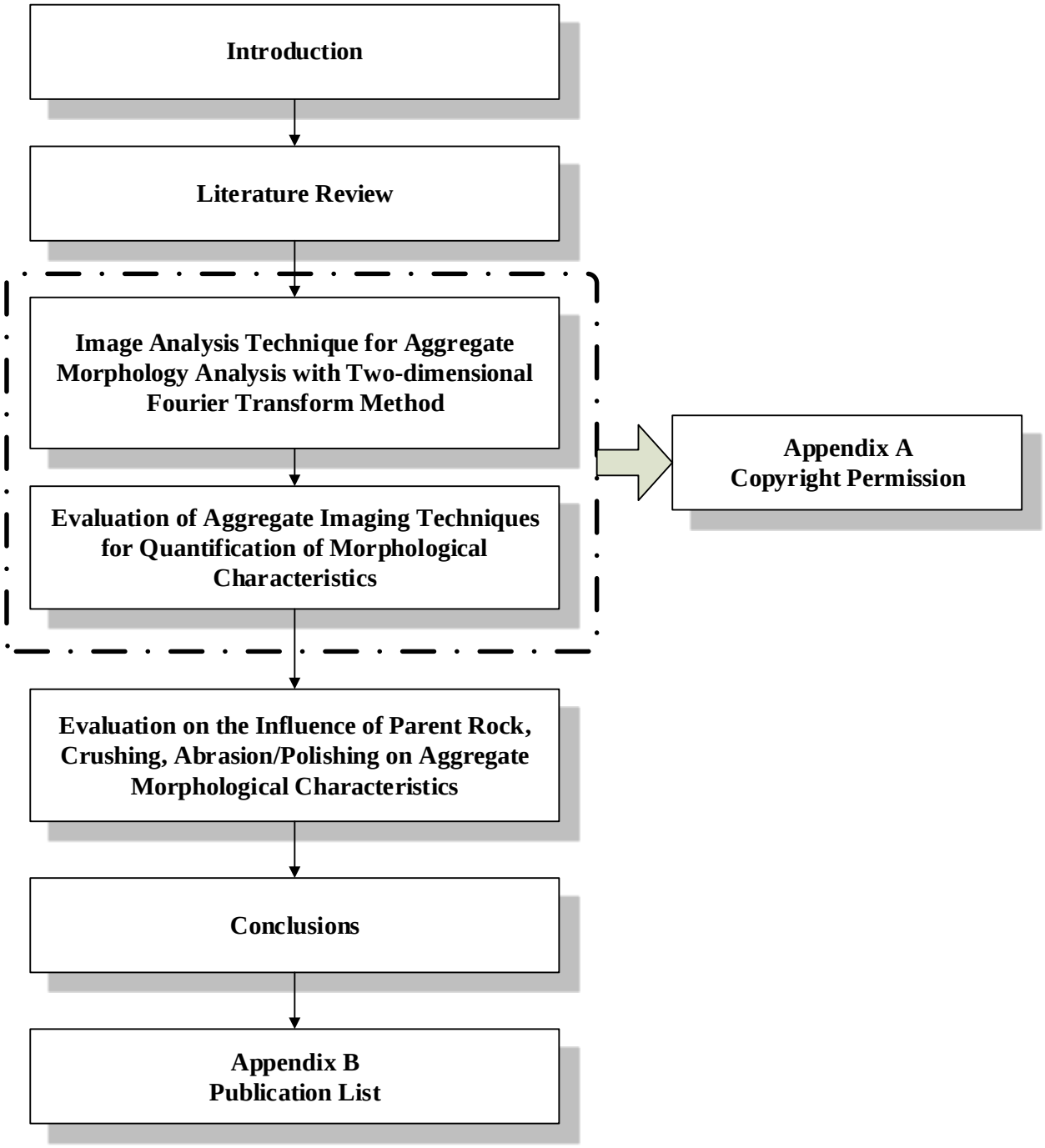

Figure 1-1 Flowchart of the dissertation

The last chapter summarizes the conclusions of this dissertation, followed by potential contributions and applications of digital imaging techniques for quantification of aggregate

morphological characteristics. Finally, recommendations on future research are made at the end of this dissertation.

Appendix A presents a copy of an email from Transportation Research Board (TRB) that gives the permission to use two published journal papers in the Transportation Research Record: Journal of the Transportation Research Board (corresponding to the content in the third chapter and the fourth chapter). Appendix B shows a publication list in the past few years.

State-of-the-art of Digital Image Analysis on Quantification of Aggregate Morphological Characteristics

2.1 INTRODUCTION

Morphological characteristics of aggregates have significant influences on the performance of construction materials, such as hot mix asphalt (HMA), and hydraulic Portland cement concrete (PCC). Consequently, quantification of morphological characteristics of aggregates is essential for quality control of both aggregates and construction. There are mainly two types of methods to measure aggregates, i.e., experimental tests and imaging techniques. Experimental tests are generally easy to conduct with inexpensive experimental instruments. However, it cannot provide separate measurements of shape, angularity and texture, and is usually labor-intensive and time-consuming.

Unlike experimental tests with labor-intensive work, imaging techniques provide one efficient means to rapidly measure shape, angularity and texture properties of aggregates. Due to the advancement of digital image techniques and availability of low-cost image processing software, imaging techniques are utilized to directly measure aggregates using computational programs to analyze digital images captured by various apparatuses, such as charged-coupled device (CCD) cameras and laser scanners (Kuo et al, 1996; Wang, et al. 1997; Jahn, et al., 2000; Tutumluer, et al., 2000; Masad, 2001; Masad, 2005a; Wang et al., 2005). However, these imaging techniques

significantly differ in the analysis methods and output different morphological parameters. This review discusses thirteen prevalent imaging techniques for aggregate morphological characteristics quantification.

2.2 IMAGING TECHNIQUES

Based on whether aggregates are moving or not during the image capture procedure, imaging techniques for quantifying aggregate morphological characteristics can be divided into three categories, including early imaging methods, dynamic digital imaging methods, and static digital imaging methods. Thirteen imaging techniques are summarized in this chapter. Table 2-1 tabulates camera setups, image information, and morphology calculation methods. Table 2-2 shows the advantages and disadvantages of these imaging techniques.

Early Imaging method

The early imaging technique involves a relatively low-cost digitizer and a microcomputer to rapidly measure aggregates with the assistant of AutoCAD and a spreadsheet program, in terms of shape, surface area, and roughness (Barksdale, et al., 1991). This technique was viable for particles larger than No. 80 (180 μm) (Prowell, et al., 2005). Aggregates are placed in clear trays; and a photocopy is made to produce two-dimensional (2D) images. These images are analyzed by a digitized table, while the thicknesses of aggregates are measured using a Vernier caliper. Shape factors are determined as elongation ratio, flatness ratio, etc.

Table 2-1 Camera Setup and Features of Aggregate Imaging Techniques

Imaging techniques		Camera setup	Image information	Morphological calculation methods		
				Shape	Angularity	Texture
Early Imaging method		Digitizer with microcomputer	2D	Shape	×	×
Dynamic digital imaging method	VDG-40 Videograder	One lines-scan CCD camera	2D	Length and width	×	×
	Computerized Particle Analyzer (CPA)		2D	Gradation and aspect ratio	×	×
	Micrometric OptiSizer (PSDA)		2D	Shape, and gradation	×	×
	Video Imaging System (VIS)		2D	Shape	×	×
	Buffalo Wire Works System		2D	Grading	×	×
	Camsizer	Two digital cameras	2D	Sphericity and aspect ratio	×	×
	WipShape	Two orthogonal cameras	3D	Grading and aspect ratio	Minimum average curve radius method	×
	University of Illinois Aggregate Image Analyzer (UIAIA)	Three orthogonal positioned cameras	2D	Sphericity and aspect ratio	Change of outline slope	Erosion and dilation technique
	Portable Image Analysis System (PIAS)	One digital camera	2D	Fourier transform method		
Static digital imaging method	Laser-based Aggregate Analysis System (LAAS)	One CCD camera	3D	Aspect ratio	Wavelet method	
	Aggregate Imaging Measurement System (AIMS II)	One camera with microscope	2D	Sphericity and aspect ratio	Gradient method	Wavelet method
	Fourier Transform interferometry (FTI) system	One CCD camera	3D	Sphericity and aspect ratio	Two-dimensional Fourier transform method	

Note: 2D=Two-dimensional, 3D=Three-dimensional, ×=not applicable.

Table 2-2 Advantages and Disadvantages of Aggregate Imaging Techniques

Imaging techniques		Aggregate size range	Advantages	Disadvantages
Early Imaging method		No. 8 – 1-inch	• Measure shape	• No angularity or texture addressed
Dynamic digital imaging method	VDG-40 Videograder	No. 16 - 1.5-inch	• Measure shape of large aggregate quantity	• Assume idealized ellipsoid as particle shape; Cannot measure angularity and texture; use one camera magnification to take images of all aggregate sizes
	Computerized Particle Analyzer (CPA)	No. 140 - 1.5-inch		
	Micrometric OptiSizer (PSDA)	No. 200 - 1.5-inch		• Separate vibratory feed systems and backlights required to scan fine and coarse samples
	Video Imaging System (VIS)	No. 16 - 1.5-inch		
	Buffalo Wire Works System PSDA	No. 200 - 1.5-inch	• Measure shape of aggregates	• Two-dimensional shape information; No angularity or texture addressed
	Camsizer	No. 50 – ½-inch	• Measure shape of large aggregate quantity • Use two cameras to capture images at different magnifications based on aggregate size	• Expensive • Assume idealized ellipsoid as particle shape • No texture addressed
	WipShape	No. 4 – 1-inch	• Measure shape of large aggregate quantity with three dimensions measured	• No texture addressed • Use one camera magnification to take images of all aggregate sizes • Separate vibratory feed systems and backlights required to scan samples
	University of Illinois Aggregate Image Analyzer (UIAIA)	No. 4 - 1.5-inch	• Measure shape of large aggregate quantity with three dimensions measured	• Use one camera magnification to take images of all aggregate sizes
	Portable Image Analysis System (PIAS)	No. 200 – 1-inch	• Measure shape, angularity and texture • Use different scans to capture images based on aggregate sizes	• Calculation is based on two dimensional outlines of aggregates
Static digital imaging method	Laser-based Aggregate Analysis System (LAAS)	No. 10 – 4-inch	• Measure three dimensions of aggregates	• Use the same scan to analyze aggregates with different sizes
	Aggregate Imaging Measurement System (AIMS II)	No. 200 – 1-inc	• Capture images at different resolution using microscope based on aggregate sizes	• Expensive
	Fourier Transform interferometry (FTI) system	No. 50 - 3/4-inch	• Measure three dimensions of aggregates with 3D image data	• Use the same scan to analyze aggregates with different sizes

(Based on Masad, et al., 2007)

Dynamic Digital Imaging Method

VDG-40 Videograder

VDG-40 Videograder is capable of detecting aggregates ranging in size from No. 16 (1.18 mm) to at least 1.5-inch (37.5 mm). Aggregates are placed into a hopper and extracted by an electromagnetic vibrator into a long feeding channel toward the separator drum. VDG-40 uses a line-scan CCD camera to capture 2D images of aggregates by calculating length and width of the aggregates. Every aggregate will be imaged as it falls in front of the backlight. An assumption that every particle is elliptical is adopted to calculate the third dimension from the captured 2D image. Currently there is no standard specification for sample size, and a minimum number of 50 particles are assumed to be statistically stable. It is worth noting that VDG-40 analyzes every particle in the sample with good correlation with manual measurements of flat and elongated aggregates (Weingart, et al., 1999; Tutumluer, et al., 2000).

Computerized Particle Analyzer

The computerized Particle Analyzer (CPA) can analyze aggregate ranging from No. 140 (106 μm) to 1.5-inch (37.5 mm) (Tyler, 2001). During the CPA test, aggregates are filled into the metal hopper and transported on to the conveyor from the bottom of the hopper to the edge where aggregates fall off a curtain between the imaging device and a backlight. It is worth noting that CPA could be used both in laboratories and on a product stream for industry. This system uses two methods to process images for shape analysis of aggregates, i.e., size method, and shape method. The size method chooses the largest chord of a particle as its diameter based on its

image; whereas the shape method uses the diameter of a circle with equivalent circumference. Results will be finally complied into a size distribution with percentage of particle counting for every size fraction in a custom software package.

Micrometric Optisizer Particle Size Distribution Analyzer (PSDA)

Micrometric Optisizer Particle Size Distribution Analyzer (PSDA) system can process aggregates with sizes ranging from No. 200 (75 μm) mesh sieve size up to 1.5-inch (37.5 mm). In the Micrometric Optisizer PSDA system, aggregates are placed into a feeding cone and gradually deposited onto a vibrating channel, which disperses and transports aggregates that fall in front of the backlight. Aggregates should be separated into coarse aggregates and fine aggregates. This system uses a CCD camera to capture 2D images of falling particles twice per second (Raunch, et al., 2002). Due to the slow imaging rate, only some aggregates are captured for further analysis of particle size gradation.

In this system, there are two ways to analyze aggregate shapes, i.e., spherical method and cubic method. The spherical method considers every profile area of the imaged aggregate as a circle by taking sphere of equivalent area, and volume can be calculated using the equivalent radius from the aforementioned circle. On the contrary, the cubic method converts the imaged aggregate profile into a square of equivalent area, and the volume is calculated using the equivalent side dimension from the aforementioned square.

Video Image System (VIS)

The Video Image System (VIS) can analyze aggregates sizing from No. 16 (1.18 mm) to 1.5-inch (37.5 mm). Like the Micrometric Optisizer system, the VIS system uses a sample holder to accommodate a large number of aggregates that is fed onto a vibrating chute, and uses a line-scan CCD camera to capture images of falling aggregates. These 2D images can be further analyzed in the VIS software package to generate reports.

Buffalo Wire Works Particle Size Distribution Analyzer (PSDA)

Buffalo Wire Works Particle Size Distribution Analyzer (PSDA) has the capability of analyzing particles raging from No. 200 (75 μm) sieve size to 1.5-inch (37.5 mm). Similar to the aforementioned four imaging techniques, Buffalo Wire Works PSDA uses a line-scan CCD camera to capture images of falling particles in front of a backlight. These 2D images can be further analyzed to generate form factor defined as follows:

$$\text{Form factor} = (\text{Perimeter}_{\text{circle}}/\text{Perimeter})^2 \qquad (2\text{-}1)$$

where Perimeter is the perimeter of imaged aggregate profile; $\text{Perimeter}_{\text{circle}}$ is the perimeter of an equivalent circle that has the same area as imaged aggregate profile.

VDG-40, CPA, Micrometric Optisizer, VIS, and Buffalo Wire Works PSDA all use a line-scan CCD camera to measure aggregates as they fall in front of backlighting. Differences between the five imaging systems are physical configurations and software packages. Like Micrometric Optisizer and VIS, Buffalo Wire Works PSDA does not capture images for every particle, and requires separate feeding systems and backlights to scan coarse and fine aggregates.

Camsizer

Camsizer system analyzes aggregates ranging from No. 50 (300 μm) to ¾-inch (19.5 mm) using two optically-matched CCD cameras to automatically capture images at different resolutions as aggregates fall in front of the backlighting (Retsch Technology-Camsizer, 2011). Aggregates fall off at the end of the hopper and are transported using a vibrating tube and finally fall between the light source and the camera. When aggregates are falling, this system use two cameras to capture digital images, one taking images of coarse aggregates and the other one detecting fine particles.

WipShape

WipShape system is generally used for coarse aggregate analysis. It uses two orthogonally positioned synchronized cameras to capture images as aggregates pass on a mini-conveyor (1st version) or on a rotating circular lighting table (the latest version). It has the capability of quickly analyzing many aggregates to output size distribution curves and shape measurement summaries by size classes, and even angularity using the minimum average curve radius method.

Both Camsizer and WipShape use two CCD cameras to capture images of aggregates. However, the two techniques are different from their instrumental setups. Camsizer generates 2D data to determine shape; whereas WipShape can generate 3D shape information as the two cameras capture images from two orthogonal views.

University of Illinois Aggregate Image Analyzer (UIAIA)

University of Illinois Aggregate Image Analyzer (UIAIA) uses three orthogonally positioned cameras to capture projections of aggregates as they are individually placed on the conveyer belt. The 3D shape of each particle can be established based on three projections captured with three cameras using a sensor that detect the aggregate, as it passes by a certain position on the belt. This system can distinguish flat and elongated aggregates and automatically calculate angularity and texture for coarse aggregates. However, aggregates with a similar color to the conveyer belt cannot be measured. The enhanced-UIAIA is equipped with three progressive-scan color cameras and four light-emitting diode (LED) illumination lights with a dimmer control. A blue background is used on the conveyor to capture high resolution color images of aggregates. An advanced color thresholding scheme is used so that different types of aggregates of various colors can be measured under optimized light intensity and with minimized shadows.

Based on images captured in UIAIA, shape is described using sphericity, flatness ratio and elongation ratio. Angularity is defined by angularity index (AI) method, shown in Figure 2-1. The AI method traces the changes of slope of the two-dimensional profile outline of the imaged particle and uses a weighted average value of its angularity determined from three views (front, top, side images). Eq.2-2 shows the calculation of angularity for each image; and Eq.2-3 is used to calculate AI.

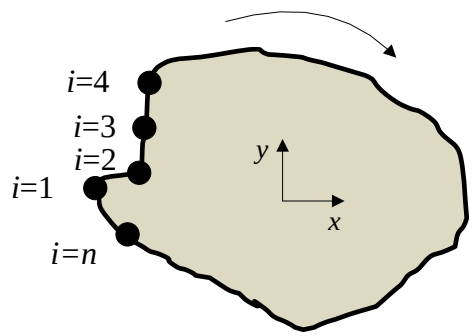

Figure 2-1 Illustration of an n-sided polygon approximating the outline of a particle (Rao, et al., 2002)

$$\text{Angularity} = \sum_{e=0}^{170} e \times P(e) \tag{2-2}$$

$$\text{AI} = \frac{(\text{Angularity} \times \text{Area})_{front} + (\text{Angularity} \times \text{Area})_{top} + (\text{Angularity} \times \text{Area})_{side}}{\text{Area}_{front} + \text{Area}_{top} + \text{Area}_{side}} \tag{2-3}$$

where e is the starting angle value for each $10°$ class interval and $P(e)$ is the probability that change in angle α ranges from e to e+10; Area_{front}, Area_{top}, and Area_{side} represent areas of imaged profiles within the front image, top image and side image, respectively.

Surface texture is analyzed using erosion and dilation technique (Masad, et al., 2000), shown in Figure 2-2, in which the left figure is the original aggregate image. Surface irregularity is lost during the erosion-dilation process as a percentage of the area in the original image is texture, defined by Eq.2-4; and surface texture (ST) is defined by Eq.2-5.

$$\text{Texture} = \frac{A_1 - A_2}{A_1} \times 100\% \tag{2-4}$$

$$\text{ST} = \frac{(\text{Texture} \times \text{Area})_{front} + (\text{Texture} \times \text{Area})_{top} + (\text{Texture} \times \text{Area})_{side}}{\text{Area}_{front} + \text{Area}_{top} + \text{Area}_{side}} \tag{2-5}$$

where A_1 and A_2 are areas of aggregates before and after erosion-dilation cycles, respectively.

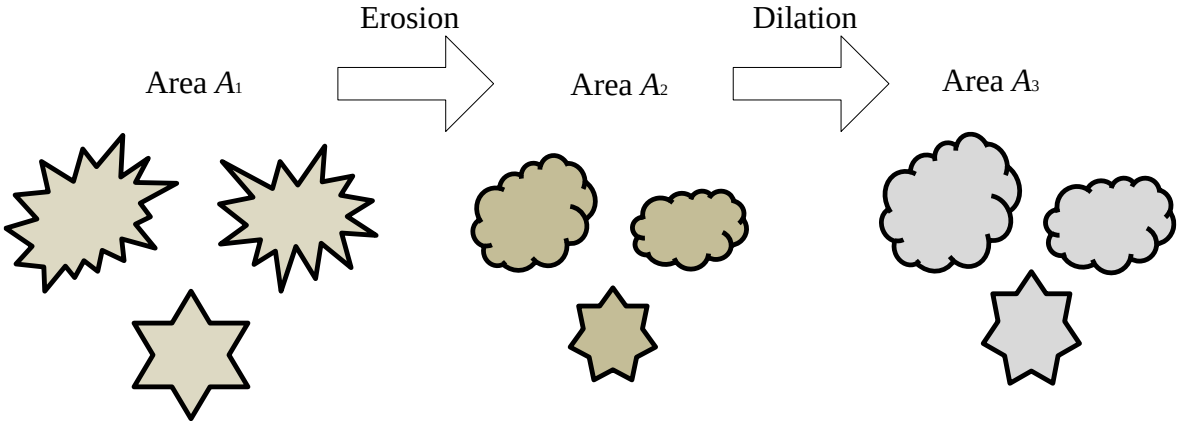

Figure 2-2 Illustration of erosion and dilation technique (Masad, et al., 2000)

Portable Image Analysis System (PIAS)

The Portable Image Analysis System (PIAS) uses an integral pocket camera to capture 2D images of both coarse and fine aggregates with different resolutions depending on aggregate sizes (Wang, et al., 2008). Images are transformed into binary images to acquire aggregate profile outlines, and morphological characteristics of aggregates are determined by shape factor, angularity factor, and texture factor using fast Fourier transform method in MATLAB software.

360 points are selected from each aggregate profile and transformed into radial coordinates with the origin of the coordinate system as the center of gravity. Coordinates of the 180 points are analyzed in terms of Fourier series. Among Fourier coefficients, shape is represented by changes of aggregate profiles at low frequencies, followed by angularity at intermediate frequency, and then texture represented by changes at high frequencies (Wang, et al., 2004; Masad, et al., 2005b). Shape factor, angularity factor, and texture factor are defined using the following equations.

$$\alpha_s = \frac{1}{2}\sum_{n=1}^{4}\left(\left(\frac{a_n}{a_0}\right)^2 + \left(\frac{b_n}{a_0}\right)^2\right) \tag{2-6}$$

$$\alpha_a = \frac{1}{2}\sum_{n=5}^{25}\left(\left(\frac{a_n}{a_0}\right)^2 + \left(\frac{b_n}{a_0}\right)^2\right) \tag{2-7}$$

$$\alpha_t = \frac{1}{2}\sum_{n=26}^{180}\left(\left(\frac{a_n}{a_0}\right)^2 + \left(\frac{b_n}{a_0}\right)^2\right) \tag{2-8}$$

where α_s, α_a, and α_t are shape factor, angularity factor, and texture factor, respectively; a_0 is the zero-frequency coefficient; a_n and b_n are real parts and imaginary parts of Fourier coefficients, respectively; n=1, 2, …, 180.

It has been shown that PIAS can effectively assess coarse aggregate morphology using MATLAB programs and images with high enough resolutions (Wang, et al., 2009). However, PIAS cannot detect aggregate thickness because captured aggregate profiles are two-dimensional.

Static Digital Imaging method

Laser-based Aggregate Scanning System (LASS)

Laser-based Aggregate Scanning System analyzes aggregates ranging from No. 10 to 4 inches. The LASS captures images of aggregate particles using a laser line scanner with a 120 mm scan width (Haas, et al., 2002). The laser scanner moves on a horizontal gantry and passes over particles scattered on the aggregate platform to acquire the 3D surface of aggregates (Kim, et al., 2003). By reconstructing the 3D surfaces of aggregates from laser scanner images, grain size distribution, angularity, and texture can be determined using the wavelet method.

Aggregate Image Measurement System (AIMS II)

Aggregate Image Measurement System (AIMS II) can analyze aggregates of a wide size range, i.e., from No. 200 to 1 inch. AIMS II uses a digital camera with an autofocus microscope to automatically capture images with different resolutions depending on aggregate sizes. This system measures three-dimensions of aggregates to determine sphericity and aspect ratios, including flatness ratio and elongation ratio. It can also calculate the angularity of aggregates of all sizes using the gradient method and the texture of coarse aggregates using the wavelet method (Masad, et al., 2001). The influence of shape on angularity is normalized using the division of measurements to the equivalent ellipse dimensions.

Figure 2-3 shows an illustration of the difference in gradient between particles. Angularity is defined by Equation 2-9. Texture is defined by Equation 2-10 at a given level using the wavelet method.

$$\text{Angularity} = \sum_{\theta=0}^{360-\Delta\theta} \frac{\left|R_{P\theta} - R_{EE\theta}\right|}{R_{EE\theta}} \tag{2-9}$$

$$\text{Texture} = \frac{1}{3N} \sum_{i=1}^{3} \sum_{j=1}^{N} \left(D_{i,j}\left(x, y\right)\right)^2 \tag{2-10}$$

where θ is inclination of gradient vectors on particle boundary point; $\Delta\theta$ is the change of inclination of gradient vectors; $R_{P\theta}$ is the radius of the particle at a directional angle of θ; $R_{EE\theta}$ is the radius of an equivalent ellipse at the same θ, N denotes the level of decomposition; $D_{ij}(x,y)$ is wavelet coefficient; i takes values of 1, 2, and 3, for the three detailed images of texture, and j is the wavelet coefficient index.

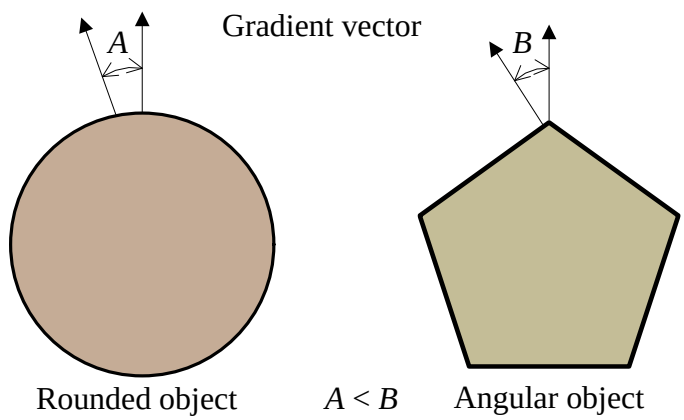

Figure 2-3 Illustration of the difference in gradient between particles (Chandan, et al., 2004)

Fourier Transform interferometry (FTI) system

The Fourier Transform interferometry (FTI) system is capable of analyzing aggregates ranging from No. 50 sieve size to 3/4 inch. The FTI system uses a CCD camera to capture images of both coarse and fine aggregates. Based on the images, 3D coordinates of aggregate top surfaces can be generated from the images. In the FTI system, shape is defined based on 3D coordinates by sphericity, flatness ratio and elongation ratio. Both angularity and texture are determined from the 3D coordinates within varying square areas using the 2D Fourier transform method. Angularity factor and texture factor are defined by Equation 2-11 and Equation 2-12.

$$\text{Angularity factor} = \sum_{n=1}^{N1}\left(\left(\frac{a_n}{a_0}\right)^2 + \left(\frac{b_n}{a_0}\right)^2\right) \tag{2-11}$$

$$\text{Texture factor} = \sum_{n=N1+1}^{N}\left(\left(\frac{a_n}{a_0}\right)^2 + \left(\frac{b_n}{a_0}\right)^2\right) \tag{2-12}$$

where a_0 is the zero-frequency coefficient; a_n and b_n are real and imaginary parts of Fourier coefficients, respectively; N is the square side length in terms of pixels; and $N1$ is the critical square side length in terms of pixels, depending on matrix sizes of square areas that selected on aggregate surfaces.

By plotting the relationship between angularity factor and square side length *N*, angularity is defined as the slope in the plot. Similarly, texture is defined as the slope of the relationship between texture factor and square side length *N*.

2.3 SUMMARY

Different from manual measurements using a caliper and visual judgment using the Krumbein roundness chart, measurements using imaging technique require both corresponding instrumental setup and well-trained operators. In general, imaging techniques are able to rapidly measure aggregates by providing reliable aggregate morphological quantifications without either labor-intensive tests or human subjectivity. Even though some apparatuses of these imaging techniques are expensive, the unit costs of incremental tests are low. Therefore, the imaging techniques have the capability of automatically detecting morphological characteristics with accurate and reliable results. However, the following issues should be taken into consideration for further improvements.

(*i*) The imaging techniques vary in analysis methods, in which results are sometimes incomparable to each other. For instance, some imaging techniques analyze 2D images while others utilize 2D projections to reconstruct 3D surface of aggregates.

(*ii*) Some imaging techniques can only analyze coarse aggregates; whereas other techniques can analyze aggregate with wide size ranges, including both coarse and fine aggregates.

Consequently, it is difficult to objectively evaluate aggregate morphological characteristics and further compare the evaluation results using different imaging techniques.

Image Analysis Technique For Aggregate Morphology Analysis with Two-dimensional Fourier Transform Method

Wenjuan Sun, Linbing Wang, and Erol Tutumluer

3.1 ABSTRACT

This paper presents some results of the NCHRP 4-34 Laser Detection and Ranging project. A high-resolution Fourier transform interferometry (FTI) system was developed for aggregate morphology characterization with the use of a fiber-optic coupler to form a Young's double-pinhole interferometer. The FTI system used a charge-coupled device camera to capture fringe images of aggregates with a size ranging from ¾ in. to No. 50 and to reconstruct three-dimensional surfaces of aggregates on the basis of fringe distortions from the captured digital images. A program was developed in MATLAB to quantify morphologic characteristics of

---

W. Sun, Charles E. Via, Jr., Department of Civil and Environmental Engineering, and L. Wang, Charles E. Via, Jr., Department of Civil and Environmental Engineering; Center for Smart Infrastructure and Sensing Technology, Virginia Tech Transportation Institute, Virginia Polytechnic Institute and State University, Blacksburg, VA 24061. E. Tutumluer, Department of Civil and Environmental Engineering, University of Illinois at Urbana–Champaign, 205 North Mathews Avenue, Urbana, IL 61801. Corresponding author: W. Sun, sunwj@vt.edu.

Transportation Research Record: Journal of the Transportation Research Board, No. 2267, Transportation Research Board of the National Academies, Washington, D.C., 2012, pp. 3–13.

DOI: 10.3141/2267-01

aggregates from a variety of sources. The output results include sphericity, flatness ratio, elongation ratio, angularity, and texture for each individual aggregate particle. In this paper, only the morphologic characteristics of seven types of coarse aggregate with sizes ranging from ¾ in. to No. 4 are presented. These aggregates were also analyzed with the Aggregate Image Measurement System (AIMS) II and the University of Illinois aggregate image analyzer (UIAIA) for further comparison. The FTI system is easy to operate and can rapidly quantify morphologic characteristics of aggregates. The FTI results of these aggregates are generally consistent with the results of AIMS II and UIAIA with regard to roughness rankings despite minor differences for several aggregates.

3.2 INTRODUCTION

Morphologic characteristics of coarse and fine aggregates have a significant influence on the performance of pavements. Shape, angularity, and texture are prevalent morphologic descriptors, which influence the aggregate interactions and strengths of bonds with binders, such as asphalt, cement, and lime (*1*). The interactions and bond strengths are vital to the rheological properties (i.e., compatibility, consolidation, and workability) and friction resistance. Therefore, characterization of aggregate morphology is important for better quality control of aggregates and for improvement of the field performance of pavements.

There are two fundamental ways to measure the shape, angularity, and texture of aggregates: direct and indirect methods. Direct methods measure aggregate morphologic properties by visual inspection, by digital image analysis, or by manual measurement of three dimensions of aggregates with calipers (AASHTO T304, AASHTO TP56, and ASTM D3398). Indirect

methods use a packing of aggregates flowing through an orifice of a specific size or utilizing compacted aggregate specimens exposed to pressure or shear forces; the methods are based on the assumption that uncompacted void content depends on the morphologic characteristics of aggregates (ASTM D4791 and ASTM D5821). A concern with current direct methods is that many measurements are time-consuming and laborious (*2, 3*). Moreover, no standard test method measures directly the angularity and texture of aggregates (*1*).

Motivated by advancements in digital imaging and availability of low-cost and fast image-processing software, various image techniques have been developed to provide a cost-effective means for rapid quantification of aggregate morphologic characteristics. Current imaging techniques adopt various mathematical algorithms with different instrumental setups. However, the output results are often expressed with different definitions of terms, which are sometimes incomparable to one another. Furthermore, some image-processing techniques analyze aggregates with two-dimensional (2-D) images, which are not accurate enough to represent three-dimensional (3-D) morphologic characteristics of aggregates. This paper presents an aggregate imaging system called Fourier transform interferometry (FTI), which analyzes the morphologic characteristics with Fourier transform in a MATLAB program on the basis of the 3-D aggregate surface images reconstructed from the digital images of aggregates. The setup components of the FTI system are introduced, followed by aggregate sample information and the morphologic analysis methodology; then the FTI morphologic characteristics of the aggregates are compared with results of the Aggregate Image Measurement System (AIMS) II and the University of Illinois aggregate image analyzer (UIAIA).

3.3 FTI SYSTEM

The FTI system is a 3-D surface profilometer that uses a simple fiber-optic coupler to form a Young's double-pinhole interferometer (*4*). A fiber-optic switch was adapted to control the input of laser signals into the system, with the use of laser lights with wavelengths of 675 and 805 nm. The Young's fringes were projected onto a 45 ° angled mirror for fringe projection onto the aggregate top surface. The images of aggregate top surfaces in the mirror were captured by a charge-coupled device camera and were analyzed by the Fourier transform method. The phase of the fringe pattern on the aggregate top surface was used to reconstruct the surface profile. Three images—including one image taken with visible light and two images captured with laser lights of wavelengths of 675 and 805 nm—were captured (*4*). The 675-nm image was used to generate a projected fringe pattern on the aggregate surface, whereas the 805-nm image was used for fringe identification. The visual-light image was used for edge detection of the aggregate surface boundary. The three images were used together to generate 3-D coordinates of the top surface of the aggregate (*5*). The FTI system could capture aggregate images in single- or multiple-particle mode. The resolutions in *x*-axis and *y*-axis directions are both 35.4 μm per pixel, and the measured *z*-axis resolution is 22 μm (*4*). However, the FTI system does not capture images of the aggregate bottom, unless the aggregate is flipped over to be imaged again.

Figure 3-1 is a photograph of the FTI system. It is capable of analyzing aggregates with sizes ranging from ¾-in. to No. 50. This paper reports data only for coarse aggregates with sizes ranging from 3/4 in. to No. 4; further information on the FTI system and more morphologic analysis data are available elsewhere (*6*). Figure 3-2 presents the configuration of the output data format. The output $z(x, y)$ from the FTI system is a 1,019 × 1,371 matrix, including the imaged

aggregate and the leading and trailing zeros. The $z(x, y)$ matrix gives the surface height z for every coordinate (x, y) as a 3-D surface map that has been bounded, corrected, and windowed. The data could also be interpreted as the vertical distance between a point on the aggregate top surface and the aggregate tray at the bottom.

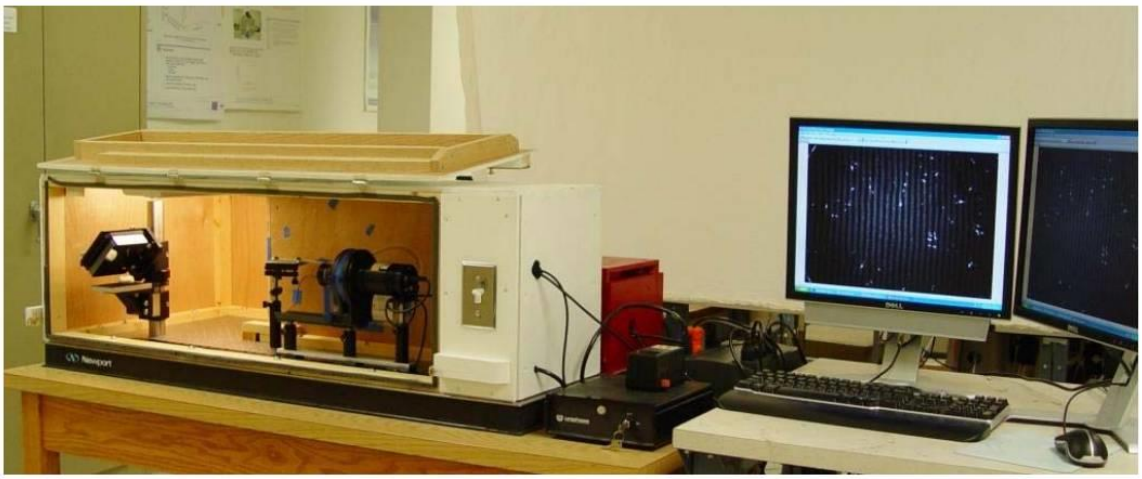

Figure 3-1 The FTI system

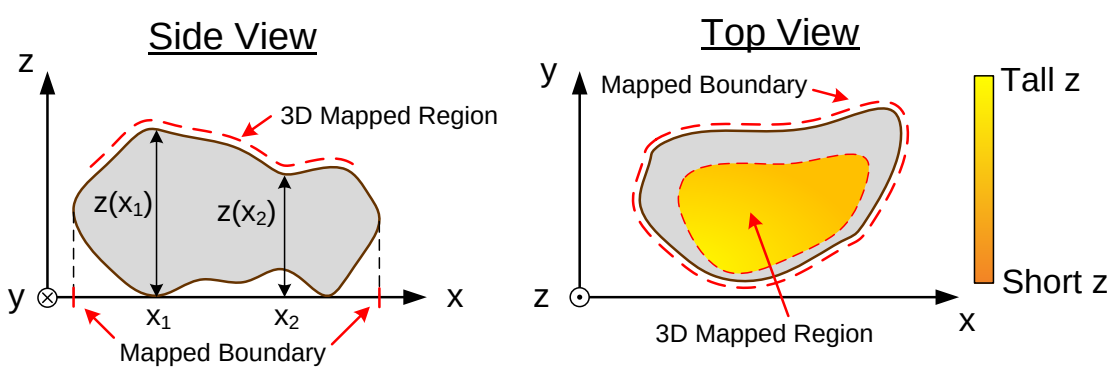

(*a*) (*b*)

Figure 3-2 Three-dimensional output data format of $z(x,y)$: (*a*) side view, and (*b*) top view. (*9*)

3.4 MORPHOLOGY ANALYSIS METHODOLOGY

The software of the FTI system included three main subroutines: a main program, an error correction program, and a morphologic analysis program. The main program was used to identify and reconstruct aggregate surfaces from digital images captured by the charge-coupled device camera. This program included semi-automated particle boundary identification and automatic fringe order identification based on a user-selected reference fringe. The error correction program was semiautomatic; with user-defined surface errors, a secondary reference fringe was selected to reprocess the $z(x, y)$ matrix to modify and improve the reconstructed surface map.

In the morphologic analysis program, all aggregate morphologic characteristics—including shape, angularity, and texture—were analyzed on the basis of the output $z(x, y)$ matrix from the error correction program. Shape was described by sphericity, flatness ratio, and elongation ratio as defined by the following equations:

$$\text{Sphericity} = \sqrt[3]{\frac{D_s D_m}{D_l^2}} \tag{3-1}$$

$$\text{Flatness Ratio} = D_s/D_m \tag{3-2}$$

$$\text{Elongation Ratio} = D_m/D_l \tag{3-3}$$

where

D_s = shortest dimension of aggregate particle;

D_l = longest dimension of aggregate particle;

D_m = dimension of aggregate particle perpendicular to both D_s and D_l.

Angularity and texture were defined with a 2-D Fourier transform method (FFT2). The discrete Fourier transform was applied to the 3-D coordinates $z(x, y)$ as a discrete function that was nonzero over the finite region $0 \le x \le N - 1$ and $0 \le y \le N - 1$ in the space domain. The 2-D N-by-N discrete Fourier transform and inverse N-by-N discrete Fourier transform relationships are given as follows (*7, 8*):

$$Z(p,q) = \sum_{x=0}^{N-1}\sum_{y=0}^{N-1} z(x,y) e^{-j\left(\frac{2\pi}{N}xp + \frac{2\pi}{N}yq\right)} \tag{3-4}$$

$$z(x,y) = \sum_{p=0}^{N-1}\sum_{q=0}^{N-1} Z(p,q) e^{j\left(\frac{2\pi}{N}xp + \frac{2\pi}{N}yq\right)} \tag{3-5}$$

$$f_x = \frac{2\pi}{N} x \tag{3-6}$$

$$f_y = \frac{2\pi}{N} y \tag{3-7}$$

where

$z(x,y)$ = 3-D coordinates of aggregate surface;

$Z(p,q)$ = discrete Fourier transform coefficient matrix of $z(x,y)$ in frequency domain;

p and q = p^{th} row and q^{th} column in $Z(p,q)$ matrix;

j = the imaginary root;

f_x and f_y = frequencies in x and y directions, respectively.

This approach is similar to the one-dimensional Fourier analysis method (*9*). High frequency and small magnitude represent surface textures of aggregates; low frequency and large magnitude

represent gentle slopes and flat planes, corresponding to aggregate shape; intermediate frequency is related to angularity (*9, 10*). Therefore, a critical step was to determine threshold values of frequencies that separate shape, angularity, and texture from one another. Figure 3-3 presents the schematic configuration of the roughness matrix. Roughness matrices were selected as square matrices sampled on the aggregate surface with variant matrix sizes. Angularity factor (AF) and texture factor (TF) are defined by the following equations in MATLAB:

$$\text{Angularity Factor (AF)} = \sum_{p=1}^{NA}\sum_{q=1}^{NA}\left[\left(a(p,q)/a_0\right)^2 + \left(b(p,q)/a_0\right)^2\right] \tag{3-8}$$

$$\text{Texture Factor (TF)} = \sum_{p=1}^{N}\sum_{q=1}^{N}\left[\left(a(p,q)/a_0\right)^2 + \left(b(p,q)/a_0\right)^2\right] - \text{AF} \tag{3-9}$$

where

a_0 = average value of $z(x,y)$;

$a(p,q)$ and $b(p,q)$ = real and imaginary parts of FFT2 coefficients at p^{th} row and q^{th} column;

N = size of $z(x,y)$ matrix;

N_A = threshold value.

N_A represents the value with which a 3-D surface is reconstructed with the use of the inverse of FFT2 coefficients that have their frequencies $< 2\pi N_A/N$ in either x-direction or y-direction. These FFT2 coefficients are considered to only contribute to angularity if the average value of absolute differences between the original surface and reconstructed surface using the inverse is > 0.2 mm, the spatial spacing discernible by unaided human eyes (*11*). The other Fourier coefficients are considered to contribute to texture only.

As indicated in Equations 3-8 and 3-9, the size of the $z(x, y)$ matrix N has a large influence on both AF and TF values; that is, values of both AF and TF would increase with increased $z(x, y)$ matrix size, because the total number of pixels on the x–y plane increases by an order of N^2. Consequently, it is necessary to figure out parameters to describe the relationship between N^2 and angularity and texture characteristics of aggregates. Figure 3-4 plots the relationship between AF, TF, and the corresponding area of roughness matrix (on the order of N^2) for some 1/2-in. aggregates. AF and TF values follow a linear relationship in both AF and TF plots. Furthermore, aggregates with more angular surfaces, such as blast furnace slag, tend to have steeper slopes in the AF plot, and aggregates with rougher surfaces tend to show steeper slopes in the TF plot. Therefore, the linear relationships (slope) in the AF and TF plots are defined as the angularity and texture of an aggregate, respectively.

Figure 3-5 shows how to separate texture from angularity on an aggregate surface by the FFT2 method. Figure 3-5*a* presents an original 3-D surface on a roughness matrix. Reconstructed surfaces were achieved by conducting an inverse Fourier transform to the Fourier coefficients with frequencies smaller than some frequencies (f_1, f_2, and f_3) shown in Figure 3-5*b*. Figure 3-5*c* plots the differences Δz between the original surface and the reconstructed surface at different frequencies. The reconstructed surface increasingly approached the angular and textured original surface and the difference Δz dramatically decreased as more high-frequency components were included in the reconstructed surface. When frequency f_2 was used to separate angularity from texture, the average value of the absolute difference between the original surface and the reconstructed surface was exactly <0.2 mm; therefore, f_2 is the critical frequency for this original surface shown in the first column.

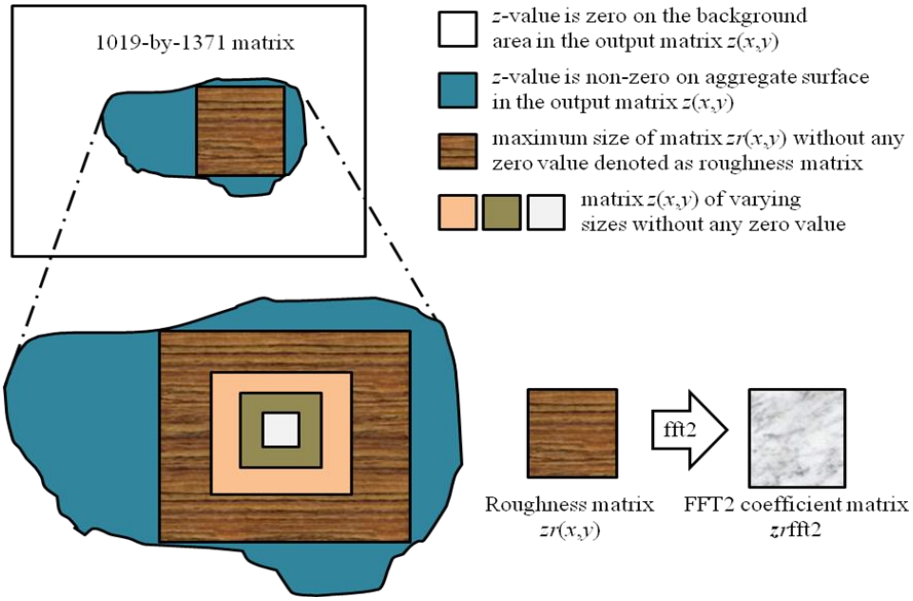

Figure 3-3 Schematic configuration of roughness matrix.

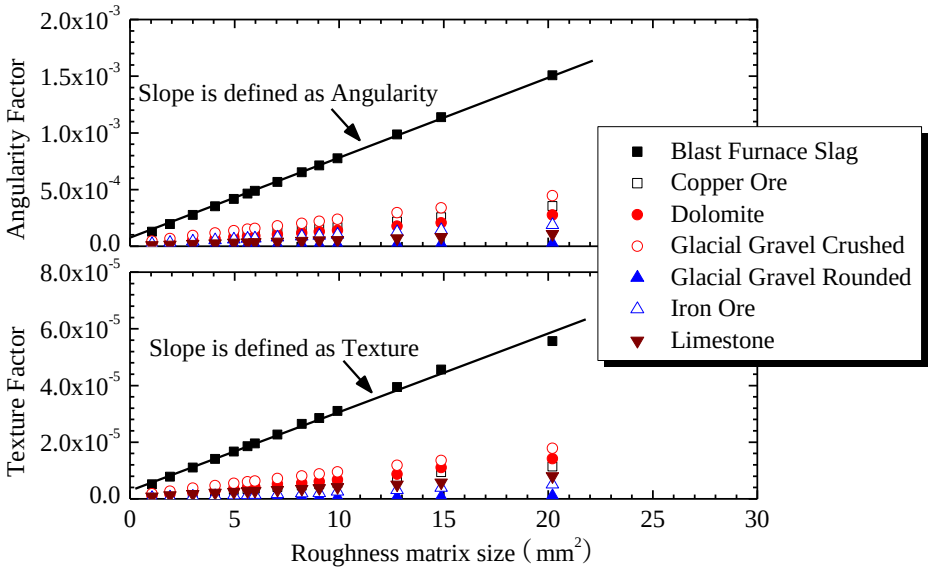

Figure 3-4 Angularity and texture of some ½-in. aggregates in FTI system.

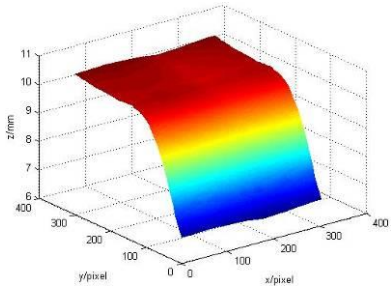

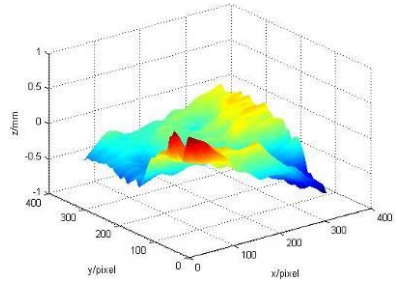

z_1=ifft2(zrfft(frequency≤f_1))

Average(abs(Δz)) ≤1 mm

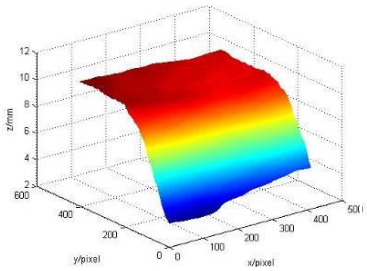

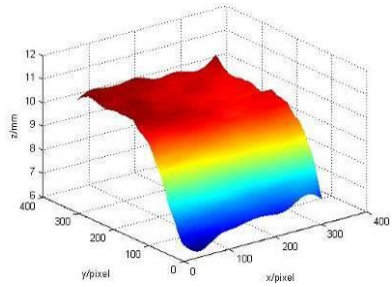

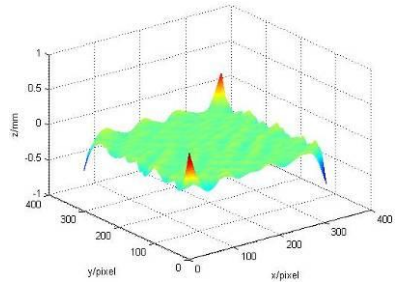

$z(x,y)$

(a)

z_2=ifft2(zrfft(frequency ≤f_2))

Average(abs(Δz)) ≤0.2 mm

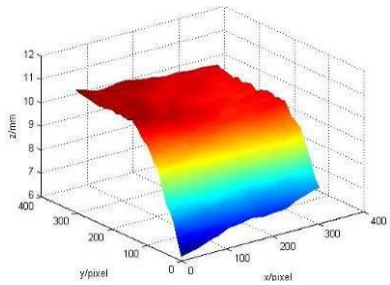

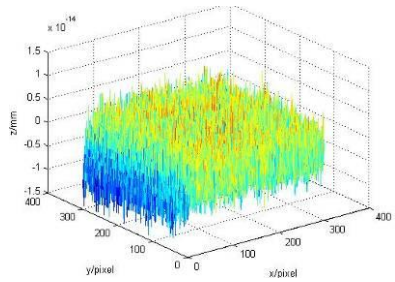

z_3=ifft2(zrfft(frequency ≤f_3))

Average(abs(Δz)) ≤1 ×10^{-14} mm

(b)

(c)

Figure 3-5 Separation between angularity and texture in roughness matrix: 301 ×301 pixel-by-pixel in x-y plane, millimeters on z-axis: (a) original 3-D $z(x,y)$, (b) reconstructed 3-D surface, and (c) $\Delta z = z(x,y) - z_i$ (i = 1, 2, 3, 4).

Table 3-1 Aggregate Types and Physical Properties

Aggregate type	Origin	Description	LAA loss (%)	Bulk dry SpGr (g/cm^3)	24 hr soak absorption (%)
Blast Furnace Slag	Wayne, MI	• Color: 5R 5/0 to 5R 1/0 • Poorly developed crystalline structure	43	2.27	3.18
Copper Ore	Keweenaw, MI	• Mixture of colors, including 5R 9/0, 5BG 8/2, 5R 8/6, and 5R 2/8 • Fine to coarse grains	19	2.64	0.95
	Houghton, MI		16	2.76	2.12
Dolomite	Mackinac, MI	• Color: 5R 9/4 to 5R 6/8 • medium to coarse crystals	27	2.78	0.52
	Monroe, MI	• Color: 5R 6/7 • Well defined small euhedral dolomite crystals	45	2.45	4.16
Glacial Gravel Crushed	Kent, MI	• Various colors • With crushed surfaces	17	2.73	0.71
Glacial Gravel Rounded	Kent, MI	• Various colors • Very smooth texture	19	2.68	1.10
Iron Ore	Marquette, MI	• Color: 10PB 2/2 with 5R 2/1 • Very fine grained and hard metamorphic rock	11	--	--
Limestone	Schoolcraft, MI	• Color: 5R 9/4 • Very fine subcrystalline texture	25	2.65	0.64
	Arenac, MI	• Color: 10PB 7/0 • Very fine crystalline with abundant frosted quartz sand grains	42	2.56	2.13

Note: LAA = Los Angeles Abrasion; Bulk dry SpGr = Bulk dry specific gravity; color in the Description column is named according to Munsell color system.

3.5 Aggregate Imaging and Analysis

Seven types of aggregate were analyzed with the FTI system, including blast furnace slag, copper ore, dolomite, glacial gravel crushed, glacial gravel rounded, iron ore, and limestone. For each type of aggregate, there were four size ranges: passing a 1-in. sieve and retained on a ¾-in.

sieve (referred to as ¾ in.), passing a ¾-in. sieve and retained on a ½-in. sieve (referred to as ½ in.), passing a ½-in. sieve and retained on a ⅜-in. sieve (referred to as ⅜ in.), and passing a ⅜-in. sieve and retained on a No. 4 sieve (referred to as No. 4). Table 3-1 lists the aggregate types and their physical properties. In this study, all aggregates are dry aggregates.

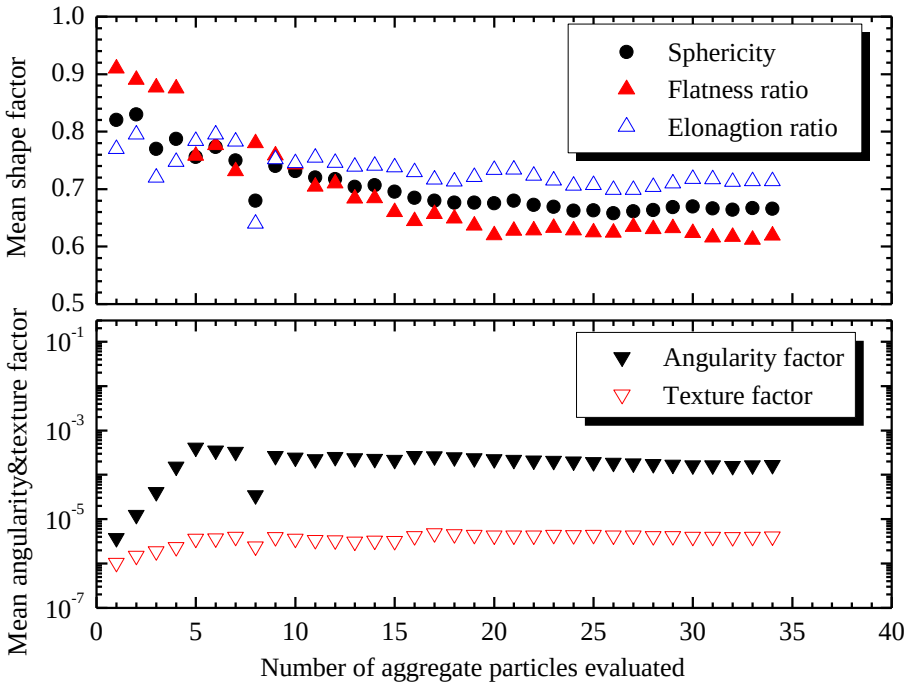

Figure 3-6 Asymptotic analysis to determine required sample size for ¾-in. dolomite aggregates.

Asymptotic analysis was performed to determine the required sample size for aggregate evaluations, which approach stable results as the sample size increases. Figure 3-6 plots the mean values of shape factor, angularity factor, and texture factor for 3/4-in. dolomite aggregates. As shown in this figure, 30 aggregate particles were sufficient to reach stable morphologic analysis results for the five morphologic characteristics. Further statistical analysis suggested that a 30-aggregate sample was large enough to provide a normal distribution and to achieve statistics-

stable results. Statistical analyses of other aggregates at each size range led to the same sample size requirement of 30. Therefore, 30 aggregate particles were analyzed within an aggregate size range for every aggregate type, with a result of 840 aggregate particles.

Table 3-2 Mean Values of FTI Morphological Parameters

Aggregate size		Sphericity	Flatness ratio	Elongation ratio	Angularity	Texture
3/4"	Blast Furnace Slag	0.72	0.72	0.73	2.74×10^{-4}	6.38×10^{-6}
	Copper Ore	0.69	0.66	0.72	2.69×10^{-4}	4.97×10^{-6}
	Dolomite	0.66	0.62	0.71	1.58×10^{-4}	3.90×10^{-6}
	Glacial Gravel Crushed	0.74	0.71	0.77	2.31×10^{-4}	3.86×10^{-6}
	Glacial Gravel Rounded	0.68	0.59	0.75	0.84×10^{-4}	1.60×10^{-6}
	Iron Ore	0.67	0.73	0.65	1.01×10^{-4}	2.13×10^{-6}
	Limestone	0.69	0.71	0.70	0.99×10^{-4}	2.52×10^{-6}
1/2"	Blast Furnace Slag	0.72	0.76	0.72	2.44×10^{-4}	9.57×10^{-6}
	Copper Ore	0.69	0.69	0.71	0.98×10^{-4}	4.69×10^{-6}
	Dolomite	0.70	0.80	0.68	0.60×10^{-4}	2.86×10^{-6}
	Glacial Gravel Crushed	0.74	0.77	0.74	1.46×10^{-4}	2.70×10^{-6}
	Glacial Gravel Rounded	0.70	0.71	0.71	0.97×10^{-4}	3.54×10^{-6}
	Iron Ore	0.67	0.68	0.68	0.99×10^{-4}	5.17×10^{-6}
	Limestone	0.66	0.78	0.62	1.90×10^{-4}	4.60×10^{-6}
3/8"	Blast Furnace Slag	0.73	0.73	0.75	2.19×10^{-4}	9.48×10^{-6}
	Copper Ore	0.70	0.72	0.71	1.39×10^{-4}	4.39×10^{-6}
	Dolomite	0.74	0.75	0.75	0.87×10^{-4}	3.59×10^{-6}
	Glacial Gravel Crushed	0.79	0.80	0.80	1.47×10^{-4}	6.94×10^{-6}
	Glacial Gravel Rounded	0.79	0.78	0.80	1.09×10^{-4}	4.81×10^{-6}
	Iron Ore	0.57	0.64	0.57	10.9×10^{-4}	77.5×10^{-6}
	Limestone	0.69	0.72	0.68	3.32×10^{-4}	15.9×10^{-6}
No. 4	Blast Furnace Slag	0.70	0.66	0.73	14.7×10^{-4}	60.0×10^{-6}
	Copper Ore	0.60	0.59	0.64	42.5×10^{-4}	190.0×10^{-6}
	Dolomite	0.56	0.55	0.58	15.7×10^{-4}	82.3×10^{-6}
	Glacial Gravel Crushed	0.69	0.71	0.69	2.48×10^{-4}	9.33×10^{-6}
	Glacial Gravel Rounded	0.73	0.77	0.73	2.48×10^{-4}	14.4×10^{-6}
	Iron Ore	0.58	0.53	0.63	21.6×10^{-4}	74.2×10^{-6}
	Limestone	0.65	0.63	0.67	12.5×10^{-4}	91.8×10^{-6}

3.6 STATISTICAL ANALYSIS OF AGGREGATE CHARACTERISTICS

Statistical analysis was conducted to quantify the distribution of aggregate morphologic characteristics of the seven types of aggregates. Table 3-2 presents the mean values of the morphologic characteristics of these aggregates. Figure 3-7 shows a photograph of all the ¾-in. aggregates. Figures 3-8 through 3-12 show distributions of the morphologic characteristics of the ¾-in. aggregates analyzed in the FTI system. The *x*-axes show the morphologic characteristics of aggregates, such as sphericity, angularity, texture; the *y*-axes present the cumulative percentages, calculated by dividing the number of aggregate particles that is less than or equal to the corresponding value of the morphologic characteristics by the total number of observations.

Figure 3-8 plots the distribution of sphericity. Crushed glacial gravel and blast furnace slag have greater values of sphericity than the other types of aggregates, whereas dolomite and iron ore have smaller values. Sphericity distributions of rounded glacial gravel and limestone are close. Figure 3-9 shows the distribution of the flatness ratio. Dolomite and rounded glacial gravel have small values of flatness ratios, whereas iron ore has the greatest value of flatness ratio. Figure 3-10 presents the distribution of the elongation ratio. Of all aggregates, crushed glacial gravel has the greatest elongation ratio, whereas iron ore has the smallest elongation ratio. All other types of aggregates have close distributions of the elongation ratio.

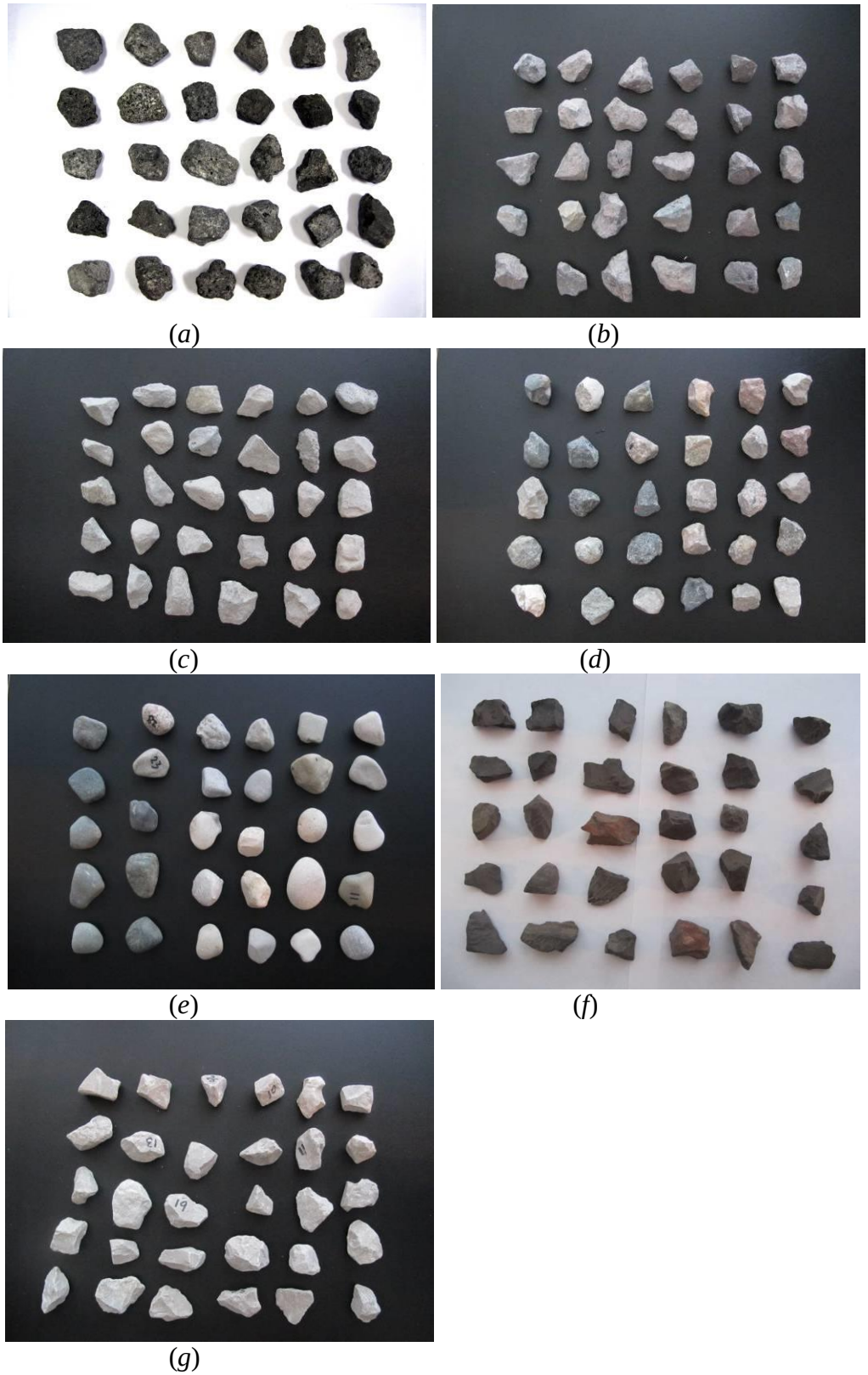

Figure 3-7 ¾-in. aggregates: (*a*) blast furnace slag, (*b*) copper ore, (*c*) dolomite, (*d*) crushed glacial gravel, (*e*) rounded glacial gravel, (*f*) iron ore, and (*g*) limestone.

Figure 3-11 plots the FTI angularity distribution of ¾-in. aggregates. Crushed glacial gravel has the greatest angularity values. The rounded glacial gravel and iron ore have much smaller values of angularity than other aggregates. Figure 3-12 shows the FTI texture distribution of ¾-in. aggregates. As expected, rounded glacial gravel has the smoothest surface, whereas blast furnace slag has the roughest surface. Copper ore and dolomite have similar surface textures; iron ore and limestone have close values of surface texture.

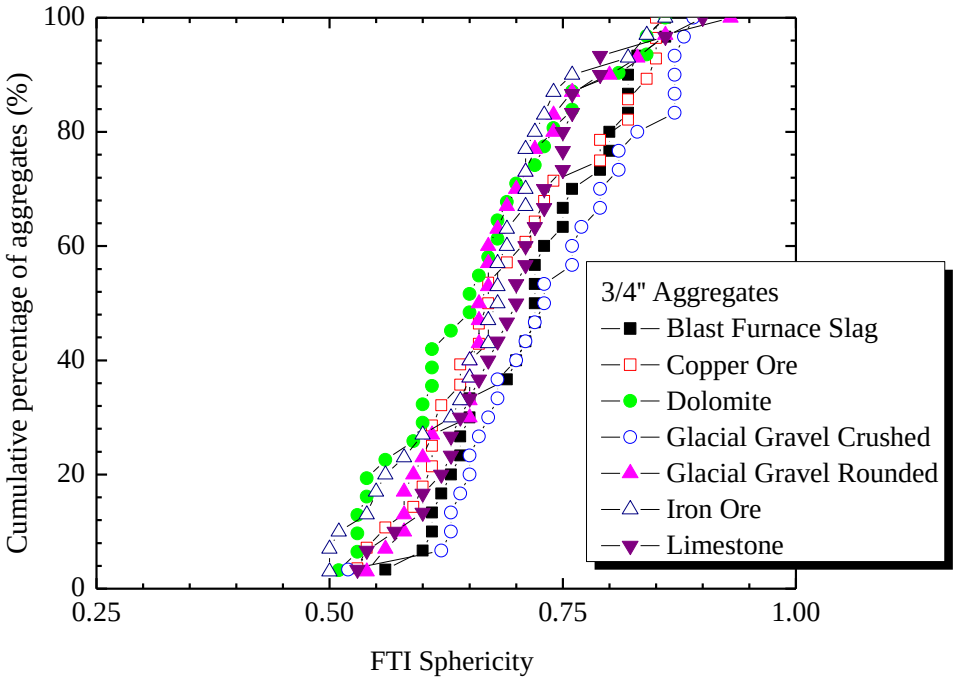

Figure 3-8 FTI sphericity distributions of ¾-in. aggregates

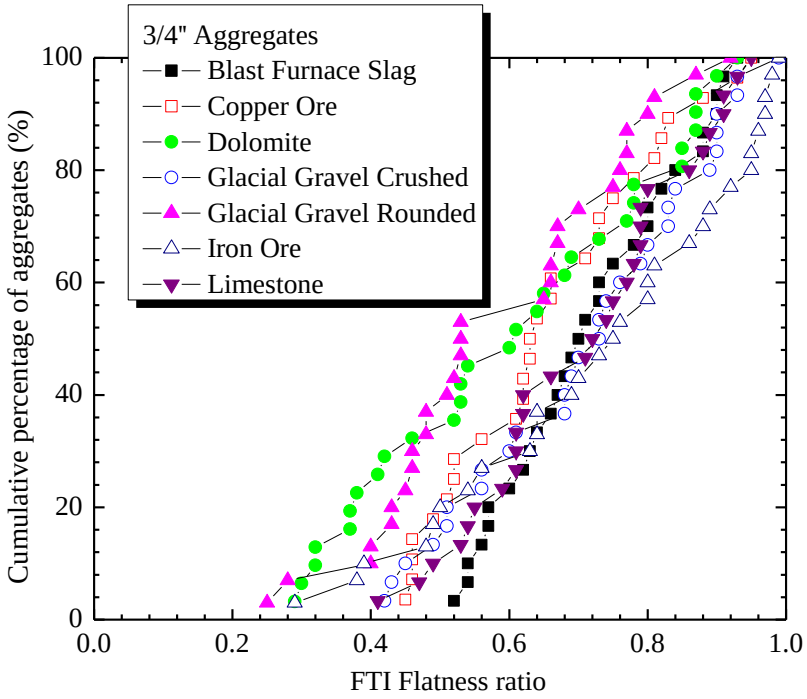

Figure 3-9 FTI flatness ratio distributions of ¾-in. aggregates

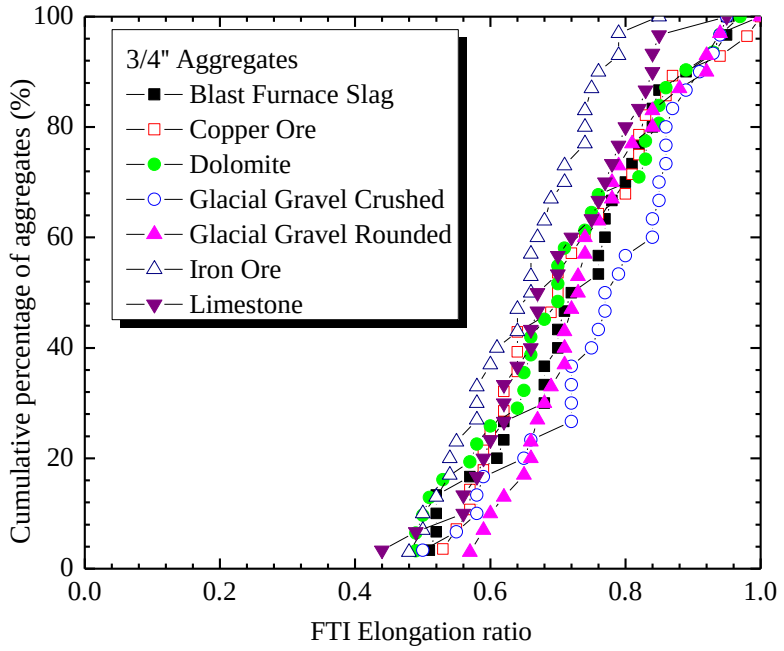

Figure 3-10 FTI elongation ratio distributions of ¾-in. aggregates

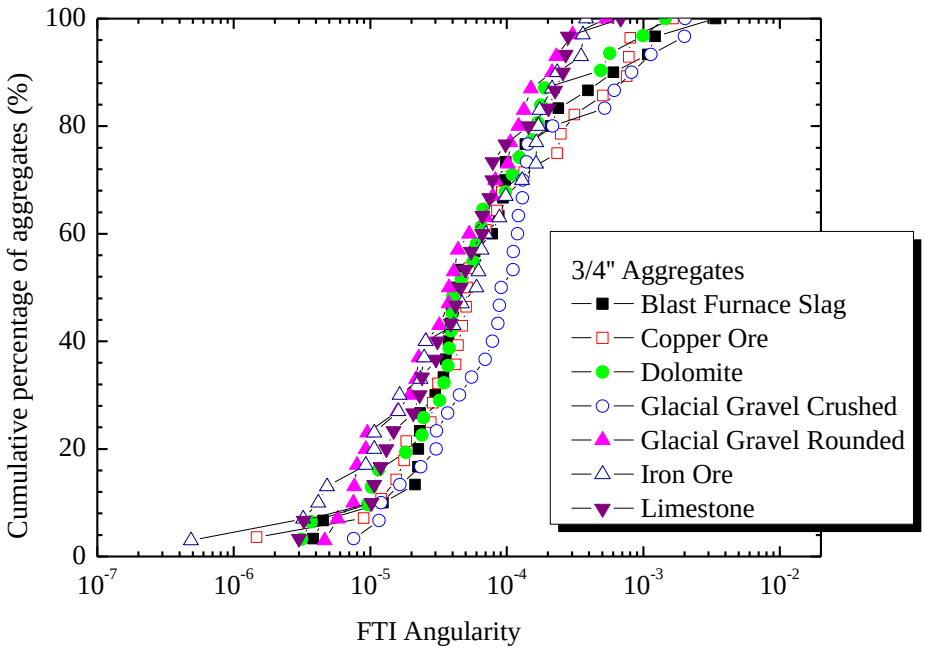

Figure 3-11 FTI angularity distributions of ¾-in. aggregates

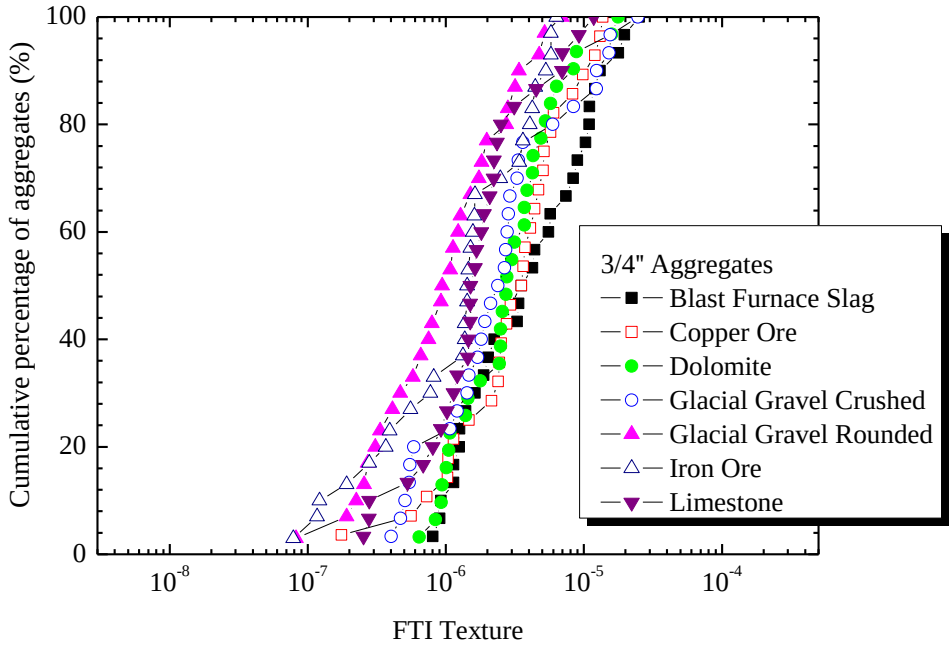

Figure 3-12 FTI texture distributions of ¾-in. aggregates

3.7 DISCUSSION OF RESULTS

For an evaluation of the reliability of the FTI system, all ¾-in. aggregate samples were also analyzed with the AIMS II and the UIAIA for comparison. Visual judgments from Figure 3-7 indicate that blast furnace slag has angular and rough surfaces and that rounded glacial gravel has the least angular and smooth surface. Table 3-3 presents the average values and standard deviations for the seven types of aggregates by FTI, AIMS II, and UIAIA methods.

In FTI results for ¾-in. aggregates, the average FTI angularity indices of blast furnace slag and copper ore were 2.74×10^{-4} and 2.69×10^{-4}, respectively; the average FTI texture indices were 6.38×10^{-6} for blast furnace slag and 4.97×10^{-6} for copper ore. Both blast furnace slag and copper ore have large values of angularity and texture, indicating angular and rough surfaces. These two materials are followed by crushed glacial gravel and dolomite. On the contrary, rounded glacial gravel, iron ore, and limestone have smooth surfaces with less angularity than the other aggregates.

In AIMS II results for ¾-in. aggregates, rounded glacial gravel has the smallest values of angularity (1,532.39) and texture (161.95), indicating the smoothest surfaces with the least angularity. According to AIMS II results, iron ore has the most angular surface, followed by copper ore; rounded glacial gravel has the smoothest surface texture, followed by iron ore and dolomite. In UIAIA results of all ¾-in. aggregates, crushed glacial gravel is the most angular type of aggregate with the roughest surfaces, followed by blast furnace slag; this sequence is inconsistent with the ranking based on the results by FTI and AIMS II. The iron ore aggregates

cannot be imaged because their color is similar to that of the UIAIA conveyor and therefore could not be resolved.

Table 3-3 Statistics of Angularity and Texture in FTI, AIMS II, and UIAIA Systems

¾-in. Aggregates			Blast Furnace Slag	Copper Ore	Dolomite	Glacial Gravel Crushed	Glacial Gravel Rounded	Iron Ore	Limestone
Angularity	FTI	Average	2.74×10^{-4}	2.69×10^{-4}	1.58×10^{-4}	2.31×10^{-4}	0.84×10^{-4}	1.01×10^{-4}	0.99×10^{-4}
		SD	6.59×10^{-4}	3.52×10^{-4}	3.07×10^{-4}	3.25×10^{-4}	1.13×10^{-4}	1.12×10^{-4}	1.39×10^{-4}
	AIMS II	Average	2968.15	3138.48	2689.25	2590.37	1532.39	3160.48	2757.89
		SD	930.95	625.82	690.57	736.76	660.06	722.55	761.4
	UIAIA	Average	439.24	373.62	337.34	486.73	254.01	na	348.93
		SD	115	76.26	62.38	110.12	84.35	na	59.11
Texture	FTI	Average	6.38×10^{-6}	4.97×10^{-6}	3.90×10^{-6}	3.86×10^{-6}	1.60×10^{-6}	2.13×10^{-6}	2.52×10^{-6}
		SD	6.28×10^{-6}	4.49×10^{-6}	3.93×10^{-6}	5.54×10^{-6}	1.66×10^{-6}	1.93×10^{-6}	2.74×10^{-6}
	AIMS II	Average	503.65	334.79	254.41	379.34	161.95	201.34	294.77
		SD	181.8	118.19	117.84	152.53	97.89	80.18	103.36
	UIAIA	Average	1.69	0.95	1.09	2.09	0.98	na	0.82
		SD	1.18	0.28	0.84	0.73	0.55	na	0.25

Note: FTI = Fourier transform interferometry; AIMS II = aggregate image measurement system II; UIAIA = University of Illinois aggregate image analyzer; SD = standard deviation; na = not applicable.

It is impossible to compare angularity and texture results of the seven types of aggregates directly with different morphologic descriptors. Consequently, the angularity and texture rankings in Figure 3-13 were adopted. All data in this figure were generated from Table 3-3, with the average value divided by the smallest average value in both angularity ranking and texture ranking for each type of aggregate. As shown in this figure, FTI, AIMS II, and UIAIA roughness rankings reach an agreement that rounded glacial gravel aggregates are considered the least angular and very smooth and that blast furnace slag aggregates are angular aggregates with rough

texture. The angularity and texture rankings are generally consistent with visual judgments despite little difference.

In angularity and texture rankings, the three image analysis techniques cannot give exactly the same rankings for angularity and texture. Possible reasons are that the mathematic algorithms to calculate angularity and texture differ from one another and that the image resolutions captured by each image system differ from one another. Compared with AIMS II and UIAIA, the FTI system has the advantage of taking the true 3-D surface data of aggregates into morphologic analysis.

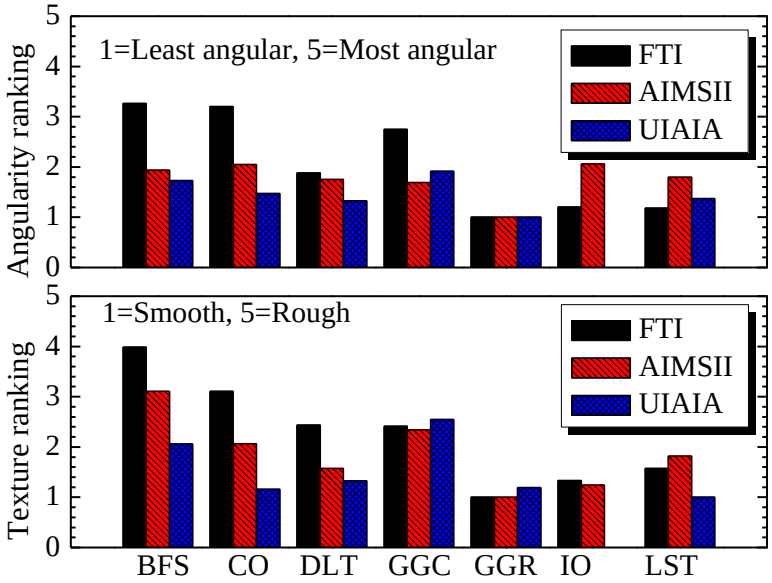

Note: BFS=Blast furnace slag; CO=Copper ore; DLT=Dolomite; GGC=Glacial glacial crushed; GGR=Glacial gravel rounded; IO=Iron ore; LST=limestone

Figure 3-13 Angularity and texture ranking of ¾-in. aggregates.

3.8 CONCLUSION AND FUTURE RESEARCH

Aggregate morphologic characteristics - including shape, texture, and angularity - have a significant influence on the performance of unbounded granular layers, pavements of hot-mix asphalt, and hydraulic Portland cement concrete. Considerable research has been conducted to understand aggregate morphologic characteristics. Imaging techniques provide a convenient means to determine the morphologic properties of coarse and fine aggregates and can successfully separate angularity from texture. This paper presents a reliable aggregate image technique to quantify the morphologic characteristics of aggregates.

This objective was achieved with the FTI system, which consists of a charge-coupled device camera, a fringe source, and MATLAB programs. Aggregates were placed on the aggregate tray under an angled mirror, and the charge-coupled device camera captured aggregate images from the angled mirror. Three images—including a visible light image and two images taken with laser lights of wavelengths of 675 and 805 nm—were captured for further analysis. The three images were analyzed with MATLAB software implementing the Fourier transform method to generate a matrix of 3-D coordinates of the aggregate surfaces. The 3-D coordinate matrix was further analyzed with FFT2 to quantify the aggregate shape, angularity, and texture.

The following conclusions can be drawn on the basis of aggregate imaging procedures and quantification results:

1. The FTI system is able to measure coarse aggregate surface morphologic characteristics with sieve sizes ranging from ¾ in. to No. 4. Image processing with Fourier transform is capable of

generating accurate 3-D coordinates with a resolution up to 35.4 μm per pixel in *x*-axis and *y*-axis directions and 20 μm in the *z*-axis direction.

2. The FFT2 method can be applied to the 3-D coordinate matrix to quantify shape, angularity, and texture of coarse aggregates. Statistical analyses of the FTI results demonstrated the capability of FFT2 to rank coarse aggregates quantitatively and the ranking results of shape, texture, and angularity were generally consistent with their qualitative ranking based on judgments with unaided eyes.

3. Comparison of FTI results with AIMS II and UIAIA results shows that the three systems can analyze aggregates with rational rankings, even though there are some differences. Blast furnace slag and crushed glacial gravel have higher angularity than other aggregates, followed by iron ore and copper ore. All methods showed rounded glacial gravel to have the smoothest surface texture.

Future research to improve the FTI system and implementation should be conducted in the following areas:

1. Further evaluation of the FTI system should be conducted on more aggregates from various sources for the robustness of the FTI system. It is essential to test the validity and repeatability of the FFT2 analysis method further. The FTI system requires the operator's judgment to select a threshold value to identify the aggregate profile and choose reference rows to reconstruct 3-D surfaces. Further research should focus on improving operation automaticity.

2. Further research should also focus on applying morphologic characteristics to pavement engineering in real projects and on evaluating pavement performance in relation to various morphologic characteristics. For instance, the FTI system may be extended to imaging the surface of pavements for calculating rutting depth and cracking densities and for monitoring pavement deformation.

3.9 ACKNOWLEDGMENTS

The research reported here was performed under NCHRP Project 4-34: Application of LADAR in the Analysis of Aggregate Characteristics. The authors extend their sincere gratitude to the project panel, including Ervin L. Dukatz, Jr., Edward T. Harrigan, William G. Eager, Julie E. Kliewer, Jorge A. Prozzi, Alan C. Robords, William H. Skerritt, G. P. Jayaprakash, and Richard C. Meininger. The authors also thank Anbo Wang, Evan Lally, Cris Harris, Yang Lu, Yu Zhou, Cristian Druta, and Ashley Stanford for their dedicated contributions. The authors acknowledge generous help and strong support from Richard C. Meininger for coordinating the use of the AIMS II at FHWA. Sincere thanks are extended to Yuanjie Xiao, who helped facilitate the scanning of aggregate particles with the UIAIA system. Finally, the authors appreciate the useful comments and suggestions from all reviewers.

3.10 REFERENCES

1. Al-Rousan, T., E. Masad, E. Tutumluer, and T. Pan. Evaluation of Image Analysis Techniques for Quantifying Aggregate Shape Characteristics. *Construction and Building Materials,* Vol. 21, 2006, pp. 978–990.

2. Rao, C., and E. Tutumluer. Determination of Volume of Aggregates: New Image Analysis Approach. In *Transportation Research Record: Journal of the Transportation Research Board, No. 1721,* TRB, National Research Council, Washington, D.C., 2000, pp. 73–80.

3. Fletcher, T., C. Chandan, E. Masad, and K. Sivakumar. Aggregate Imaging System for Characterizing the Shape of Fine and Coarse Aggregates. In *Transportation Research Record: Journal of the Transportation Research Board, No. 1832,* Transportation Research Board of the National Academies, Washington, D.C., 2003, pp. 67–77.

4. Lally, E. M. *Fourier Transform Interferometry for 3D Mapping of Rough and Discontinuous Surfaces.* PhD dissertation. Virginia Polytechnic Institute and State University, Blacksburg, 2010.

5. Lally, E. M., J. Gong, and A. Wang. Method of Multiple References for 3D Imaging with Fourier Transform Interferometry. *Optic Express,* Vol. 18, No. 17, 2010, pp. 17591–17596.

6. Wang, L., W. Sun, E. M. Lally, A. Wang, and E. Tutumluer. *Application of LADAR in the Analysis of Aggregate Characteristics.* NCHRP 4-34 Final Report. Transportation Research Board of the National Academies, Washington, D.C., 2011.

7. Wang, R. Y. *Two-Dimensional Fourier Transform.* Harvey Mudd College, Claremont, Calif., 2007. http://fourier.eng.hmc.edu/e101/lectures/Image_Processing/node6.html.

8. *MATLAB User Manual.* MathWorks, Natik, Mass., 2011.

9. Wang, L., X. Wang, L. Mohammad, and C. Abadie. Unified Method to Quantify Aggregates Shape Angularity and Texture using Fourier Analysis. *Journal of Material in Civil Engineering,* Vol. 17, No. 5, 2005, pp. 498–504.

10. Smith, S. W. *The Scientist and Engineer's Guide to Digital Signal Processing,* 2nd ed. California Technical Publishing, San Diego, 1999.

11. Brandon, D., and W. D. Kaplan. *Microstructural Characterization of Materials.* Wiley, New York, 1999.

The Geology and Properties of Earth Materials Section peer-reviewed this paper.

Evaluation of Aggregate Imaging Techniques for Quantification of Morphological Characteristics

Linbing Wang, Wenjuan Sun, Erol Tutumluer, and Cristian Druta

4.1 ABSTRACT

Aggregate morphological characteristics, including shape, angularity, and surface texture, have a significant impact on the engineering properties of construction materials such as hot-mix asphalt and hydraulic cement concrete. Consequently, the quantification of morphological characteristics of aggregates is essential for quality control of both aggregate production and pavement construction. Imaging techniques provide a cost-effective means for measuring the aggregate morphological characteristics conveniently without tedious work. However, these imaging

---

L. Wang, 301N Patton Hall, and W. Sun, 301 Patton Hall, Charles E. Via, Jr., Department of Civil and Environmental Engineering, Virginia Polytechnic Institute and State University, Blacksburg, VA 24061. E. Tutumluer, Department of Civil and Environmental Engineering, University of Illinois at Urbana–Champaign, 205 North Mathews Avenue, Urbana, IL 61801. C. Druta, Virginia Tech Transportation Institute, Virginia Polytechnic Institute and State University, 3500 Transportation Research Drive, Blacksburg, VA 24060. Corresponding author: L. Wang, wangl@vt.edu.

Transportation Research Record: Journal of the Transportation Research Board, No. 2335, Transportation Research Board of the National Academies, Washington, D.C., 2013, pp. 39–49.

DOI: 10.3141/2335-05

techniques adopt various mathematical methods with different instrument setups and result in different definitions of morphological descriptors that are usually incomparable with each other. This paper evaluates prevalent imaging techniques used for aggregate morphological characteristics analysis, including equipment cost, repeatability, reliability, accuracy, and measured morphological parameters. Three imaging techniques (second-generation Aggregate Imaging Measurement System, first-generation University of Illinois aggregate image analyzer, and Fourier transform interferometer system), are further evaluated by comparing the analysis results of seven types of aggregates passing a ¾-in. sieve and retained on a ½-in. sieve with manual measurements and visual rankings. Analysis of variance between measurements using different methods is also conducted to evaluate the accuracy of each aggregate imaging system. From the data analysis, recommendations that depend on morphological characteristics of most interest to engineers are made for the selection of appropriate imaging-analysis techniques.

4.2 INTRODUCTION

Aggregates are an important component in asphalt concrete, cement concrete, granular bases, and treated bases. The morphological characteristics of aggregates, including shape, angularity, surface texture, and surface area, significantly affect the workability, durability, fatigue response, and friction properties of both hydraulic Portland cement concrete (PCC) and hot-mixed asphalt (HMA) pavements (*1–3*). Consequently, a great deal of research has been conducted to gain a better understanding of the morphological characteristics of various aggregates and to establish the relationship between aggregate morphological characteristics and field performance of pavements (*4, 5*). Because of the advancements in imaging techniques and the availability of

low-cost, rapid image processing software, digital-imaging techniques provide a reliable means for rapidly quantifying the morphological characteristics of aggregates.

Historically, tremendous efforts have been made to quantify aggregate morphological characteristics by using imaging techniques and to correlate these characteristics to pavement performance at both the state and the national levels. Some national efforts in the past few years focused on evaluation of direct measurement methods that used two-dimensional (2-D) image analysis and semi-three-dimensional (semi-3-D) (i.e., 2.5-D) methods. However, 2-D or 2.5-D image analysis may not be accurate enough to represent 3-D morphological characteristics of aggregates. Besides, current imaging techniques use different image acquisition methods and different definitions of shape, angularity, and texture, sometimes making the morphological characterization results incomparable to one another. Consequently, it is vital to determine the quantification methods of aggregate morphological characteristics that are valid and accurate.

This paper evaluates the most widely used image analysis techniques for aggregate morphological analysis. A comparison between features of different aggregate imaging techniques is presented and is followed by definitions of the morphological descriptors in the second-generation Aggregate Imaging Measurement System (AIMS II), the first-generation University of Illinois aggregate image analyzer (UIAIA), and the Fourier transform interferometry (FTI) system. Then, those three imaging techniques are adopted to quantify the morphological characteristics of seven types of ½-in. aggregates (i.e., aggregates passing a ¾-in. sieve and retained on a ½-in. sieve). The analysis results are compared to manual measurements and visual rankings for further evaluation of the three aggregate imaging systems. Each of three

operators manually measured three dimensions of each aggregate particle with calipers three times, and the average value of the measurements of each particle was used in this paper as the manually measured results.

4.3 Comparison Between Aggregate Imaging Techniques

Imaging techniques for the quantification of morphological characteristics of aggregates can be generally divided into two categories on the basis of whether the aggregates are in motion: dynamic digital-image method and static digital-image method. Tables 4-1 and 4-2 tabulate the experimental setups, estimated cost, and aggregate size ranges that each system can measure and other features of the aggregate imaging techniques. The estimated cost of each aggregate imaging system is generally higher than $20,000, and the number of cameras installed in these systems ranges from one to three.

Of the 10 existing aggregate imaging techniques, three are further evaluated in this paper: AIMS II, UIAIA, and FTI. AIMS II can image and analyze aggregates of a wide size range, from No. 200 (0.075 mm) to 1 in. (25.4 mm) Aggregates are dispersed on a round tray over a trough in a manner that provides separation between aggregates; the tray is placed on a turntable that the AIMS software can operate to rotate automatically. The system includes seven trays with different trough sizes, and the proper tray is selected on the basis of aggregate size. The tray rotates while the camera captures an image of each aggregate. The resolution of the captured image is dependent on aggregate size, ranging from 44.78 μm/pixel for coarse, 17.91 μm/pixel for No. 8 (2.36 mm), 8.96 μm/pixel for No. 16 (1.18 mm), and 4.48 μm/pixel for No. 30 (0.60 mm) to 3.36 μm/pixel for finer than No. 50 (0.3 mm).

Table 4-1 Comparison between Different Aggregate Imaging Techniques

Test Method	Aggregate Imaging System	Estimated equipment cost ($)	Analysis Speed	Accuracy	Ease of Use	Repeatability
Dynamic Digital Image Method	VDG-40 Videograder	45,000	H	M	M	L
	Computerized Particle Analyzer	25,000	H	M	M	M
	PSDA	50,000	L	M	H	L
	VIS	60,000	H	M	M	L
	Camsizer	45,000	M	M	M	L
	Winshape	35,000	H	M	M	M
	UIAIA	35,000	M	H	M	H
Statistic Digital Image Method	AIMS II	35,000	H	H	H	H
	FTI	20,000	M	H	M	H

Note: H = high; M = medium; L = low. (Based on [*5*])
PSDA = Micrometric Optimizer Particle Size Distribution Analyzer, VIS = Video Image System, UIAIA = University of Illinois Aggregate Imaging Analyzer, AIMS = Aggregate Imaging Measurement System, FTI = Fourier Transform Interferometry.

In UIAIA, all the aggregates are individually placed on a conveyor belt, with three orthogonally positioned cameras to capture the aggregates'projections. UIAIA can distinguish flat and elongated aggregates and automatically calculate angularity and surface texture as well as surface area and volume for a wide range of coarse and fine aggregates (from 76.2 to 2.38 mm). As opposed to the black-and-white cameras and black background (of the first-generation UIAIA system), the second-generation enhanced version (UIAIA II) is equipped with three progressive-scan color cameras (1,292- × 964-pixel resolution) and a blue background to capture high-resolution (0.056 mm/pixel) color images of aggregate. Moreover, an advanced color-thresholding scheme is used in the enhanced UIAIA software control. Therefore, different types of mineral aggregates of various colors can now be scanned with this system because it includes

four LED illumination lights with dimmer control that optimizes light intensity and minimizes shadows to achieve the sharpest possible images. Even though UIAIA II is now available, this paper presents results only from the first-generation UIAIA.

The FTI system is able to analyze both coarse and fine aggregates (from 19.05 to 0.30 mm) from different origins of various colors. Aggregates are dispersed on a particle tray, and a charge-coupled device camera captures images of the top surfaces of aggregates from an angled mirror. The resolution of FTI images is 35.4 μm/pixel in both *x*- and *y*-directions.

Table 4-2 Comparison of Additional Characteristics of Aggregate Imaging Techniques

Characteristic	Aggregate Imaging System	Aggregate Size Range	No. of cameras	Dimensions of Image Data	Measured Characteristics
Dynamic Digital Image Analyzer	VDG-40 Videograder	#16 - 1.5-in.	1	2	Shape
	Computerized Particle Analyzer	#140 - 1.5-in.	1	2	Shape
	PSDA	#200 - 1.5-in.	1	2	Shape
	VIS	#16 - 1.5-in.	1	2	Shape
	Camsizer	#50 - ¾-in.	2	2	Shape Angularity
	Winshape	#4 – 1-in.	2	3	Shape Angularity
	UIAIA	#8 – 1-in.	3	2	Shape Angularity Texture
Statistic Digital Image Method	AIMS II	#200 – 1-in.	1	3	Shape Angularity Texture
	FTI	#50 - ¾-in.	1	3	Shape Angularity Texture

4.4 IMAGE ANALYSIS METHODS IN AIMS II, UIAIA, AND FTI SYSTEM

AIMS II uses a digital camera with an autofocus microscope for automatic capture of images of different resolutions, which are dependent on aggregate sizes. This system measures three dimensions of aggregates to calculate sphericity and aspect ratios from images of the aggregate top surface. It can also calculate the angularity of aggregate of all sizes through use of a gradient method and quantify texture of coarse aggregates by means of the wavelet method (*7*). The influence of shape on angularity is normalized through division of measurements by use of the equivalent-ellipse dimensions.

In AIMS II, the shape properties of coarse aggregates are defined by sphericity (Equation 4-1), flatness ratio (Equation 4-2), elongation ratio (Equation 4-3), and flatness-and-elongation (FE) ratio (Equation 4-4), whereas the shape properties of fine aggregates are defined by the Form2D parameter (Equation 4-5) instead of sphericity.

$$\text{sphericity} = \sqrt[3]{\frac{D_s D_m}{D_l^2}} \tag{4-1}$$

$$\text{flatness ratio} = D_s / D_m \tag{4-2}$$

$$\text{elongation ratio} = D_m / D_l \tag{4-3}$$

$$\text{FE ratio} = D_m / D_s \tag{4-4}$$

$$\text{Form2D} = \sum_{\theta=0}^{360-\Delta\theta} \left[\frac{R_{\theta+\Delta\theta} - R_\theta}{R_\theta} \right] \tag{4-5}$$

where

D_s = shortest dimension of the aggregate particle,

D_l = longest dimension of the aggregate particle,

D_m = dimension of the aggregate particle perpendicular to both D_s and D_l,

R_θ = radius of the particle at angle θ, and

$\Delta\theta$ = incremental difference in angle.

Angularity is defined by Equation 4-6, and texture is defined by Equation 4-7 at a given level with the use of a wavelet method.

$$\text{Angularity} = \sum_{\theta=0}^{360-\Delta\theta} \frac{\left|R_{P\theta} - R_{EE\theta}\right|}{R_{EE\theta}} \tag{4-6}$$

$$\text{Texture} = \frac{1}{3N} \sum_{i=1}^{3} \sum_{j=1}^{N} \left(D_{i,j}\left(x, y\right)\right)^2 \tag{4-7}$$

where

$R_{P\theta}$ = radius of the particle at a directional angle of θ,

$R_{EE\theta}$ = radius of an equivalent ellipse at same θ,

N = level of decomposition;

i = 1, 2, and 3 for three detailed images of texture,

j = wavelet coefficient index, and

x, y = location of coefficients in transformed domain.

In the UIAIA system, shape is described by means of sphericity, flatness ratio, and elongation ratio; angularity is described by the angularity index (AI) method as illustrated in Figure 4-1. The AI method traces the changes of slope of the 2-D profile outline of the particle and uses a

weighted average value of its angularity determined from three views (front, top, and side). Equation 4-8 shows the calculation of angularity for each image, and Equation 4-9 is used to calculate AI.

$$\text{Angularity} = \sum_{e=0}^{170} e \times P(e) \tag{4-8}$$

$$\text{AI} = \frac{(\text{Angularity} \times \text{Area})_{front} + (\text{Angularity} \times \text{Area})_{top} + (\text{Angularity} \times \text{Area})_{side}}{\text{Area}_{front} + \text{Area}_{top} + \text{Area}_{side}} \tag{4-9}$$

where

e = angle starting for each interval of 10 °,

$P(e)$ = probability that changes in angle α from starting angle e to next angle e+10, and

$\text{area}_{\text{front}}$, area_{top}, and $\text{area}_{\text{side}}$ = areas of profiles of front, top and side views, respectively.

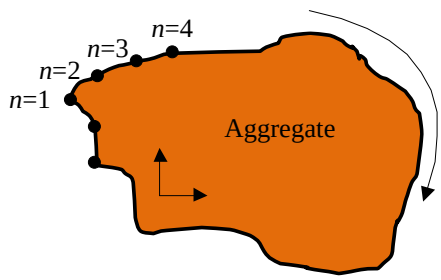

Figure 4-1 Illustration of an n-sided polygon approximating the outline of a particle (*8*).

Surface texture is analyzed through an erosion and dilation technique, illustrated in Figure 4-2, in which Figure 4-2*a* shows the original aggregate image (*9*). Surface irregularity is gradually lost during the erosion–dilation process, with the corresponding area lost as a percentage of the area

in the original image. The percentage of lost area is defined as texture in Equation 4-10, and surface texture (ST) is defined by Equation 4-11.

$$\text{Texture}=\frac{A_1-A_2}{A_1}\times 100\% \tag{4-10}$$

$$\text{ST}=\frac{(\text{Texture}\times\text{Area})_{front}+(\text{Texture}\times\text{Area})_{top}+(\text{Texture}\times\text{Area})_{side}}{\text{Area}_{front}+\text{Area}_{top}+\text{Area}_{side}} \tag{4-11}$$

where A_1 and A_2 are areas of aggregates before and after erosion-dilation cycles, respectively.

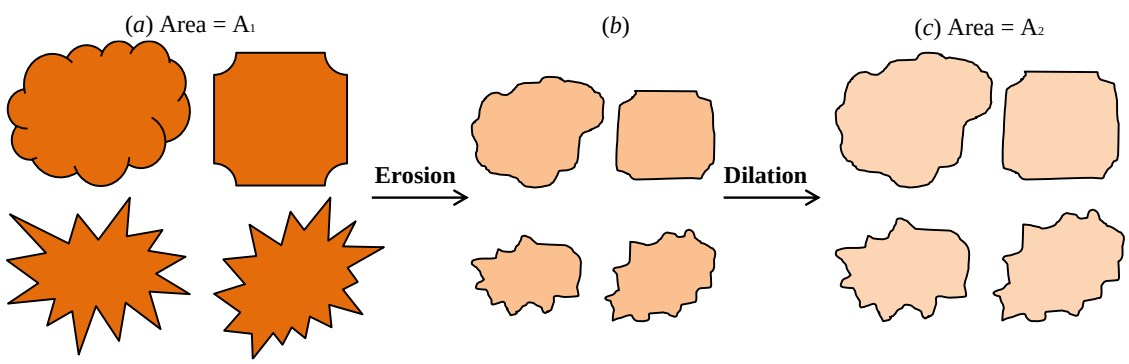

Figure 4-2 Illustration of erosion and dilation technique (*9*).

In the FTI system, shape properties of aggregates are described by sphericity, flatness ratio, elongation ratio, and FE ratio; angularity and texture are defined by using a 2-D Fourier transform method.

$$Z(p,q)=\sum_{x=0}^{N-1}\sum_{y=0}^{N-1}z(x,y)e^{-j\left(\frac{2\pi}{N}xp+\frac{2\pi}{N}yq\right)} \tag{4-12}$$

$$z(x,y)=\sum_{p=0}^{N-1}\sum_{q=0}^{N-1}Z(p,q)e^{j\left(\frac{2\pi}{N}xp+\frac{2\pi}{N}yq\right)} \tag{4-13}$$

$$\mathrm{AF} = \sum_{p=1}^{N_A}\sum_{q=1}^{N_A}\left[\left(a(p,q)/a_0\right)^2 + \left(b(p,q)/a_0\right)^2\right] \tag{4-14}$$

$$\mathrm{TF} = \sum_{p=1}^{N}\sum_{q=1}^{N}\left[\left(a(p,q)/a_0\right)^2 + \left(b(p,q)/a_0\right)^2\right] - \mathrm{AF} \tag{4-15}$$

where

$Z(p, q)$ = coefficient in p^{th} row and q^{th} column with the matrix for the discrete Fourier transform of $z(x, y)$ in frequency domain,

N = size of $z(x, y)$ matrix,

$z(x, y)$ = 3-D coordinate in x^{th} row and y^{th} column on aggregate surface,

j = imaginary root,

AF = angularity factor,

a and b = real and imaginary parts of coefficients of 2-D fast Fourier transforms (FFT2),

a_0 = average value of $z(x, y)$,

TF = texture factor, and

N_A = threshold value with which a 3-D surface is reconstructed by using the inverse of FFT2 coefficients that have their frequencies smaller than $2\pi N_A/N$ in either x- or y-direction.

The FFT2 coefficients are considered to only contribute to angularity if the average value of the absolute differences between the original surface and reconstructed surface using the inverse is greater than 0.2 mm, which is the spatial spacing discernible by unaided human eyes. Other Fourier coefficients are considered to contribute to texture only.

The roughness matrix is a $z(x, y)$ matrix of a rectangular region on an aggregate surface with an area ranging from 1.0 mm^2 to the maximum value of 25% of an aggregate surface area that is

based on the sieve size of the aggregate being analyzed (*10*). Figure 4-3 plots the relationship between AF (or TF) and the roughness matrix area for all seven types of aggregates (AF plot or TF plot) for some ½-in. aggregates. As Figure 4-3 shows, the AF and TF values follow a linear relationship in both the AF and TF plots as the area of the roughness matrix increases. Furthermore, aggregates with more angular surfaces tend to have steeper slopes in the AF plot, and aggregates with rougher surfaces tend to show steeper slopes in the TF plot. Therefore, it is reasonable to define the linear relationship (slope) in the AF and TF plots as angularity and texture of an aggregate, respectively.

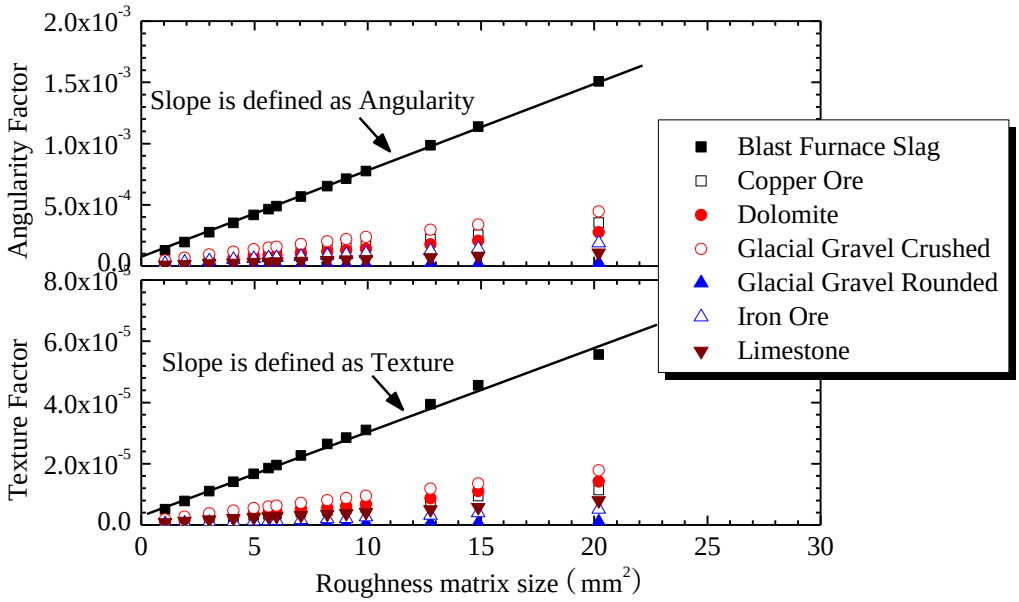

Figure 4-3 Illustrations of angularity and texture of some 1/2'' aggregates in the FTI system (*10*).

4.5 AGGREGATES

Table 4-3 lists some physical properties of the seven types of aggregates: blast furnace slag (BFS), copper ore (CO), dolomite (DLT), crushed glacial gravel (CGG), rounded glacial gravel

(RGG), iron ore (IO), and limestone (LST). Each type of aggregate was represented by thirty ½-in. samples to ensure statistical stability of the data. Further statistical analysis suggests that a 30-aggregate sample is large enough to provide a normal distribution and to achieve stable statistics for each type. All seven types of aggregate were manually measured first with a vernier caliper and then analyzed through the FTI, AIMS II, and the first-generation UIAIA system, respectively, for comparison. Figure 4-4 shows photographs of the ½-in. aggregates. As the photographs show, the surfaces of the BFS are quite angular and the roughest, while the surfaces of the RGG are the least angular and extremely smooth.

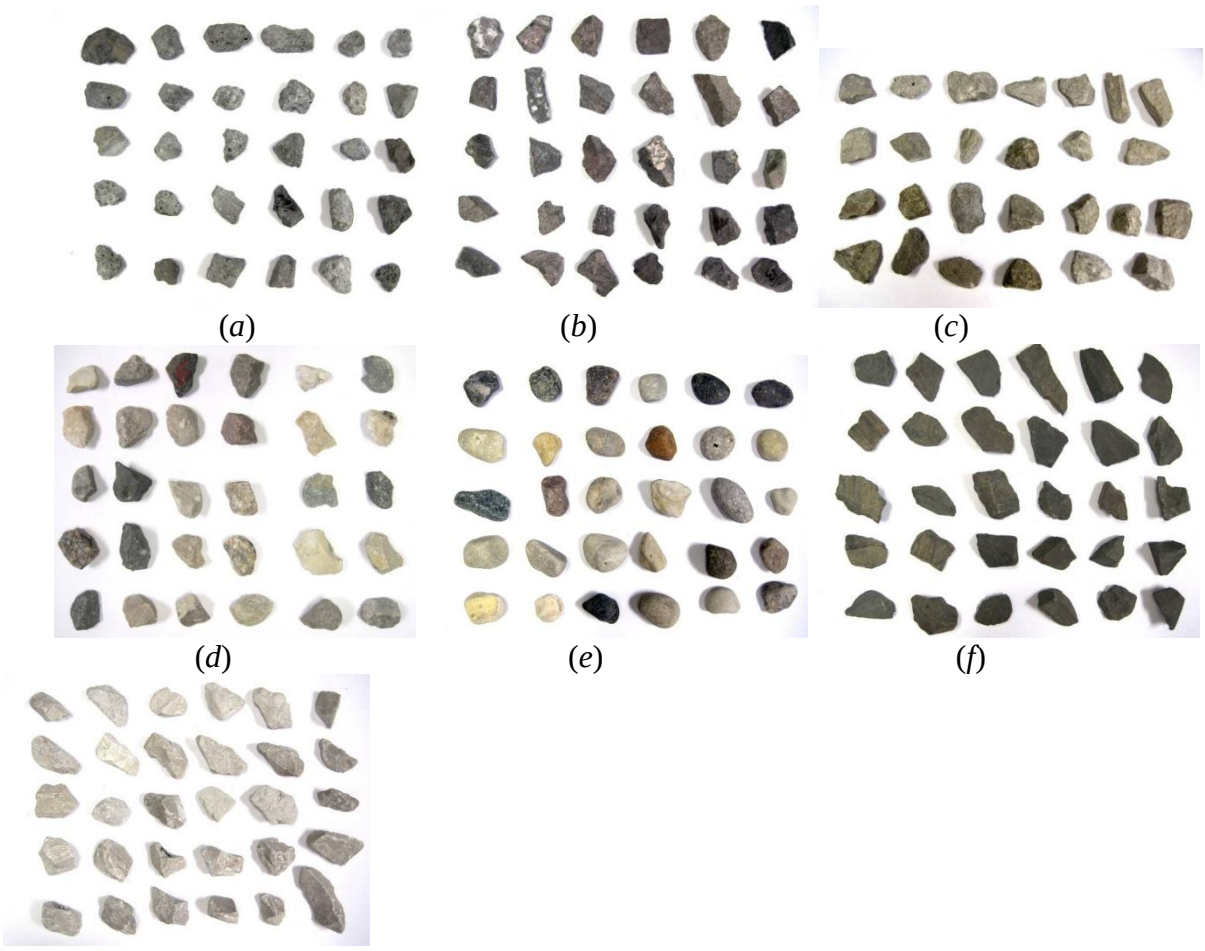

Figure 4-4 Photos of ½-in. aggregates: (*a*) BFS, (*b*) CO, (*c*) DLT, (*d*) CGG, (*e*) RGG, (*f*) IO, and (*g*) LST.

Table 4-3 Aggregate Types and the Physical Properties (*10*)

Aggregate type	Origin	Description	LAA loss (%)	Bulk dry SpGr (g/cm^3)	24 hr soak absorption (%)
BFS	Wayne, MI	• Color: 5R 5/0 to 5R 1/0 • Poorly developed crystalline structure	43	2.27	3.18
CO	Keweenaw, MI	• Mixture of colors, including 5R 9/0, 5BG 8/2, 5R 8/6, and 5R 2/8 • Fine to coarse grains	19	2.64	0.95
	Houghton, MI		16	2.76	2.12
DLT	Mackinac, MI	• Color: 5R 9/4 to 5R 6/8 • medium to coarse crystals	27	2.78	0.52
	Monroe, MI	• Color: 5R 6/7 • Well defined small euhedral dolomite crystals	45	2.45	4.16
GGC	Kent, MI	• Various colors • With crushed surfaces	17	2.73	0.71
GGR	Kent, MI	• Various colors • Very smooth texture	19	2.68	1.10
IO	Marquette, MI	• Color: 10PB 2/2 with 5R 2/1 • Very fine grained and hard metamorphic rock	11	NA	NA
LST	Schoolcraft, MI	• Color: 5R 9/4 • Very fine subcrystalline texture	25	2.65	0.64
	Arenac, MI	• Color: 10PB 7/0 • Very fine crystalline with abundant frosted quartz sand grains	42	2.56	2.13

Note: LAA=Los Angeles Abrasion; Bulk dry SpGr=Bulk dry specific gravity; BFS = Blast Furnace Slag; CO = Copper Ore; DLT = Dolomite; GGC = Glacial Gravel Crushed; GGR = Glacial Gravel Rounded; IO = Iron Ore; LST = Limestone; NA = not applicable. Color description in the Description column is named according to Munsell color system. The Munsell color system is a color system that defines color based on three dimensions: hue, value (lightness), and chroma (color purity). A color can be specified by listing three numbers for hue, value, and chroma. For example, 5R 5/0 means a red of medium lightness and barely saturated, with 5R meaning the color in the middle of the red hue band, 5/ meaning medium value (lightness), and a chroma of 0.

4.6 Analysis Results

Figure 4-5 plots the sphericity distributions of the seven types of ½-in. aggregates by means of manual measurement and AIMS II and the FTI system. Compared with the sphericity distribution of manual measurement, AIMS II sphericity is distributed in a wider range and FTI sphericity in a narrower range. Both manual measurements and FTI results show that BFS, RGG, and CGG have aggregates with relatively large values of sphericity; conversely, IO and LST have aggregates with smaller values of sphericity than the other types of aggregate.

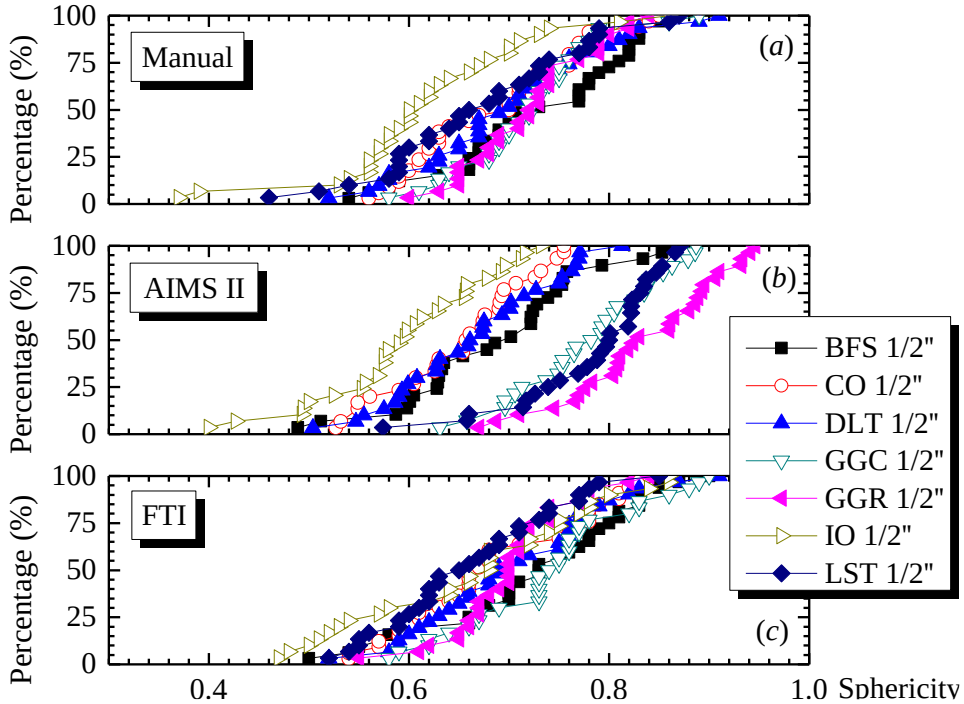

Figure 4-5 Sphericity distributions of ½-in. aggregates for various analysis methods: (*a*) manual, (*b*) AIMS II, (*c*) FTI.

Figure 4-6 plots the FE ratio distributions of all the ½-in. aggregates analyzed by manual measurement and the UIAIA, AIMS II, and the FTI system. Consistent with manual

measurements, both AIMS II and the FTI system consider IO to have the greatest values of FE ratio. Because IO was not evaluated with the UIAIA system, that system gave DLT the next-highest values of FE ratio, which were similar to those of the AIMS II and manual measurements.

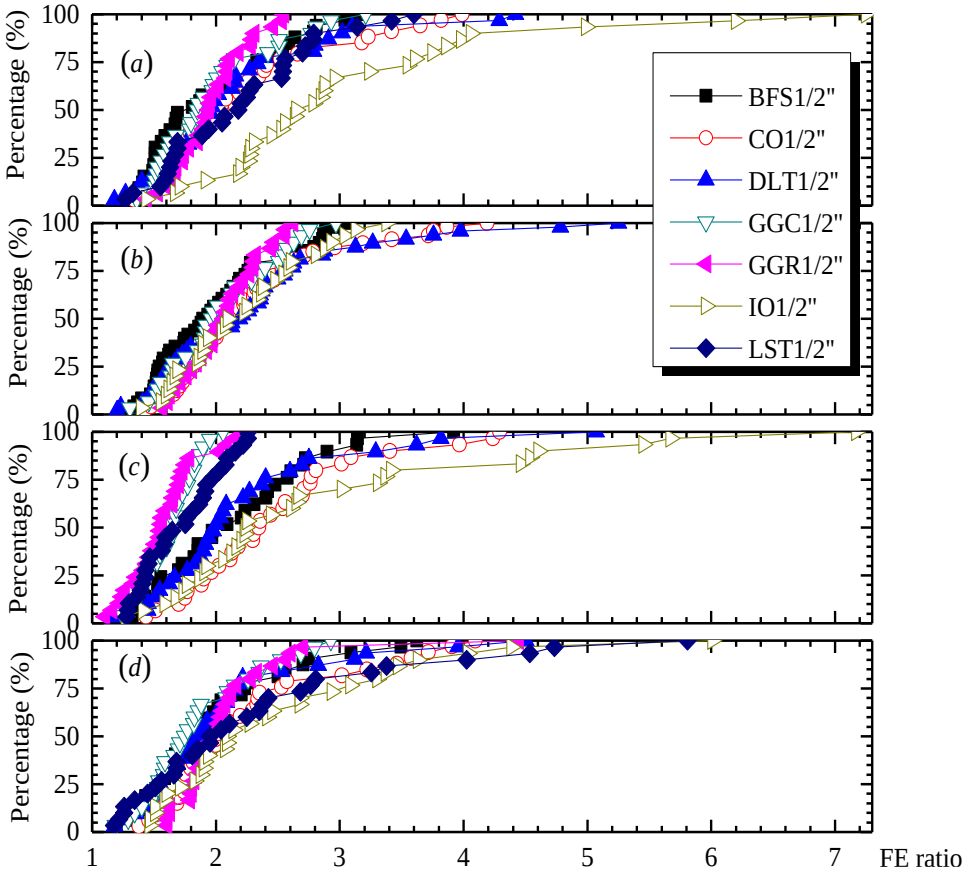

Figure 4-6 Distributions of FE ratio of ½-in. aggregates for various analysis methods: (*a*) manual, (*b*) UIAIA, (*c*) AIMS II, and (*d*) FTI.

Table 4-4 tabulates mean values and standard deviations for the seven types of ½-in. aggregates. The FTI ranking shows that aggregates from BFS are the most angular and have the roughest surfaces; LST aggregates are the second-most angular and have the second-smoothest surfaces.

DLT is the least-angular aggregate and has the smoothest surface texture. The AIMS II ranking indicates that CO is the most angular aggregate with the second-roughest surfaces; aggregates from BFS are the second-most angular and have the roughest surfaces. Aggregates of RGG are the least angular and have the smoothest surfaces. In the UIAIA ranking, aggregates of IO could not be imaged because of their dark color (although this would not be a limitation for the enhanced UIAIA II, which uses progressive color cameras and a blue background to capture digital color images of the aggregates). CGG has the most angular aggregates and the roughest surfaces, and aggregates from RGG are the least angular and have the third-smoothest surfaces.

Table 4-4 Angularity and Texture of ½-in. Aggregates Determined by FTI, AIMS II, and UIAIA

Characteristic			BFS	CO	DLT	GGC	GGR	IO	LST
Angularity	FTI	Mean	2.44×10^{-4}	0.98×10^{-4}	0.60×10^{-4}	1.46×10^{-4}	0.97×10^{-4}	1.00×10^{-4}	1.90×10^{-4}
		Standard deviation	5.18×10^{-4}	1.14×10^{-4}	1.13×10^{-4}	2.51×10^{-4}	1.11×10^{-4}	1.04×10^{-4}	4.54×10^{-4}
	AIMS II	Mean	3040.72	3126.44	2864.42	2650.92	1362.78	2932.80	2859.35
		Standard deviation	833.09	604.35	697.83	612.77	624.87	515.95	631.80
	UIAIA	Mean	367.51	394.23	333.59	458.09	239.89	NA	357.07
		Standard deviation	80.71	77	55.15	108.54	83.19	NA	51.69
Texture	FTI	Mean	9.57×10^{-6}	4.69×10^{-6}	2.86×10^{-6}	2.70×10^{-6}	3.54×10^{-6}	5.17×10^{-6}	4.60×10^{-6}
		Standard deviation	13.70×10^{-6}	5.68×10^{-6}	5.18×10^{-6}	3.37×10^{-6}	4.32×10^{-6}	6.47×10^{-6}	8.38×10^{-6}
	AIMS II	Mean	574.74	365.75	259.11	322.72	217.55	243.40	270.21
		Standard deviation	155.81	120.04	113.33	188.26	145.06	112.90	122.26
	UIAIA	Mean	1.12	1.19	0.92	2.15	1.00	NA	0.91
		Standard deviation	0.39	0.44	0.39	0.98	0.76	NA	0.27

Note: NA = not available.

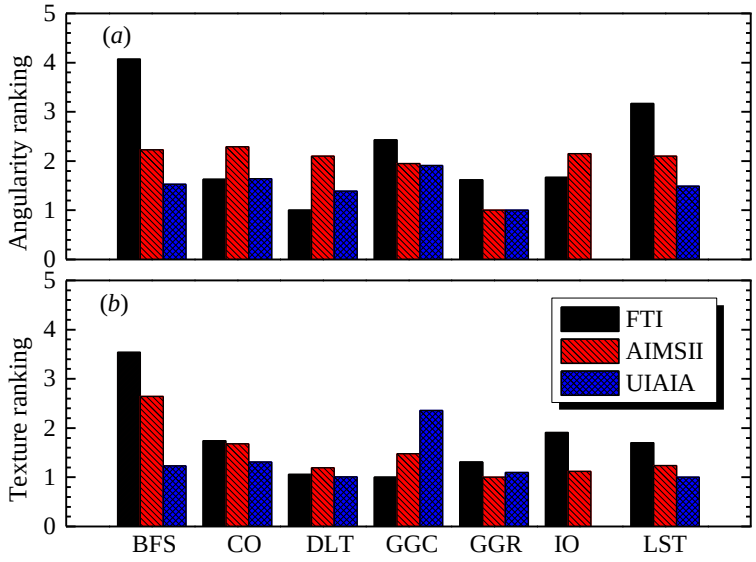

Figure 4-7 (*a*) Angularity and (*b*) texture rankings of ½-in. aggregates of various materials determined by three analysis techniques.

Because direct comparison of roughness rankings of the seven types of aggregates by means of the different morphological descriptors is not convenient, the angularity and texture rankings for ½-in. aggregates are plotted in Figure 4-7. All data in this figure are generated from Table 4-4 by simply dividing the mean value of each type of aggregate by the smallest mean value for either angularity or texture from the FTI, AIMS II, and UIAIA angularities and textures, respectively. In Figure 4-7, both AIMS II and UIAIA roughness rankings indicate that aggregates from RGG are considered the least angular and have an extremely smooth texture, whereas FTI ranks DLT aggregates as being the most angular and having an extremely smooth texture. And BFS aggregates are quite angular and have the roughest texture according to the angularity and texture rankings from all three systems.

4.7 EVALUATION AND DISCUSSION

To evaluate the three imaging techniques (AIMS II, UIAIA, and FTI) further, the following procedure was adopted: (*a*) comparison with manual measurements for shape characteristics; (*b*) analysis of variance (ANOVA) test to determine differences in the results of the various methods of testing for shape, angularity, and texture characteristics; and (*c*) comparison to visual rankings for both angularity and texture.

4.7.1 Comparison with Manual Measurements

The relationship between manual measurements and shape characteristics quantified through aggregate imaging techniques could be regressed by linear relationships. As Figure 4-8 shows, the linear relationships for sphericity and FE ratio indicate that (*a*) both AIMS II and FTI could accurately and consistently quantify the sphericity of LST aggregates with that from manual measurements, and (*b*) both UIAIA and FTI quantify the FE ratio of RGG aggregates with more consistent values than does AIMS II.

4.7.2 ANOVA Test

ANOVA is used to compare several groups of observations that are independent and may each have a different mean. A test of importance is whether all the means are statistically equal. The basic assumptions of the ANOVA test are as follows: (*a*) sample data are collected by means of a simple random sampling method; (*b*) sample groups are independent from one another; (*c*) variance is equal across groups; and (*d*) each group follows a normal distribution.

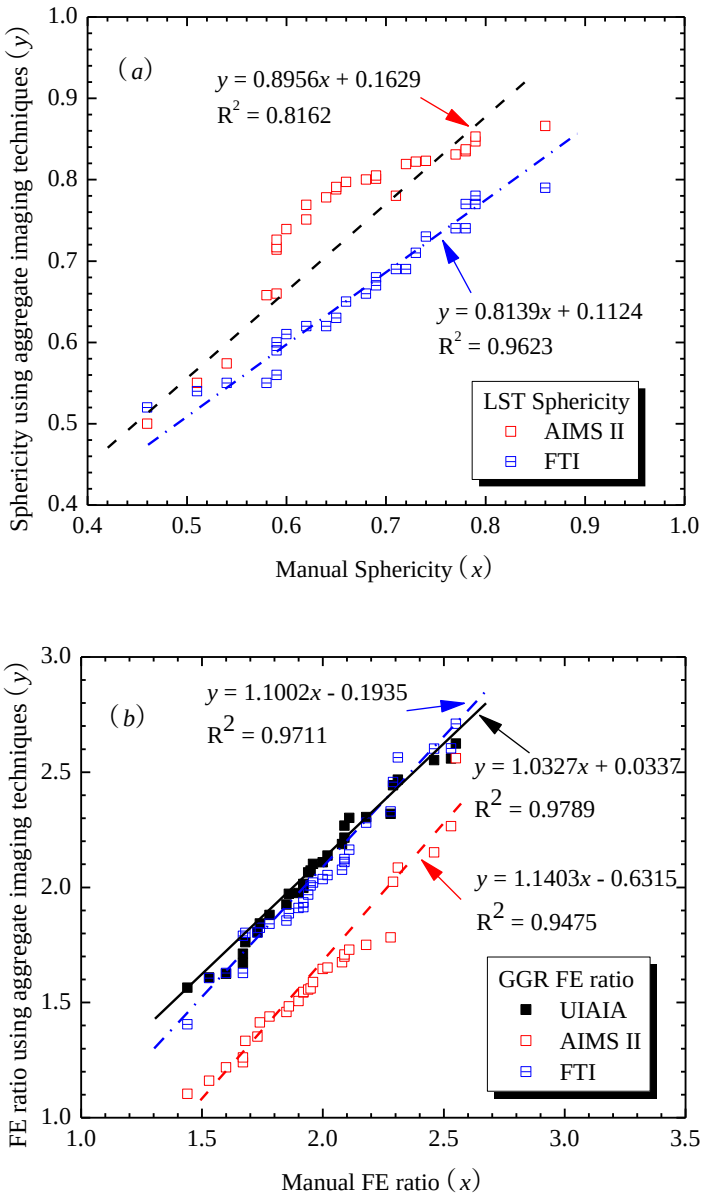

Figure 4-8 Relationship between manual measurements and shape properties of ½-in. LST aggregates acquired from image analysis techniques for (*a*) sphericity and (*b*) FE ratio.

The ANOVA tests reported in this section were used to compare sphericity and FE ratio of all the ½-in. aggregates by using the statistical software JMP (Version 9), so as to determine whether the differences between the three methods were significant for shape characteristics. Angularity and texture characteristics cannot be directly compared with each other by using

ANOVA in JMP because the descriptors for angularity and texture are defined in different terms. The ANOVA test can detect only whether significant differences exist between results obtained by different methods (i.e., FTI, AIMS II, UIAIA, and manual measurements). Once a difference between means of these groups is found, Tukey's honestly significant difference test is conducted in JMP to determine which mean is significantly different from the others.

Table 4-5 presents the method groups for the ANOVA test, and Table 4-6 tabulates the ANOVA test results. The ANOVA test for sphericity is as follows: H_0 (in which $\mu_{1s} = \mu_{2s} = \mu_{3s}$) versus *Ha* (in which at least one mean differs), where μ_{1s}, μ_{2s}, and μ_{3s} are the means of sphericity determined from the FTI system, AIMS II, and manual measurements, respectively. Set $\alpha = 0.05$, reject H_0 if p value $< \alpha$, and then perform Tukey's method to conduct a multiple comparison test to find the mean that is significantly different from others. The ANOVA test for FE ratio is as follows: H_0 (in which $\mu_{1fe} = \mu_{2fe} = \mu_{3fe} = \mu_{4fe}$) versus *Ha* (in which at least one mean differs), where μ_{1fe}, μ_{2fe}, μ_{3fe}, and μ_{4fe} are the means of the FE ratio determined from the FTI, AIMS II, UIAIA, and manual measurements, respectively. Set $\alpha = 0.05$, reject H_0 if p value $< \alpha$, and then perform Tukey's method to conduct a multiple comparison test to find the mean that is significantly different from the others.

Table 4-5 Analysis Method Groups for ANOVA Test

	Method	Group
Sphericity	FTI	1
	AIMS II	2
	Manual measurement	3
FE Ratio	FTI	1
	AIMS II	2
	UIAIA	3
	Manual measurement	4

Table 4-6 ANOVA Test Summary for Sphericity and FE ratio of ½-in. Aggregates

Aggregates	Sphericity	FE ratio
BFS	No significant difference among three means.	No significant difference among the four means.
CO	No significant difference among three means.	No significant difference among the four means.
DLT	No significant difference between three means.	The UIAIA mean is significantly smaller than the other three means.
GGC	The AIMS II mean is significantly greater than the other two means.	The AIMS II mean is significantly smaller than the other three means.
GGR	The FTI mean is the greatest one, and the AIMS II mean is the smallest one.	The AIMS II mean is significantly smaller than the other three means.
IO	No significant difference among three means.	No significant difference among the four means.
LST	The FTI mean is very close to the manual measurement mean.	The FTI mean is very close to the manual measurement mean and the UIAIA mean.

4.7.3 Comparison with Visual Ranking of Angularity and Texture

Angularity and texture of all the ½-in. aggregates were visually ranked by three operators. Mean values of the same aggregate were calculated for visually evaluated rankings from the three operators to get the final visual rankings of angularity and texture. To compare the angularity and texture rankings acquired from three imaging techniques with the visual rankings, the Spearman correlation coefficient was calculated. The Spearman correlation coefficient ρ is defined by the following equation:

$$\rho = \frac{\sum_{i=1}^{n}(x_i - \bar{x})(y_i - \bar{y})}{\sqrt{\sum_{i=1}^{n}(x_i - \bar{x})^2 (y_i - \bar{y})^2}} \tag{4-16}$$

where n is the sample size and x and y represent the visual ranking results and rankings of image analysis results, respectively. The Spearman correlation coefficient has a value ranging from −1 to 1. A Spearman correlation of zero indicates that there is no relevance between X and Y (x and y are ranks of X and Y, respectively), whereas a Spearman correlation close to 1 shows a monotonically related relationship between X and Y, even if the relationship is not linear.

The following table presents the Spearman correlation coefficients of angularity and texture obtained by comparing the ranking results for angularity and texture for the three imaging techniques with the visual ranking results.

Table 4-7 Spearson Correlation Coefficents

	Analysis Method		
Characteristics	UIAIA	AIMS II	FTI
Angularity	0.257	0.771	0.860
Texture	0.200	0.657	0.371

The Spearman correlation coefficients suggest that (*a*) all three imaging techniques can be used for the quantification of angularity and texture for all the ½-in. aggregates (and, furthermore, FTI angularity ranking has the closest correlation to visual ranking of the three imaging techniques) and (*b*) AIMS II ranking for texture has better agreement with visual ranking than the other two.

4.8 CONCLUSION

Imaging techniques can rapidly measure aggregate shape, angularity, and texture characteristics. Even though these techniques may require expensive equipment, the unit costs of incremental tests are low. Furthermore, imaging techniques can provide automatic quantification of

morphological characteristics with accurate and reliable results. The following issues should be considered for further improvement of the available techniques:

1. Imaging techniques use various analysis methods that may produce results sometimes incomparable with one another. For instance, some imaging techniques analyze 2-D images while others use 2-D projections to reconstruct 3-D surfaces of aggregates.
2. Some imaging techniques could analyze only coarse aggregates, whereas other techniques could analyze aggregates of wide size ranges, including both coarse and fine. Consequently, it is difficult to evaluate the relative merits of different imaging techniques.
3. Measurements using imaging techniques require instrument setups and well-trained operators.

After evaluation of three imaging techniques (UIAIA, AIMS II, and FTI), the following conclusions can be drawn on the basis of aggregate imaging procedures and quantification results:

1. ANOVA test results of the ½-in. aggregates demonstrate that the shape characteristics (such as sphericity) obtained through the FTI system are in good agreement with those calculated from manual measurements and AIMS II for most aggregates. The ANOVA test of the FE ratio show that FE ratio results obtained from the three aggregate imaging systems are generally in good agreement with FE ratios calculated from manual measurements.
2. Comparison of angularity and texture results shows that the three aggregate imaging systems could analyze ½-in. aggregates with reasonable angularity and texture rankings. It was found that BFS has greater values for both angularity and texture than the other aggregates; it was followed

by LST and IO. Both DLT and RGG were shown by all three aggregate imaging techniques to have extremely smooth surface textures.

However, some differences were apparent between the analyzed results from the three imaging systems. For example, aggregates from CGG were quantified as having a somewhat smooth surface texture by both AIMS II and FTI, but CGG was considered to have the roughest surface texture when UIAIA is used. Conversely, DLT aggregates were considered the least angular by FTI, while AIMS II and UIAIA rank them as the second-least angular. A possible reason for the diversities may lie in the different definitions of "angularity" and "surface texture." When angularity and texture are significantly different, these systems may be sufficiently sensitive to differentiate them; when angularity and texture are not significantly different, these systems may rank them differently. Rather than the black-and-white cameras and black background of the first-generation UIAIA, the second-generation, enhanced version of UIAIA is equipped with higher-resolution, progressive-scan color cameras and a blue background to capture high-resolution color images (0.056 mm/pixel) and to use an advanced color-thresholding scheme for improved texture quantification.

From the evaluation, which considered results from only the first-generation UIAIA system, the following analysis methods are recommended:

1. Both AIMS II and the FTI system are capable of reasonably quantifying shape properties of the seven types of ½-in. aggregates in relation to sphericity, flatness ratio, elongation ratio, and flatness-and-elongation ratio.

2. The authors recommend the use of either AIMS II or FTI to analyze aggregates for angularity, as both systems are capable of differentiating aggregates of all kinds of colors from various origins and providing results in wide numerical ranges for both angularity and texture. The authors recommend the adoption of AIMS II to quantify surface texture.

4.9 ACKNOWLEDGMENTS

This research was funded under NCHRP Project 4-34, Application of LADAR in the Analysis of Aggregate Characteristics. The authors extend their sincere gratitude to the project panel, including Ervin L. Dukatz, Jr., Edward T. Harrigan, William G. Eager, Julie E. Kliewer, Jorge A. Prozzi, Alan C. Robords, William H. Skerritt, G. P. Jayaprakash, and especially Richard C. Meininger, who coordinated the use of AIMS II at FHWA. Great appreciation is also extended to Anbo Wang, Evan M. Lally, Cris Harris, Yang Lu, Yu Zhou, Ashley Stanford, Yinning Zhang, and Yue Hou for their dedicated contributions to developing the FTI system, compiling the MATLAB program, and analyzing aggregates. The authors also acknowledge the generous help from Yuanjie Xiao and Maziar Moaveni for analyzing aggregates through use of the first-generation UIAIA system.

4.10 REFERENCES

1. Chowdhury, A., J. W. Button, V. Kohale, and D. W. Jahn. *Evaluation of Superpave Fine Aggregate Angularity Specification.* ICAP Report 201-1. International Center for Aggregate Research, Texas Transportation Institute, Texas A&M University System, College Station, 2001.

2. Masad, E. Review of Imaging Techniques for Characterizing the Shape of Aggregates Used in Asphalt Mixes. In *Proc., 9th Annual Symposium of the International Center for Aggregates Research,* Austin, Texas, 2001.

3. Al-Rousan, T., E. Masad, E. Tutumluer, and T. Pan. Evaluation of Image Analysis Techniques for Quantifying Aggregate Shape Characteristics. *Construction and Building Materials,* Vol. 21, No. 5, 2006, pp. 978–990.

4. Masad, E., D. Olcott, T. White, and L. Tashman. Correlation of Fine Aggregate Imaging Shape Indices with Asphalt Mixture Performance. In *Transportation Research Record: Journal of the Transportation Research Board, No. 1757,* TRB, National Research Council, Washington, D.C., 2001, pp. 148–156.

5. Prowell, B. D., J. Zhang, and E. R. Brown. *NCHRP 539: Aggregate Properties and the Performance of Superpave-Designed Hot-Mix Asphalt.* Transportation Research Board of the National Academies, Washington, D.C., 2005.

6. Wang, L., W. Sun, E. M. Lally, A. Wang, C. Druta, and E. Tutumluer. *NCHRP Report 724: Application of LADAR in the Analysis of Aggregate Characteristics.* Transportation Research Board of the National Academies, Washington, D.C., 2012.

7. Masad, E. A., T. Al-Rousan, J. W. Button, D. N. Little, and E. Tutumluer. *NCHRP Report 555: Test Methods for Characterizing Aggregate Shape, Texture, and Angularity.* Transportation Research Board of the National Academies, Washington, D.C., 2007.

8. Rao, C., E. Tutumluer, and I. T. Kim. Quantification of Coarse Aggregate Angularity Based on Image Analysis. In *Transportation Research Record: Journal of the Transportation Research Board, No. 1787,* Transportation Research Board of the National Academies, Washington, D.C., 2002, pp. 117–124.

9. Masad, E., and J. Button. Unified Imaging Approach for Measuring Aggregate Angularity and Texture. *Journal of Computer-Aided Civil and Infrastructure Engineering*, Vol. 15, No. 4, 2000, pp. 273–280.

10. Sun, W., L. Wang, and E. Tutumluer. Image Analysis Technique for Aggregate Morphology Analysis with Two-Dimensional Fourier Transform Method. In *Transportation Research Record: Journal of the Transportation Research Board, No. 2267,* Transportation Research Board of the National Academies, Washington, D.C., 2012, pp. 3–13.

The Geology and Properties of Earth Materials Section peer-reviewed this paper.

Evaluation of the Influence of Parent Rock, Crushing, and Abrasion on Aggregate Morphology Characteristics

5.1 ABSTRACT

The morphological characteristics and mineral compositions of aggregates have a significant influence on their mechanical performances. This paper investigates three influential factors on the morphological characteristics, including parent rock (i.e., mineral compositions and crystal structures), crushing, and abrasion/polishing. The following research is conducted: (*i*) establishing three-dimensional supercell crystal structures for five representative minerals (i.e., α-quartz, calcite, dolomite, hematite and magnetite) corresponding to four types of aggregates (i.e., quartzite/granite/aplite, limestone, dolomite, and iron ore), and calculating root-mean-square (RMS) roughness at the atomic-scale to evaluate the mineral effect on aggregate morphological characteristics; (*ii*) comparing morphological characteristics of crushed aggregates with those of natural aggregates to evaluate the influence of crushing on aggregate morphological characteristics; (*iii*) comparing changes of morphological characteristics for aggregates before and after the micro-deval abrasion/polishing test to evaluate the abrasion/polishing effect on aggregate morphological characteristics. It is found that the roughness ranking of four types of aggregates can be represented by the atomic-scale roughness ranking based on supercell crystal structures of five dominant minerals in those aggregates. However, there are some differences between the roughness ranking at the atomic-scale and the

roughness ranking at the macroscale. The crushing process will alter morphological characteristics of aggregates, resulting in more angular aggregates with rougher surface texture. The abrasion/polishing process will also alter morphological characteristics of aggregates, and the angularity and texture properties of aggregates may increase or decrease, depending on the mineral compositions and the duration of the abrasion/polishing process. These findings offer new insights into the surface roughness of aggregates.

5.2 INTRODUCTION

Research findings indicate that the mechanical performance of aggregates depend on their intrinsic properties, such as grading, morphological characteristics, mineral compositions, physical properties, and chemical properties (*1*). Tamrakar et al. (*2*) found that mechanical properties of sandstones depended on the types of rock and the content of calcium carbonate, and were independent of deposition age of rocks. Tamrakar et al. (*3*) also analyzed sandstones from the Siwalik group and concluded that the strength of sandstone mainly depends on its void content. The morphological characteristics, such as shape, angularity and surface texture, are related with the following aspects: geological factors of aggregates, composition materials (i.e., crystal structure and inherent defects), type of crushing equipment, crushing methods, abrasion/polishing, etc. Aggregate shape is related to durability, workability, shear strength, tensile strength, stiffness, and fatigue resistance of concrete. Flat and elongated aggregates are undesirable for asphalt concrete and hydrated cement concrete, and there are specifications limiting the usage of flat and elongated particles in mix design procedures. Angular aggregates with rough texture surfaces exhibit stronger interlocking and internal friction between aggregates than rounded aggregates with smooth surface textures, consequently creating better mechanical performance of asphalt concrete and cement concrete. That is because angular surface and rough

surface texture represent better interlocking effects between aggregates and the matrix with an increased surface area on the interface. Kaplan (*4-5*) found that surface texture has the greatest influence on compressive strength among all morphological characteristics (including shape factors, angularity and surface texture), without appreciable effect on workability of concrete to the degree that grading and particle shape factors do.

A shortage of natural aggregates at cost-effective transportation distances promotes the prosperity of the manufactured aggregate industry. According to the United States Geological Survey, there are crushed aggregates valued over $11 billion produced in 2013 in 50 States (*6*). Starting from blasting rocks, aggregate manufacture is followed by a series of crushing, in which crushing and abrasion during aggregate production processes can accommodate adjustment to match market demands for each aggregate gradation (*7*). Measurement results show that loading conditions in the crushing process have a great influence on shape characteristics of crushed aggregates. Generally, loading conditions that promote low coordination and Mode I fracture propagation produces flaky and rod-shape aggregates, and those that promote high coordination favor higher cubicity with increased fine generation through abrasion process and asperity breakage (*7*). On the other hand, crushing methods affect the morphological characteristics of the resulting aggregates and micro-fines, and crushing efficiency for a given petrography is crucial for producing more cubical and less elongated/flat particles, and abrasion/polishing also influence aggregate surface roughness (*7*).

Aggregates degrade under traffic loads in pavements and railway base courses that experience high stresses at the stone-on-stone contact points. During degradation, aggregates are most likely

to lose angularity and texture due to abrasion and polishing, weakening mechanical performances of pavements and railway base courses. Abrasion and polishing processes can alter angularity and texture of aggregates. Test results show that most aggregates after the micro-deval test tend to have a smoother texture. A few aggregates experience an increase in texture after the micro-deval test, attributing to asperity breakage of particles and/or removal of some surface deposits exposing on aggregate surfaces (*8*).

Previous research mainly focused on comparison of morphological characteristics of different types of aggregates using different quantification methods and on the influence of loading conditions in crushing and abrasion processes on mechanical properties of aggregates. However, in both natural and manufactured aggregates, aggregate inherent properties, such as mineral compositions and microstructures, fundamentally determine how cracks are propagated in the crushing and abrasion processes in rock weathering and aggregate crushing production, in turn impacting aggregate mechanical performances. To better predict mechanical properties of aggregates, more attention should be paid on the following three aspects: (*i*) quantification on the influence of crushing on aggregate morphological characteristics; (*ii*) quantification on the influence of abrasion/polishing on aggregate morphological characteristics; and (*iii*) investigation on the fundamental mechanism of why aggregates consisting of different minerals would turn out different morphological characteristics. This paper quantitatively evaluates the influence of parent rock, crushing, and abrasion on morphological characteristics of the most commonly used aggregates, including glacial/aplite/granite/quartzite, dolomite, limestone, and iron ore.

5.3 MATERIALS AND METHOD

Table 5-1 tabulates physical properties of four types of No. 57 aggregates (passing through the 1-in. sieve and retaining on the No. 4 sieve). The four types of aggregates are from Michigan State, including rounded glacial gravel, dolomite, limestone and iron ore. Each type of No. 57 aggregates are discretized into four categories according to the size range: ¾-in. (passing through 1-in. sieve and retaining on ¾-in. sieve), ½-in. (passing through ¾-in. sieve and retaining on 1/2-in.), 3/8-in. (passing through ½-in. sieve and retaining on 3/8-in. sieve) and No. 4 (passing through 3/8-in. sieve and retaining on No. 4 sieve). There are 30 particles in each size range for every type of aggregate, which is 480 particles in total. All these aggregates are measured by the two-dimensional Fourier transform (FFT2) method based on digital images of aggregates in the Fourier transform interferometry (FTI) system, with the image resolution of 35.4 μm/pixel in both *x* and *y* directions.

Table 5-2 tabulates aggregate information of Staunton aggregates used for the stone matrix asphalt (SMA)-9.5 mix in Virginia State. There are four types of Staunton aggregates, including No. 8 (2.38 mm) aplite from Piney River, No. 10 (No.4 to 0) limestone from Staunton, No. 68 (3/4-in. to No. 8) aplite from Piney River, and No. 78 (1/2-in. to No. 8) quartzite and arkose from Stuarts Draft. There are 120 particles in each type of aggregate, which is 480 particles in total. All these aggregates are measured by the FFT2 method in the improved FTI system with a replacement of a new charge-coupled device (CCD) camera that is capable to capture images at a higher speed with a better image resolution of 28.47 μm/pixel in both *x* and *y* directions.

Both granite and aplite are commonly used aggregates from intrusive igneous rock, with dominant minerals of feldspar and quartz. Quartz (SiO_2) is selected as a mineral representation of rounded glacial gravel and aplite for surface roughness analysis of crystal structure at the atomic scale. Limestone is a sedimentary rock composed largely of calcium carbonate ($CaCO_3$), with two different crystal forms, mineral calcite and aragonite. Calcite is selected as a mineral representation of limestone for its surface roughness of crystal structure at the atomic-scale. Dolomite is an anhydrous carbonate mineral composed of calcium magnesium carbonate ($CaMg(CO_3)_2$). The surface roughness of dolomite crystal structure is analyzed at the atomic-scale. The primary iron-bearing minerals in iron ore are usually in the form of magnetite ($Fe^{2+}Fe^{3+}{}_2O_4$) and hematite (α-Fe_2O_3). Consequently, the surface roughness characteristics of both magnetite and hematite are analyzed to represent the morphological characteristics of iron ore aggregates at the atomic-scale. In total, there are five crystal structures for four types of aggregates, including α-quartz for quartzite/granite, calcite for limestone, dolomite for dolomite, and hematite and magnetite for iron ore. Table 5-3 tabulates selected properties of the five minerals with lattice parameters of the five crystal structures. Figure 5-1 through Figure 5-5 plot the supercell structures and unit cells of α-quartz, calcite, dolomite, hematite and magnetite, respectively.

The root-mean-square (RMS) roughness is a representation of surface roughness of supercell crystal structure at the atomic-scale, and the RMS roughness can be calculated by Eq. (5-1).

$$\text{root-mean-square (RMS) roughness} = \sqrt{\frac{1}{MN}\sum_{i=1}^{M}\sum_{j=1}^{N}\left(z\left(x_i, y_j\right) - \mu_z\right)^2} \tag{5-1}$$

where RMS roughness is the root mean square average of profile height deviations from the mean surface μ_z, recorded within the evaluation length $z\left(x_i, y_j\right)$; *M* and *N* are the dimensions in *x* and *y* directions in the height matrix.

Table 5-1 Aggregate Types and Physical Properties of LADAR Aggregates

Aggregate type	Origin	Lithographic description	LAA loss (%)	Bulk dry SpGr (g/cm^3)	24 hr soak absorption (%)	Aggregate size	Total particle number
Dolomite	Mackinac, MI	Light tan to light gray, medium to coarse crystals	27	2.78	0.52	No. 57	120
	Monroe, MI	Tan, well defined small euhedral dolomite crystals	45	2.45	4.16		
Glacial Gravel Rounded	Kent, MI	Various colors, very smooth texture	19	2.68	1.10	No. 57	120
Iron Ore	Marquette, MI	Black with hints of brown, very fine grained and hard metamorphic rock	11	N/A	N/A	No. 57	120
Limestone	Schoolcraft, MI	Light tan with very fine subcrystalline texture	25	2.65	0.64	No. 57	120
	Arenac, MI	Light gray, very fine crystalline with abundant frosted quartz sand grains	42	2.56	2.13		

Note: LAA=Los Angeles Abrasion; Bulk dry SpGr=Bulk dry specific gravity; N/A=not available.

Table 5-2 Aggregate Information for SMA-9.5 Mix

Aggregate fraction	Aggregate size	Aggregate type	Plant	Particle number
Staunton	No. 8	Aplite	Piney River	120
	No. 10	Limestone	Staunton	120
	No. 68	Aplite	Piney River	120
	No. 78	Quartzite and Arkose	Stuarts Draft	120

Table 5-3 Selected Properties and Lattice Parameters of Major Minerals in Typical Aggregates

Mineral	Quartz	Calcite	Dolomite	Hematite	Magnetite
Category	Silicate mineral	Carbonate mineral	Carbonate mineral	Oxide mineral	Oxide mineral Spinel group
Hardness	7	3	3½~4	5~6	6
Cleavage	None	3 planes at 75 º	3 planes at 74 º	None	None (in granular form)
Note	Very common; may occur in many rock types; glassy; translucent to transparent; may be colored; very resistant to weathering; chief mineral in sandstone.	Very common; occurs in many rock type; chief mineral in limestone; vigorous reaction with dilute HCl.	Common; with calcite in dolomitic limestone or dolostone (>50% dolomite); vigorous reaction with dilute HCl only when powdered.	Reddish gray, black, blackish red; magnetic after heating; common accessory mineral in many rock types.	Black; magnetic; common accessory mineral in many rock types.
Chemical formula	SiO_2	$CaCO_3$	$(CaMg)CO_3$	α-Fe_2O_3	$Fe^{2+}Fe^{3+}{}_2O_4$
Crystal symmetry	Trigonal rhomboheidral $\bar{3}$	05.AB.05	04.DA.05	04.CB.05	Isometric 4/m $\bar{3}$/2m
Unit cell	$a = b = 4.8012(1)$ Å $c = 16.002$ Å $\alpha = 90^\circ$ $\beta = 90^\circ$ $\gamma = 120^\circ$ Z = 3	$a = b = 4.9896(2)$ Å $c = 17.0610(11)$ Å $\alpha = 90^\circ$ $\beta = 90^\circ$ $\gamma = 120^\circ$ Z = 6	$a = b = 4.9133$ Å $c = 5.4052$ Å $\alpha = 90^\circ$ $\beta = 90^\circ$ $\gamma = 120^\circ$ Z = 3	$a = b = 5.038(2)$ Å $c = 13.7712(12)$ Å $\alpha = 90^\circ$ $\beta = 90^\circ$ $\gamma = 120^\circ$ Z = 6	$a = b = c = 8.397$ Å $\alpha = 90^\circ$ $\beta = 90^\circ$ $\gamma = 90^\circ$ Z = 8
Crystal system	Trigonal	Trigonal hexagonal	α-quartz: Trigonal β-quartz: Hexagonal	Trigonal	Isometric hexoctahedral
Primary aggregate	Quartzite / Granite / Aplite/Glacial	Limestone	Dolomite	Iron Ore	

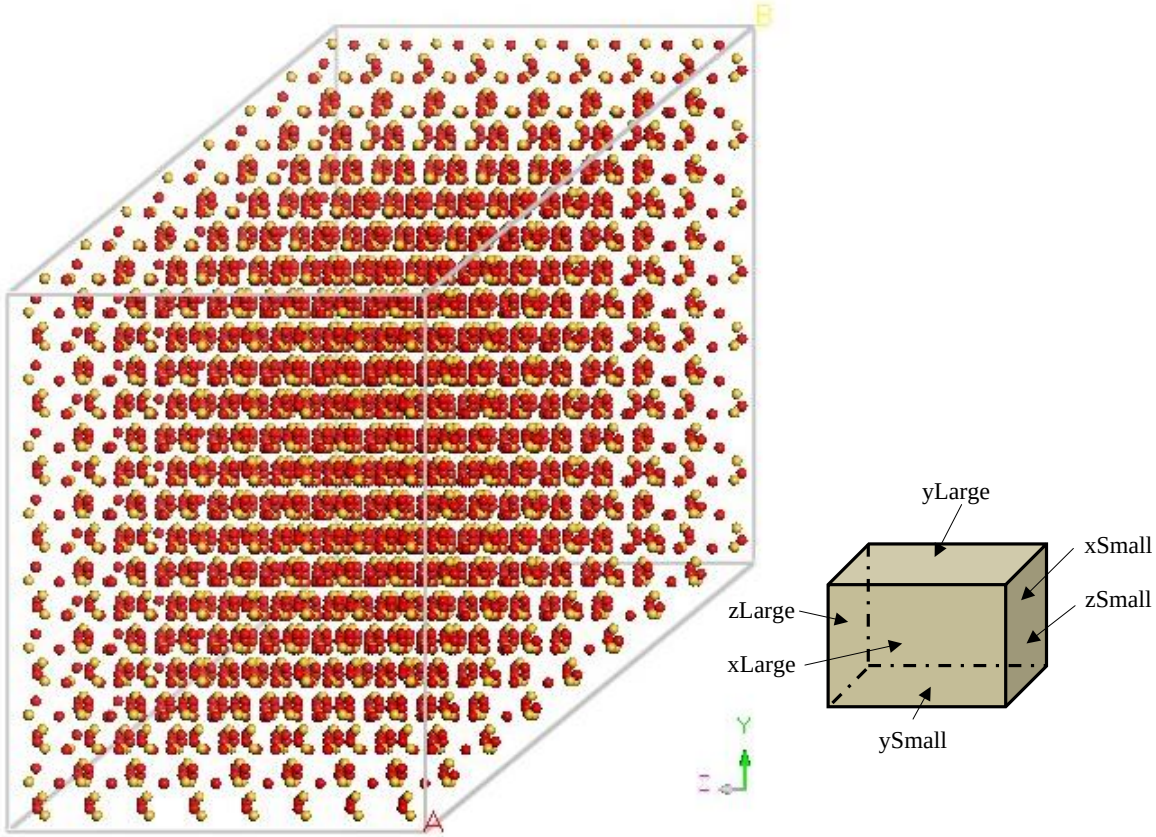

(*a*)

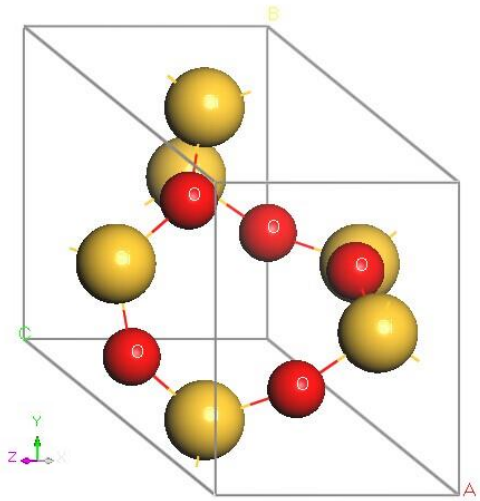

(*b*)

Figure 5-1 (*a*) 8×8×8 α-quartz supercell structure, (*b*) unit cell of α-quartz

Note: yellow balls represent silicate atoms (Si), and red balls represent oxygen atoms (O).

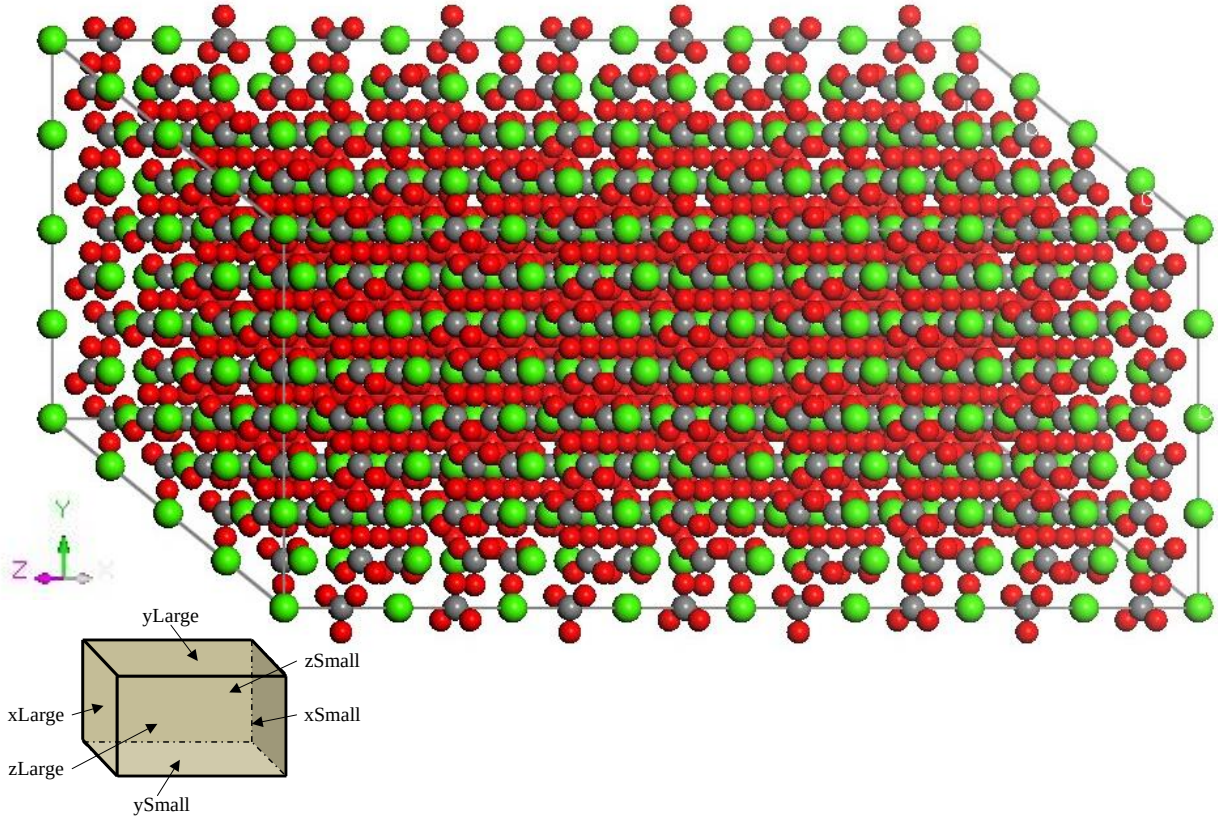

(*a*)

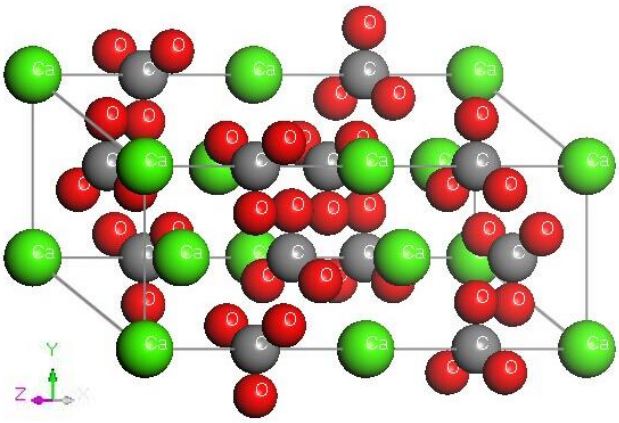

(*b*)

Figure 5-2 (*a*) 4×4×4 calcite supercell structure, (*b*) unit cell of calcite

Note: Green balls represent Calcium atoms (Ca), red balls represent oxygen atoms (O), and grey balls represent carbon atoms (C).

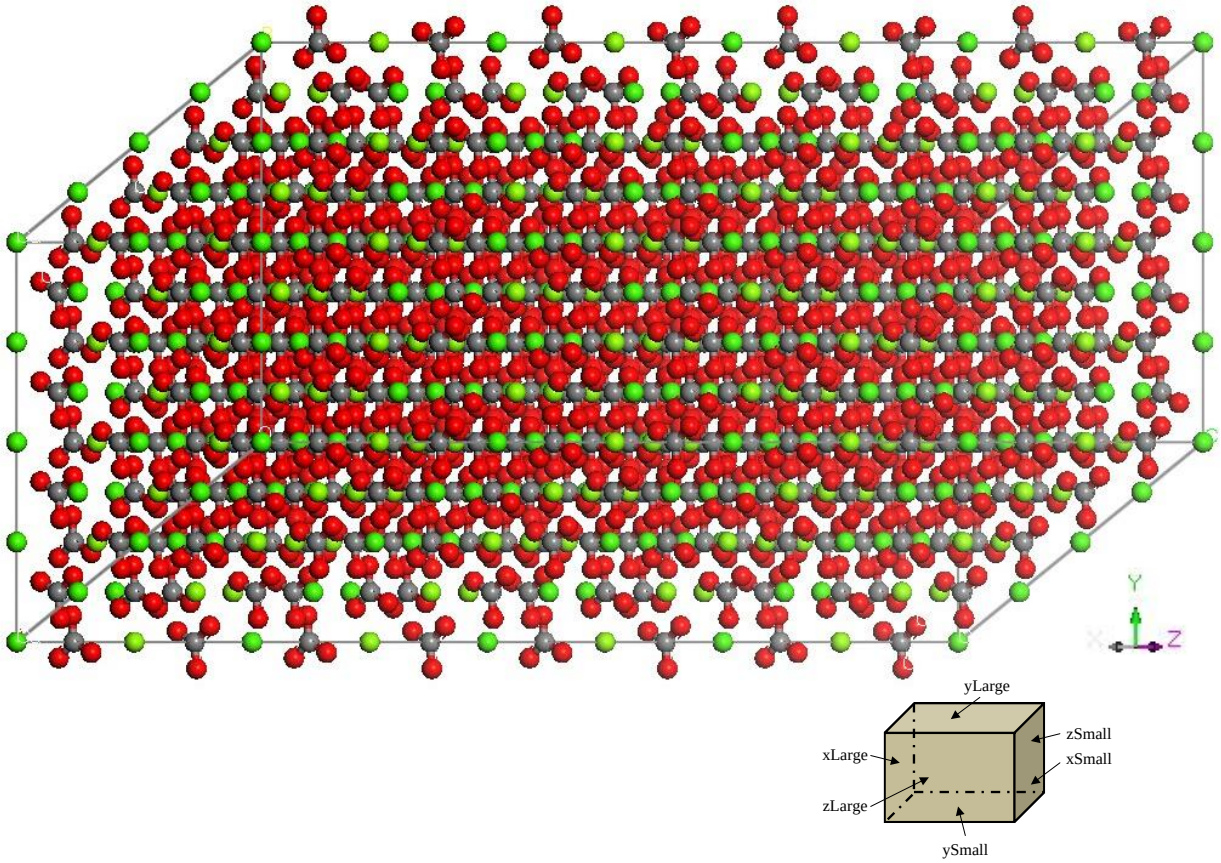

(*a*)

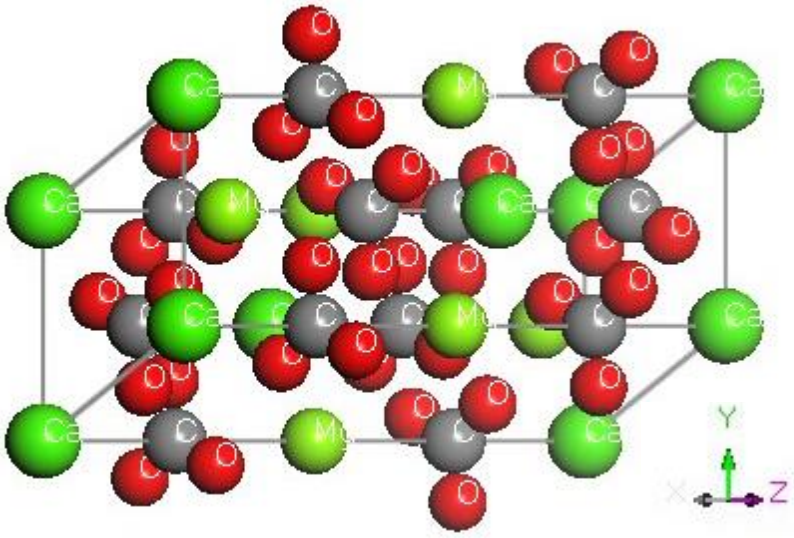

(*b*)

Figure 5-3 (*a*) 4×4×4 dolomite supercell structure, (*b*) unit cell of dolomite

Note: Green balls represent calcium (Ca) and magnesium (Mg) atoms, red balls represent oxygen atoms (O), and grey balls represent carbon atoms (C).

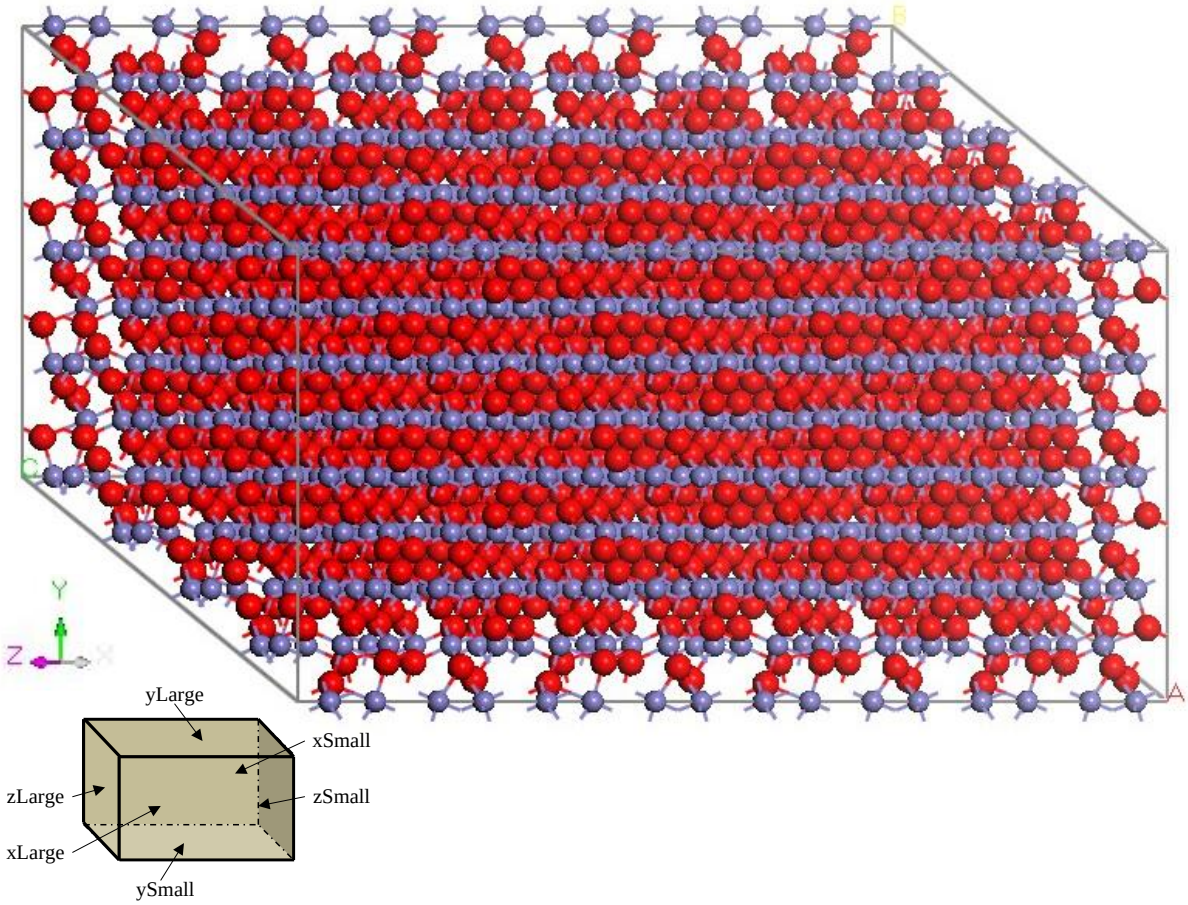

(*a*)

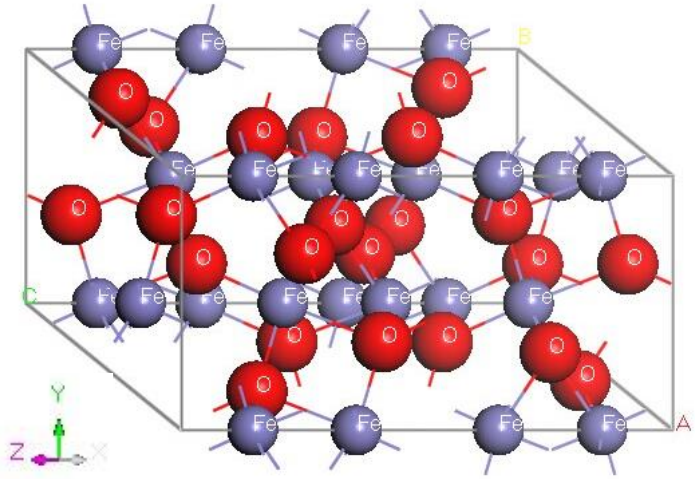

(*b*)

Figure 5-4 (*a*) 4×4×4 hematite supercell structure, (*b*) unit cell of hematite

Note: purple balls represent iron atoms (Fe), and red balls represent oxygen atoms (O).

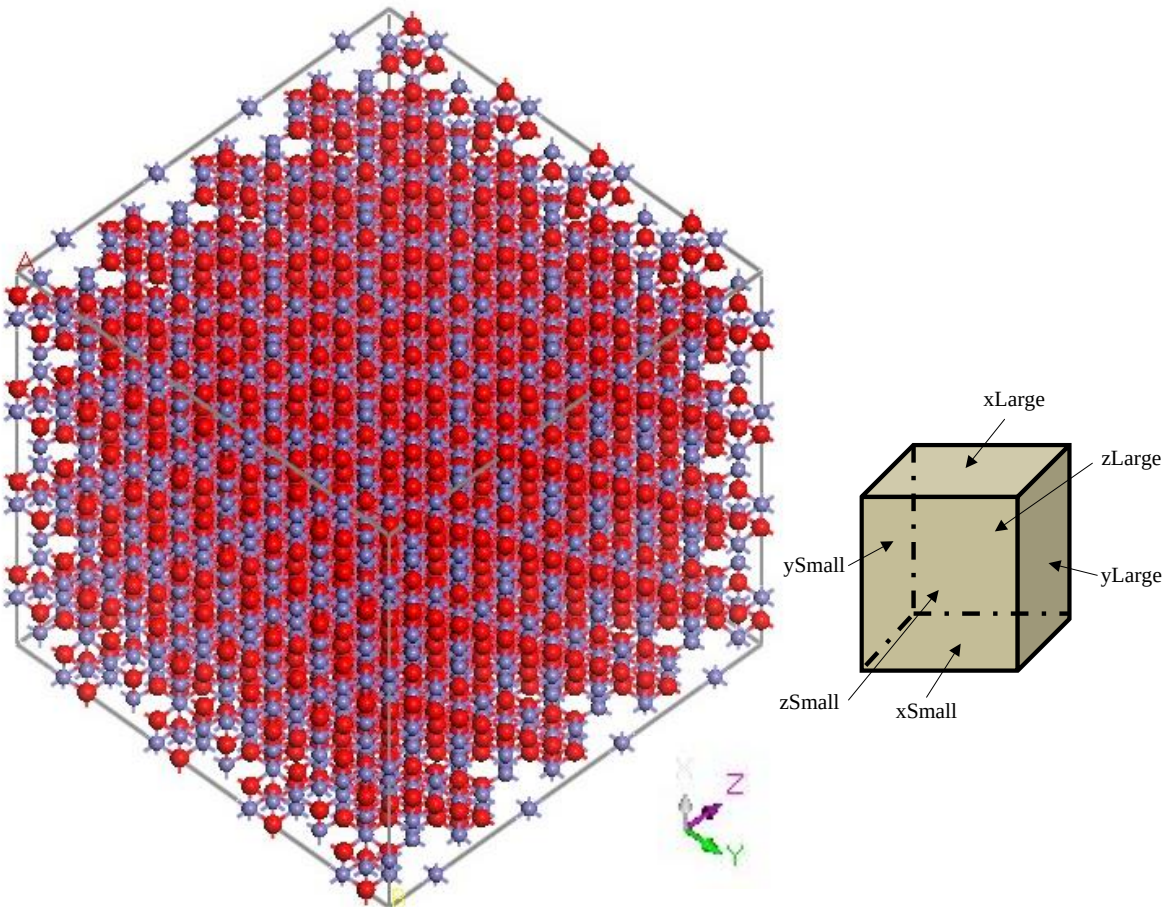

(*a*)

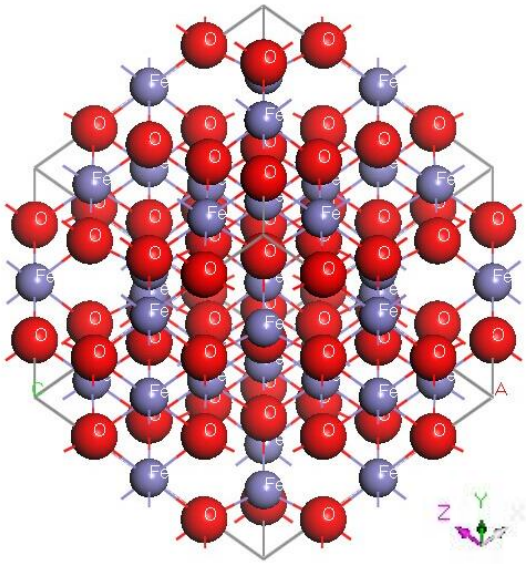

(*b*)

Figure 5-5 (*a*) 4×4×4 magnetite supercell structure, (*b*) unit cell of magnetite

Note: purple balls represent iron atoms (Fe), and red balls represent oxygen atoms (O).

To evaluate how the crushing process alters aggregate morphological characteristics, both natural and crushed aggregates consisting of the same type of material are measured using the FTI system, including sphericity, flatness ratio, elongation ratio, angularity, and texture. Rounded glacial gravel (GGR) is selected as natural aggregates, and crushed glacial gravel (GGC) is selected as crushed aggregates. Table 5-4 tabulates physical properties and origins of GGC and GGR. Both types of aggregates are from Kent, MI, with the size varying from 3/4-in. (19.05 mm) to No.4 (4.75 mm), and a total number of 120 particles in each type. The FTI results of natural aggregates at the same size range are compared to those of crushed aggregates to quantify the influence of the crushing process on morphological characteristics.

Table 5-4 Physical Properties and Origins of Nature and Crushed Glacial Gravels

Aggregate type	Origin	Lithographic description	LAA loss (%)	Bulk dry SpGr (g/cm^3)	24 hr soak absorption (%)	Aggregate size
Rounded Glacial Gravel	Kent, MI	Various colors, very smooth texture	19	2.68	1.10	¾-in., ½-in., 3/8-in., No.4
Crushed Glacial Gravel	Kent, MI	Various colors, with crushed surfaces	17	2.73	0.71	¾-in., ½-in., 3/8-in., No.4

Note: LAA loss=Los Angeles Abrasion loss; Bulk dry SpGr=Bulk dry specific gravity; ¾-in. aggregates = aggregates passing through 1-in. sieve and retaining on ¾-in. sieve, ½-in. aggregates = aggregates passing through ¾-in. sieve and retaining on ½-in. sieve, 3/8-in. aggregates = aggregates passing through ½-in. sieve and retaining on 3/8-in. sieve, No.4 aggregates = aggregates passing through 3/8-in. sieve and retaining on No.4 sieve.

The micro-deval test is widely used to study the abrasion and polishing effects of aggregates in pavement surfaces, as it provides a good indicator of coarse aggregate quality, such as abrasion resistance and durability of aggregates. In micro-deval tests, aggregates mixed with steel balls, which are 9.5 mm in diameter and emerged in water, are rotated at a rotation speed of 100 ± 5 rpm

for two hours. To investigate the abrasion/polishing effect, morphological characteristics of aggregates are measured before and after the micro-deval test. All the aggregates are photographed using a digital camera, and these aggregate images are transformed to grey-scale images to identify aggregate boundaries and further quantify morphological characteristics. The Fourier transform method are used to analyze on coordinates of aggregate boundaries before and after the micro-deval test. The variations of morphological characteristics throughout the micro-deval test are analyzed to evaluate the abrasion effect on aggregate morphological characteristics (*9*). Table 5-5 tabulates the lithologic description and aggregate size ranges of four types of coarse aggregates, including Maymead granite, Salem quartzite, Broadway dolomite and Strasburg limestone. Both standard micro-deval test according to AASHTO T327-00 and micro-deval abrasion/polishing test are conducted on the four types of aggregates. Micro-deval abrasion / polishing test is designed to be performed at a time interval of 15 minutes, 30 minutes and 45 minutes, respectively; that is 15 minutes, 45 minutes and 90 minutes of abrasion / polishing on aggregates in the micro-deval abrasion / polishing test (*9*).

Table 5-5 Lithological Description of Four Types of Aggregates (*9*)

Aggregate origin	Lithologic description	Insoluble residue (%)	Aggregate size range				
			1.5-in. - 1-in.	1-in. - 3/4-in.	3/4-in. - 1/2-in.	1/2-in. - 3/8-in.	3/8-in. - No.4
Maymead	Granite	NA	x	x	x	x	x
Salem	Quartzite	NA		x	x	x	
Broadway	Dolomite	18		x	x	x	x
Strasburg	Limestone	1.9		x	x	x	

Note: NA = not available

5.4 MINERAL EFFECT

To investigate the effect of break surface angle on the surface roughness of five supercell structures, a set of slice planes with different angles are used to cut the supercell structures, and

two cutoff planes are formed. The atomic-scale RMS roughness of both cutoff planes are analyzed according to Eq. (5-1) with more than 80 slice planes selected for each supercell structure. Figure 5-6 plots the relationship between the RMS roughness and the angle α of the slice plane from the ySmall plane for five supercell structures. It is found there is no evident correlation between the atomic-scale RMS roughness and the angle α of the slice plane for any supercell structure.

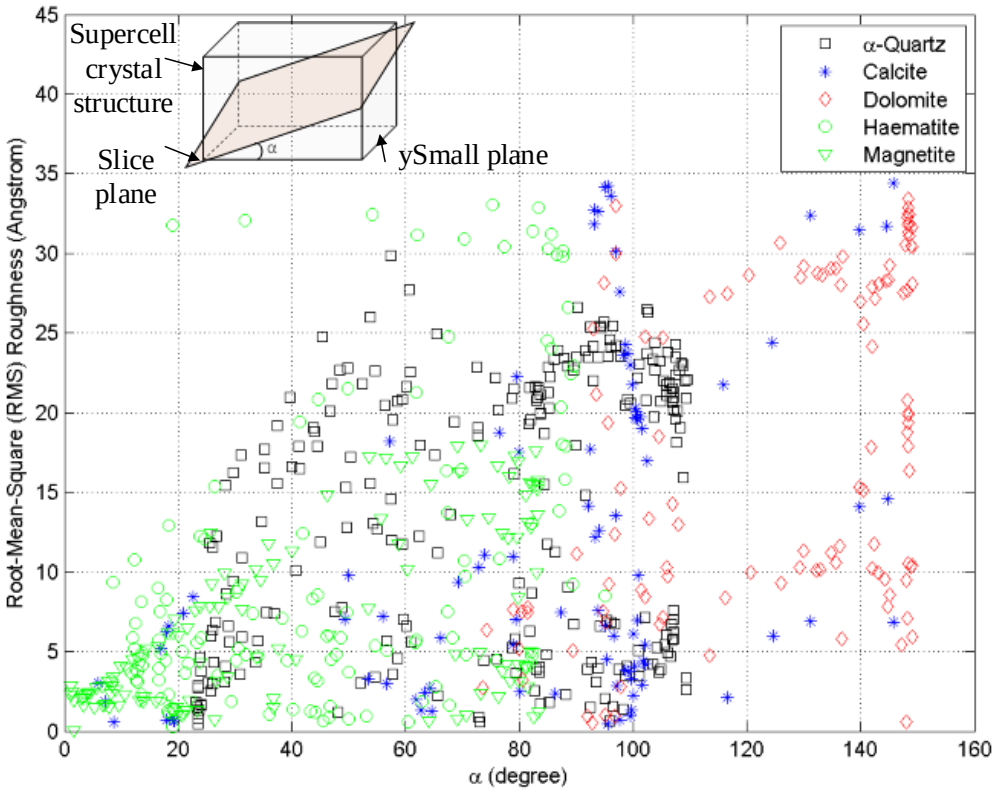

Figure 5-6 Relationship between root-mean-square (RMS) roughness and angle of the slice plane (α) from ySmall plane for α-quartz 8×8×8 supercell structure (black square), calcite 4×4×4 supercell structure (blue star), dolomite 4×4×4 supercell structure (red square), haematite 4×4×4 supercell structure (green circle), and magnetite 4×4×4 supercell structure (green triangle).

Table 5-6 tabulates the calculated results for the RMS roughness for the five supercell crystal structures: α-quartz, calcite, dolomite, haematite and magnetite. Figure 5-7 plots the mean, maximum, and minimum for five supercell structures. As we can see from this figure, the mean values of RMS roughness from maximum to minimum is as follows: magnetite, haematite, calcite, α-quartz and dolomite, representing the surface roughness from smooth to rough at the atomic-scale.

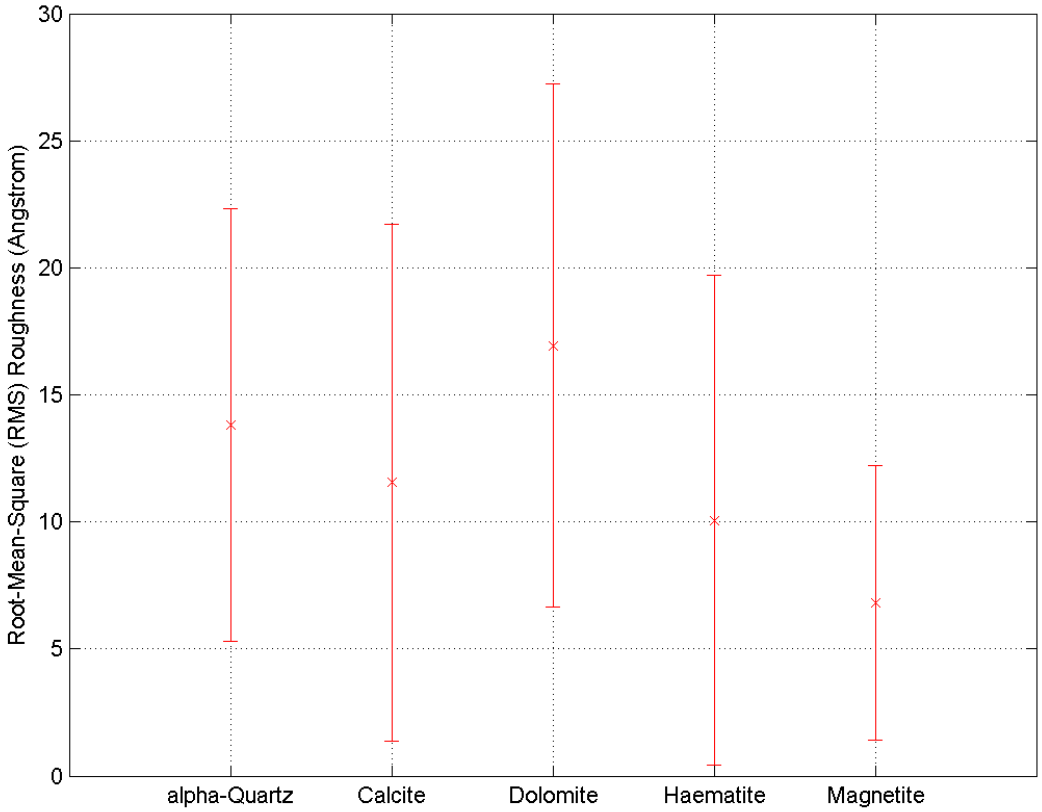

Figure 5-7 Root-mean-square (RMS) roughness of α-quartz 8×8×8 supercell structure, calcite 4×4×4 supercell structure, dolomite 4×4×4 supercell structure, haematite 4×4×4 supercell structure, and magnetite 4×4×4 supercell structure.

Table 5-7 tabulates the roughness ranking according to mean values of FTI texture of four types of coarse aggregates. Figure 5-8 plots the surface texture distributions for four types of coarse aggregates measured by the FTI system. It is found that iron ore has the roughest surface texture, followed by limestone, dolomite, and rounded glacial gravel, according to the FTI texture results. Conversely, the roughness ranking from rough to smooth is limestone, dolomite, iron ore, and rounded glacial gravel, according to AIMS II texture results.

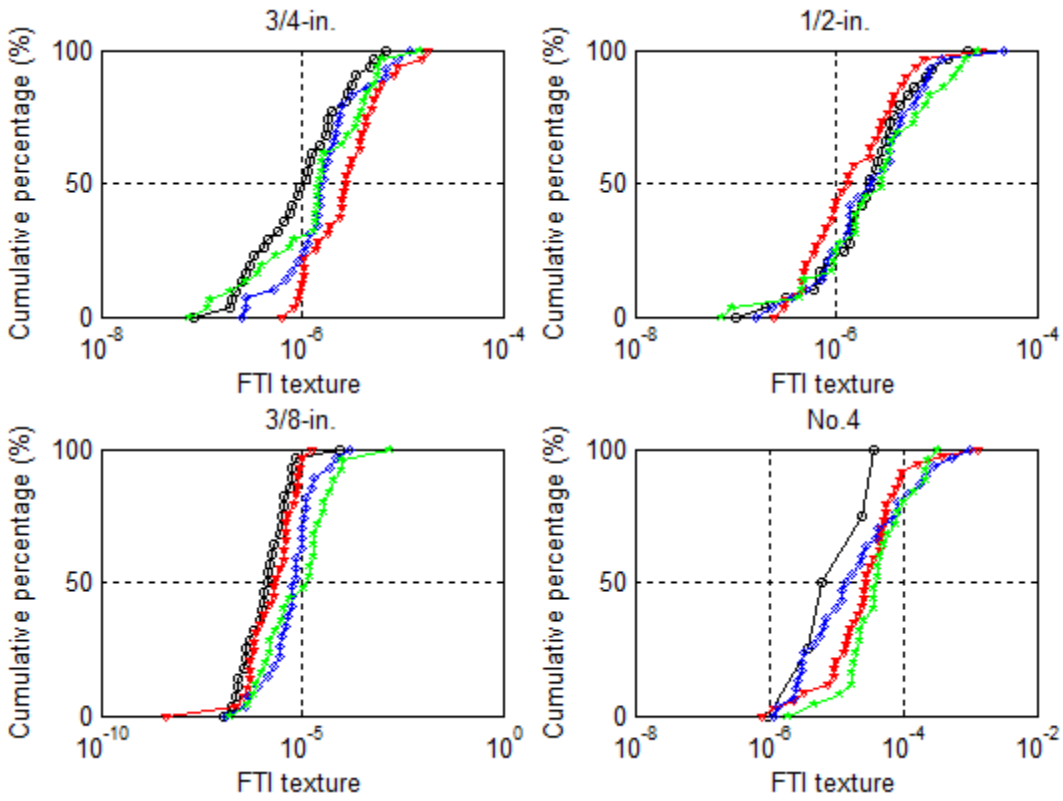

Figure 5-8 FTI texture distribution of LADAR aggregates, using the FTI system with image resolution of 35.4 μm/pixel in *x* and *y* directions and 22 μm in *z* direction, black dot, red triangle, blue diamond, and green pentagram represent rounded glacial gravel, dolomite, limestone and iron ore, respectively.

Table 5-6 Root-mean-square (RMS) Roughness on Six Surfaces of Five Crystal Structures

Aggregate Material	Mineral	Supercell size	Root-mean-square (RMS) Roughness (Angstrom)	
			Mean value	Standard deviation
Granite	α-Quartz	8×8×8	13.8114	8.5016
Limestone	Calcite	4×4×4	11.5422	10.1627
Dolomite	Dolomite	4×4×4	16.9374	10.3028
Iron Ore	Hematite	4×4×4	10.0584	9.6304
	Magnetite	4×4×4	6.8244	5.4067

Table 5-7 Roughness Ranking Results for Four Types of Aggregates using the FTI and AIMS II Systems

Aggregate size	¾-in.	½-in.	3/8-in.	No. 4	No. 57	Roughness ranking
Fourier Transform interferometry (FTI)	Dolomite	Dolomite	Iron Ore	Limestone	Iron Ore	Rough
	Limestone	Iron Ore	Limestone	Dolomite	Limestone	
	Iron Ore	Limestone	Glacial Gravel Round	Iron Ore	Dolomite	↓
	Glacial Gravel Round	Glacial Gravel Round	Dolomite	Glacial Gravel Round	Glacial Gravel Rounded	Smooth
The second generation of Aggregate Image Measurement System (AIMS II)	Iron Ore	Limestone	Dolomite	Limestone	Limestone	Rough
	Dolomite	Dolomite	Limestone	Iron Ore	Dolomite	
	Limestone	Iron Ore	Iron Ore	Dolomite	Iron Ore	↓
	Glacial Gravel Round	Glacial Gravel Round	Glacial Gravel Round	Glacial Gravel Round	Glacial Gravel Rounded	Smooth

Table 5-8 Roughness Ranking for Four Types of Aggregates using Different Methods

Aggregate size			¾-in.		½-in.		3/8-in.		No. 4	
Aggregate type	Mineral	Atomic-scale	FTI	AIMS II	FTI	AIMS II	FTI	AIMS II	FTI	AIMS II
Glacial Gravel Round	α-Quartz	3	1	1	1	1	2	1	1	1
Limestone	Calcite	2	3	2	2	4	3	3	4	4
Dolomite	Dolomite	4	4	3	4	3	1	4	3	2
Iron Ore	Hematite	1	2	4	3	2	4	2	2	3
	Magnetite									

Note: Numbers of 1 to 4 represent roughness ranking order, representing roughness from smooth to rough.

Figure 5-9 plots the histograms of FTI texture and the distributions of FTI texture for four aggregate fractions from Staunton, Virginia. The four aggregate fractions are 13-1078 Staunton No. 10 limestone, 13-1078 Staunton No. 8 aplite, 13-1078 Staunton No. 68 aplite, and 13-1078 Staunton No. 78 aplite. The dominant minerals for limestone and aplite are calcite and quartz, respectively. As we can see from this figure, both 13-1078 Staunton No. 68 aplite and 13-1078 Staunton No. 78 aplite have much greater surface texture values than 13-1078 Staunton No. 10 limestone. Conversely, 13-1078 Staunton No. 8 aplite has smaller texture values than 13-1078 Staunton No. 10 limestone. This is validated by surface roughness ranking at the atomic-scale. As Figure 5-7 shown, the mean RMS roughness of calcite is smaller than that of α-quartz, indicating the limestone tends to have a smoother aggregate surface than aplite; however, there is a wide overlapping range of the RMS roughness between α-quartz and calcite, representing that limestone and aplite aggregates have similar roughness characteristics.

Table 5-8 tabulates the roughness rankings for rounded glacial gravel, limestone, dolomite, and iron ore, according to the mean RMS roughness of more than 160 cutoff surfaces acquired from over 80 slice planes at the atomic-scale. This uses the mean value of surface texture analyzed through the FFT2 method with the FTI system and the wavelet method with the second generation of aggregate image analysis system (AIMS II) at macroscale. The roughness ranking at the atomic-scale is capable to represent the roughness ranking at the macroscale to some extent; however, the roughness rankings at different scales cannot correlate with each other very well. Possible reasons are as follows: (*i*) actual aggregates consist of complicated microstructures, with a great variety of minerals, micro voids and defects; these complicated microstructures and mineral compositions are not considered in the roughness analysis of

supercell crystal structures at the atomic-scale, which may have influences on roughness features of aggregates at the macroscale. (*ii*) In natural environment, the transportation process will alter aggregate morphological characteristics in the degradation from rock to aggregates and soils. (*iii*) In aggregate plants, aggregate morphological characteristics may be altered in both the crushing and abrasion/polishing processes. Consequently, surface texture at the macroscale may be different from that at the atomic-scale, since the following influential factors cannot be considered in roughness analysis at the atomic-scale, including complicated microstructures and mineral compositions, transportation process in aggregate degradation, crushing, and abrasion/polishing in aggregate production.

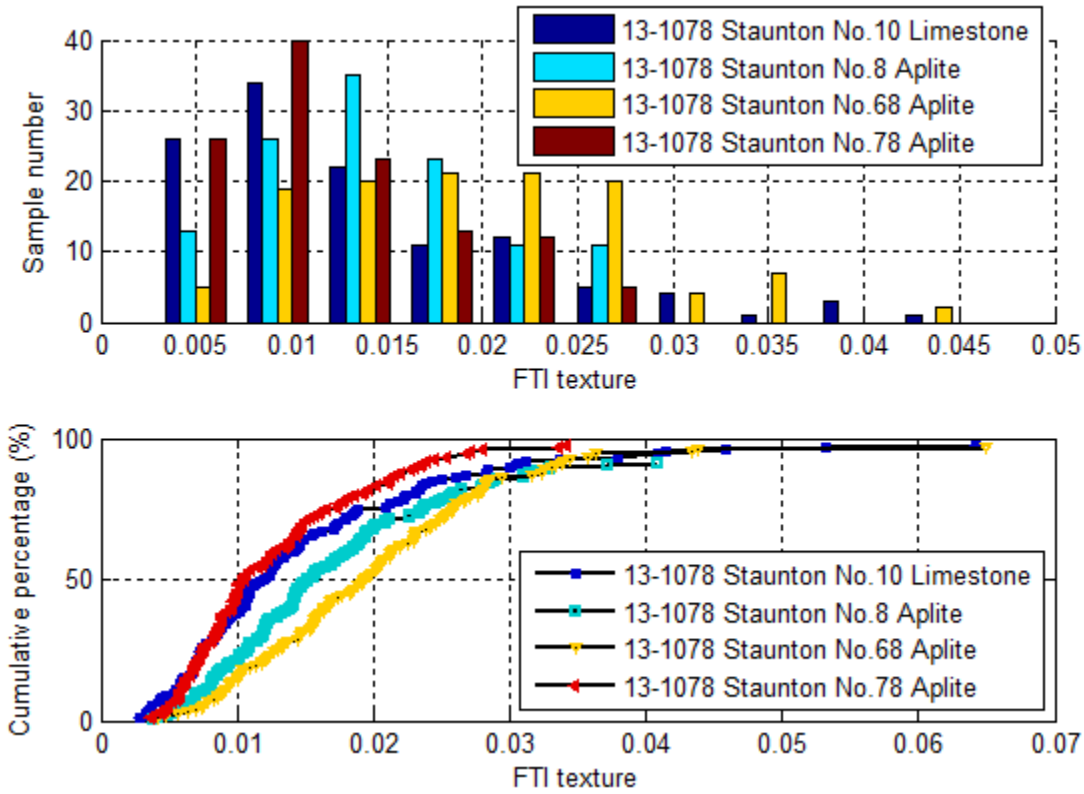

Figure 5-9 (*a*) histogram bar plot of FTI texture, and (*b*) FTI texture distributions for 13-1078 Staunton No. 10, No. 8, No. 68 and No. 78 aggregates, using the improved FTI system.

Table 5-9 Mean Values and Standard Deviations of Morphological Characteristics of Natural and Crushed Glacial Aggregates

Aggregate size			3/4-in.	1/2-in.	3/8-in.	No. 4	No.8	No.16
Sphericity	GGR	Average	0.68	0.70	0.79	0.73	0.53	0.39
		STD	0.09	0.06	0.12	0.11	0.12	0.14
	GGC	Average	0.74	0.74	0.79	0.69	0.58	0.30
		STD	0.10	0.09	0.06	0.13	0.16	0.10
Flatness ratio	GGR	Average	0.59	0.71	0.78	0.77	0.58	0.63
		STD	0.17	0.16	0.17	0.25	0.21	0.22
	GGC	Average	0.71	0.77	0.80	0.71	0.70	0.60
		STD	0.17	0.15	0.13	0.16	0.21	0.16
Elongation ratio	GGR	Average	0.75	0.71	0.80	0.73	0.54	0.32
		STD	0.11	0.11	0.14	0.18	0.21	0.14
	GGC	Average	0.77	0.74	0.80	0.69	0.55	0.22
		STD	0.12	0.12	0.11	0.16	0.22	0.11
Angularity	GGR	Average	8.44×10^{-5}	9.71×10^{-5}	1.09×10^{-5}	2.48×10^{-5}	2.22×10^{-2}	4.21×10^{-2}
		STD	1.13×10^{-4}	1.11×10^{-4}	1.94×10^{-4}	2.04×10^{-4}	1.48×10^{-2}	2.49×10^{-2}
	GGC	Average	2.31×10^{-4}	1.46×10^{-4}	1.47×10^{-4}	2.48×10^{-4}	2.41×10^{-2}	5.54×10^{-2}
		STD	4.25×10^{-4}	2.51×10^{-4}	1.98×10^{-4}	2.66×10^{-4}	1.49×10^{-2}	1.87×10^{-2}
Texture	GGR	Average	1.60×10^{-6}	3.54×10^{-6}	4.81×10^{-6}	1.44×10^{-5}	N/A	N/A
		STD	1.66×10^{-6}	4.32×10^{-6}	1.54×10^{-5}	1.54×10^{-5}	N/A	N/A
	GGC	Average	3.86×10^{-6}	2.69×10^{-6}	6.94×10^{-6}	9.33×10^{-6}	N/A	N/A
		STD	5.54×10^{-6}	3.37×10^{-6}	1.00×10^{-5}	1.64×10^{-5}	N/A	N/A

Note: GGC = crushed glacial gravel, GGR = rounded glacial gravel, STD = standard deviation, N/A = not available.

5.5 CRUSHING EFFECT

Figure 5-10 plots the distributions of morphological properties of both GGR and GGC coarse aggregates. Table 5-9 tabulates the mean values and standard deviations of morphological characteristics of the GGR and GGC aggregates. The comparison between GGR and GGC fine aggregates indicates that no significant difference is observed on the sphericity values between GGC and GGR aggregates. The average values of the flatness ratio and elongation ratio of all the

GGC fine aggregates are generally smaller than those of the GGR fine aggregates, except for the No.16 aggregates. The values of flatness ratio and elongation ratio of GGC aggregates are greater than those of GGR aggregates, indicating that crushed aggregates (i.e., GGC) generally tend to be less flat and less elongated than natural aggregates (i.e., GGR). In the meantime, an increase in the angularity and texture values from GGR to GGC aggregates is observed in all the aggregates of all sizes. The increase of angularity and texture values from GGR to GGC suggests that both coarse and fine GGC aggregates are more angular with rougher surface textures than GGR aggregates. A possible reason that crushed aggregates have greater values of angularity and texture for fine aggregates is that fine aggregates are easier to be crushed.

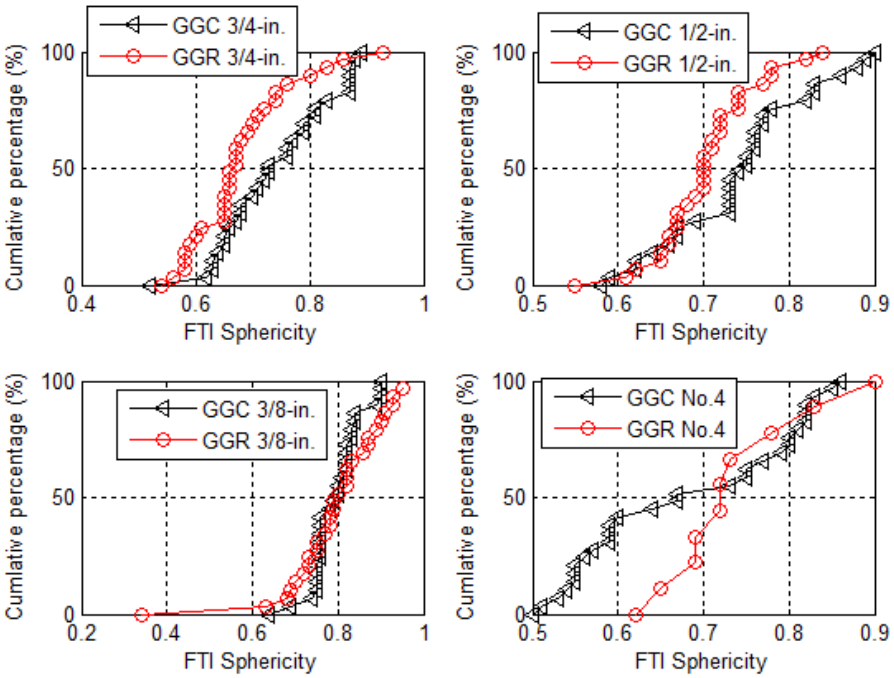

(*a*) Sphericity

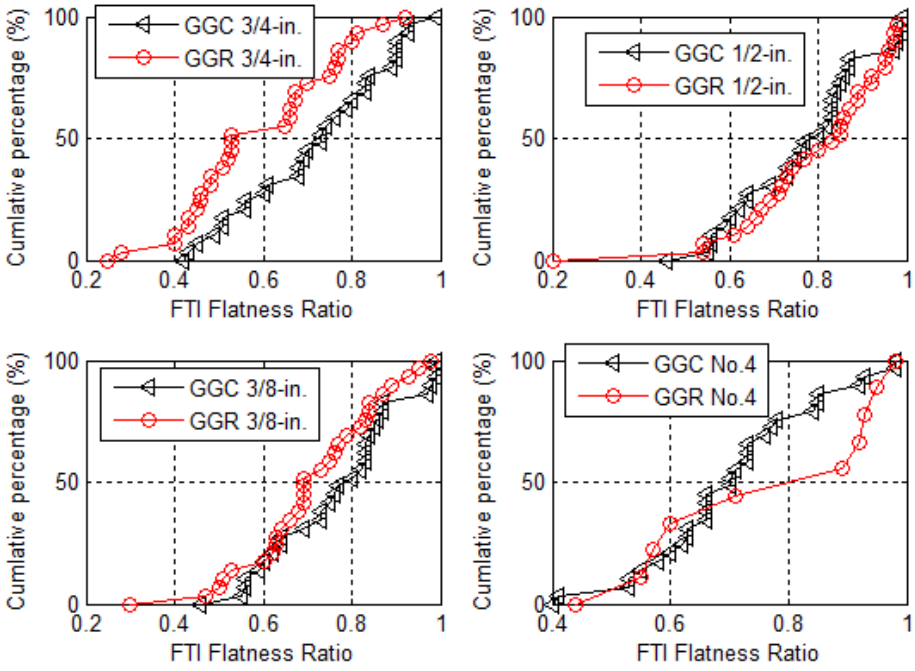

(*b*) Flatness ratio

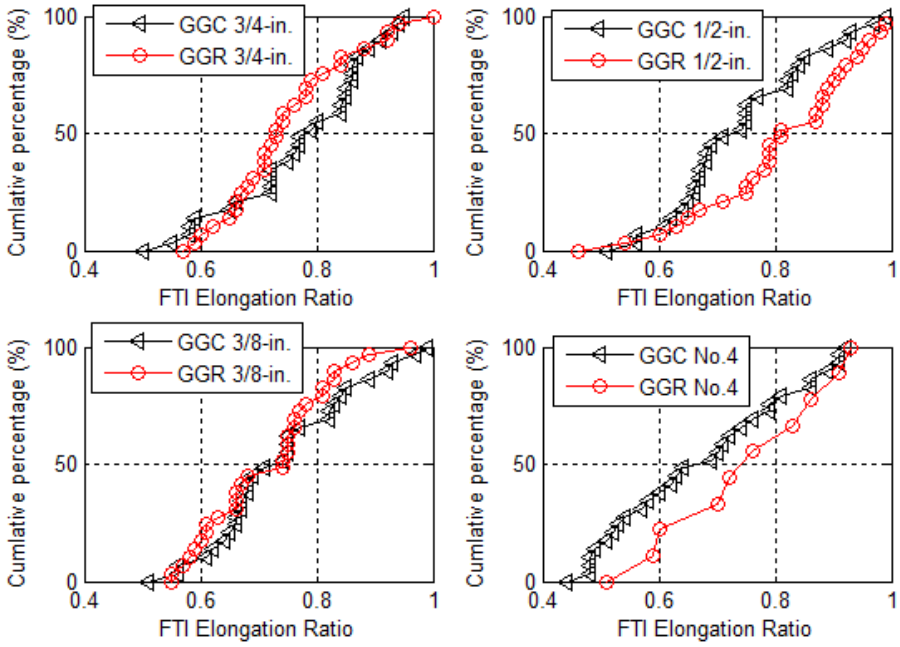

(*c*) Elongation ratio

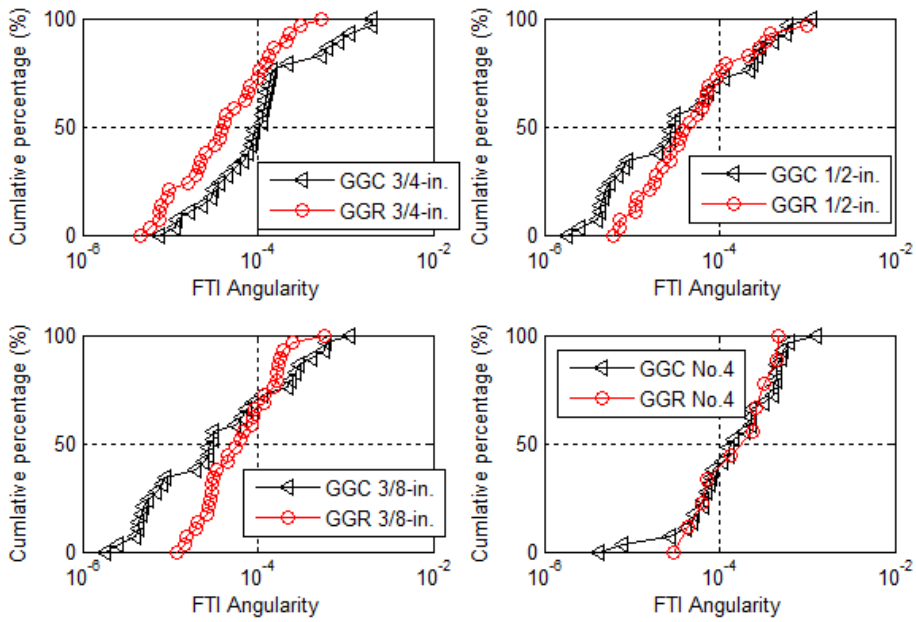

(*d*) FTI Angularity

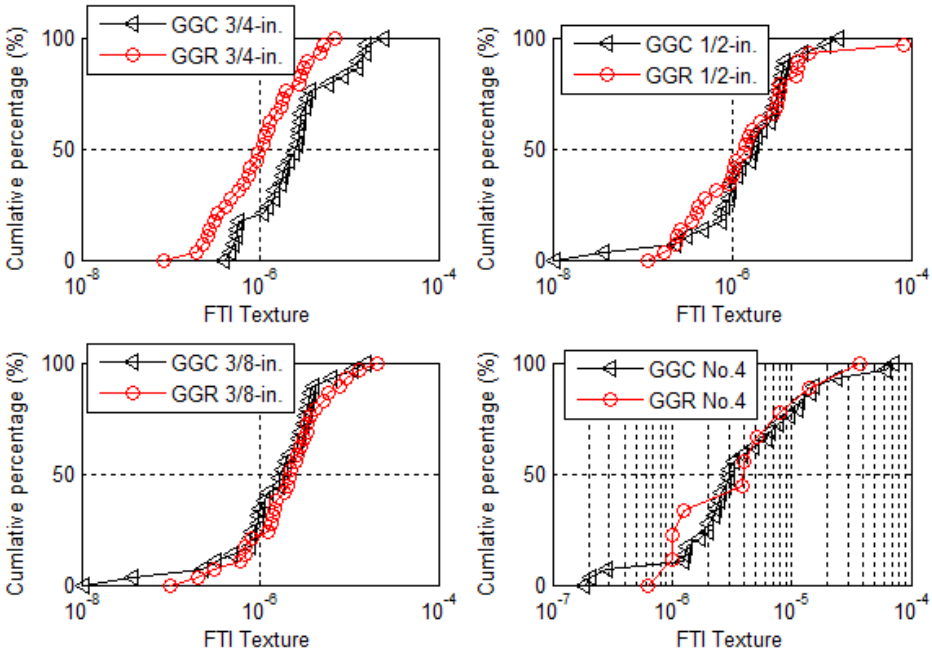

(*e*) FTI Texture

Figure 5-10 Distributions of morphological characteristics for glacial gravel rounded and glacial gravel crushed aggregates

5.6 ABRASION/POLISHING EFFECT

Figure 5-11 plots the abrasion losses in both AASHTO T 327 micro-deval test and micro-deval abrasion/polishing test at 15 minutes, 45 minutes, and 90 minutes, respectively. As shown in Figure 5-11(a), aggregates of abrasion loss from the greatest to the least are as follows: Strasburg limestone, Salem quartzite, Maymead granite, and Broadway dolomite. As shown in Figure 5-11(b), the abrasion loss increases with the increase of abrasion duration; Strasburg limestone shows the greatest abrasion loss in the last 45 minutes of abrasion.

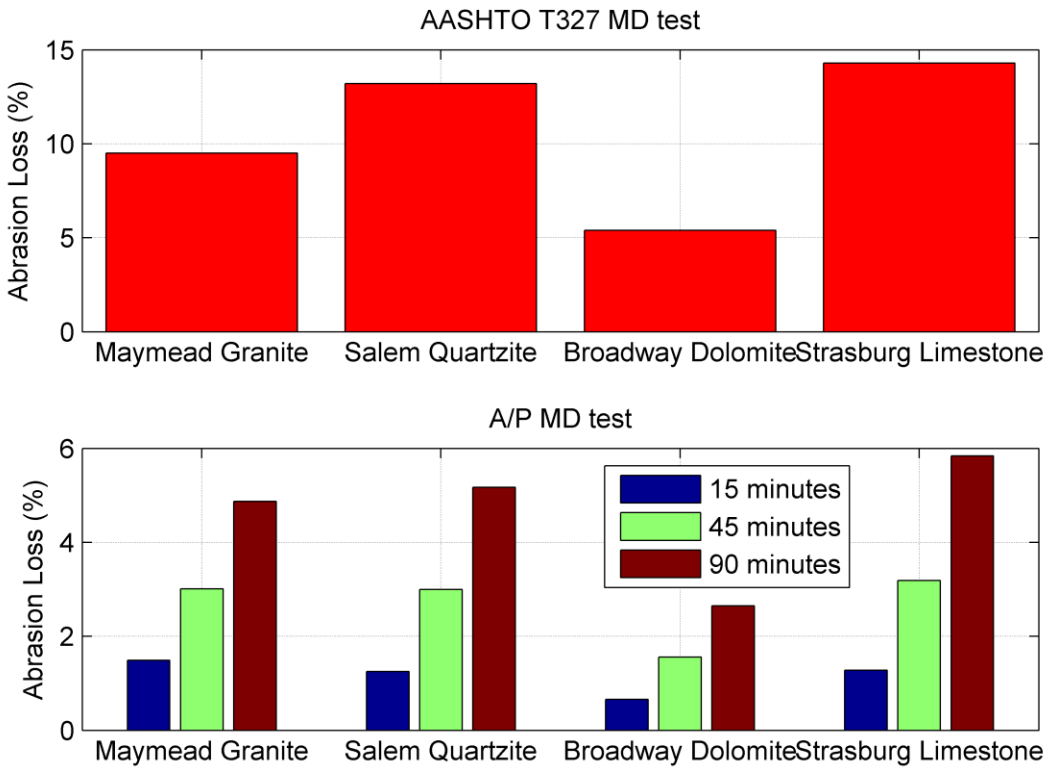

Figure 5-11 Abrasion loss in AASHTO T327 Micro-deval (MD) test and Micro-Deval Abrasion/Polishing (MD A/P) Test

Figure 5-12 plots the change of angularity and texture throughout the 90 minutes of the micro-deval abrasion/polishing test for four types of aggregates. The angularity loss and texture loss denotes the difference in either angularity or texture of an aggregate surface before and after the micro-deval test. A negative change in angularity or texture indicates that an aggregate has become less angular and smoother in surface texture after the micro-deval test, whereas a positive value of angularity loss and texture loss indicates a more angular aggregate with a rougher surface texture. Intuitively, abrasions in the micro-deval test would be most likely to break sharp corners of aggregates, decreasing aggregate angularity and/or texture throughout the abrasion process, which corresponds to negative values in angularity loss and texture loss. As shown in this figure, both Maymead granite and Strasburg limestone show a decrease in angularity, yet only the angularity of Salem quartzite increases through the micro-deval abrasion/polishing test. Conversely, the angularity of Broadway dolomite gradually decreases in the first 45 minutes of abrasion and then increases in the last 45 minutes of abrasion. In terms of texture, Maymead granite, Salem quartzite, and Strasburg limestone all gradually decrease throughout the abrasion test, and only Broadway dolomite shows an increase in texture due to abrasion. A possible reason for the increase in angularity and texture after the micro-deval test is as follows: the micro-deval test causes surface breakage for some aggregates, forming into angular aggregates with a rougher texture; that is to say that positive values of angularity loss and texture loss are achieved after the micro-deval abrasion/polishing test. The inconsistent changes of angularity loss and texture loss throughout the micro-deval abrasion/polishing tests indicate that the micro-deval test might change the angularity and texture characteristics of aggregates, and that the abrasion duration does have an influence on angularity and texture.

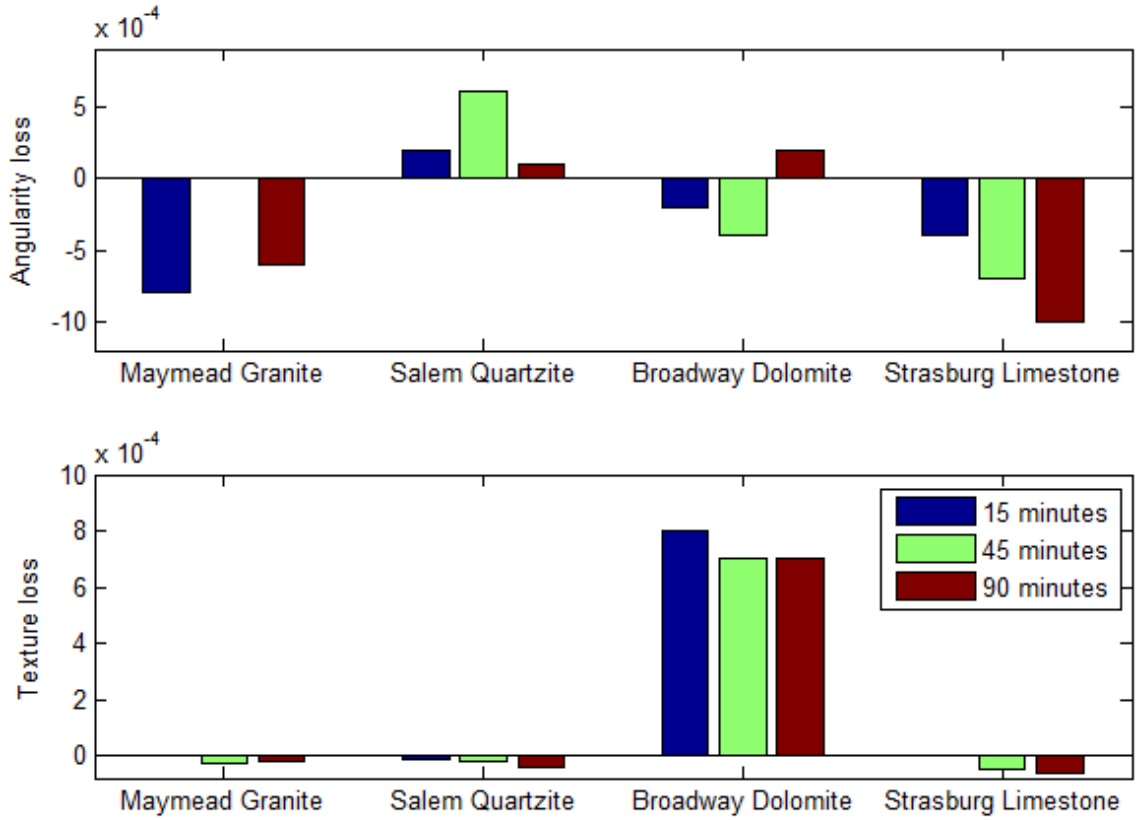

Figure 5-12 Variation of angularity and texture throughout A/P micro-deval test

Figure 5-13 plots the abrasion loss, roughness loss, angularity loss, and texture loss throughout the micro-deval abrasion/polishing test for the four types of aggregates. Roughness loss is defined as the sum of angularity loss and texture loss. It is apparent that abrasion loss linearly increases as the micro-deval abrasion/polishing test duration increases. The angularity and texture of both Maymead granite and Strasburg limestone decrease after the micro-deval test; the Starsburg limestone shows decreases in texture after the abrasion process with a decrease in angularity in the initial 45 minutes of abrasion and an increase in angularity in the second 45 minutes of abrasion. Conversely, both angularity and texture of Broadway dolomite increase

after the micro-deval test, indicating the breakage of aggregate surface asperities during the abrasion process.

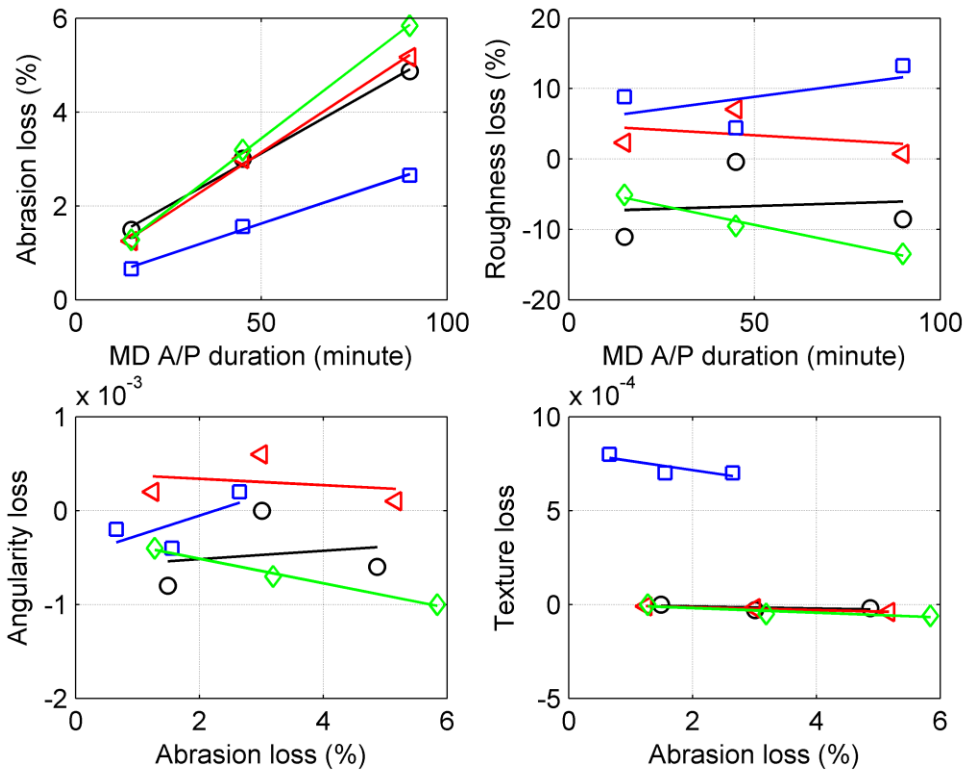

Figure 5-13 Abrasion loss, roughness loss, angularity loss and texture loss throughout micro-deval abrasion/polishing test. Note: black dots, red triangles, blue squares and green diamonds represent Maymead granite, Salem quartzite, Broadway dolomite and Strasburg limestone, respectively.

5.7 CONCLUSIONS

Aggregate morphological characteristics are related to parent rock (i.e., mineral compositions, crystal structure and inherent defects), crushing, and abrasion/polishing processes. Roughness of five supercell structures is analyzed at the atomic-scale to evaluate the mineral effects on

roughness and further compared with roughness ranking at the macroscale. Crushing effect is investigated by comparing morphological characteristics between natural aggregates and crushed aggregates of glacial gravel. Abrasion/polishing effect is evaluated by measuring angularity and surface texture of four types of aggregates before and after the micro-deval abrasion/polishing test. The following conclusions can be drawn.

(*i*) α-quartz is selected as the representative mineral of granite/aplite/gravel glacial, dolomite is selected as the representative mineral of dolomite, calcite is selected as the representative mineral of limestone, and haematite and magnetite are selected as representative minerals for iron ore. Investigations on atomic-scale roughness for five crystal structures show that the roughness ranking from rough to smooth is as follows: calcite, dolomite, α-quartz, and haematite and magnetite. However, the roughness ranking at the macroscale level is different from that at the atomic-scale. At the macroscale level, the FTI roughness ranking is as follows: iron ore, limestone, dolomite and rounded glacial gravel, and the AIMS II roughness ranking is as follows: limestone, dolomite, iron ore, and rounded glacial gravel. A possible reason for the difference between the atomic-scale roughness ranking and the macroscale roughness ranking may be that roughness analysis of crystal structures at the atomic-scale may not be able to represent roughness characteristics at the macroscale. That is because the following aspects are not considered in the roughness analysis at the atomic-scale: actual mineral compositions and inherent defects and voids, crushing effect, and abrasion/polishing effect.

(*ii*) Evaluations on morphological characteristics of glacial gravel aggregates show that the crushing process has a large influence on aggregate morphological characteristics. Crushed

glacial ravel aggregates are flatter and more elongated with more angular surfaces and rougher texture, compared with natural aggregates (rounded glacial gravel aggregates) with less angular surfaces and smoother texture surfaces.

(*iii*) Comparing the angularity and texture results of four types of aggregates before and after the micro-deval test can be used to identify aggregates that have great weight loss due to poor abrasion/polishing resistance from those that exhibit small weight loss due to fragmentation. Throughout 90 minutes of the micro-deval test process, Strasburg limestone shows gradual decreases in both angularity and texture, Maymead granite shows decreases in both angularity and texture, and Salem quartzite shows an increase in angularity and a decrease in texture. On the other hand, Broadway dolomite shows a decrease in angularity at initial 45 minutes, indicating abrasions and loss of aggregate asperity, and then increases at the second 45 minutes in angularity, indicating breakage of aggregate asperity; conversely, Broadway dolomite increases in surface texture throughout the 90 minutes of micro-deval test.

5.8 REFERENCES

1. Khanal, S. and Tamrakar, N.K. Evaluation of quality of crushed-limestone and -siltstone for road aggregates. *Bulletin of the Department of Geology*, Tribhuvan University, Kathmandu, Nepal, 12, 2009, 29-42.

2. Tamrakar, N.K., Yokota, S., and Nakamura, M. *Some mechanical properties of Siwalik sandstones and their relation to petrographic properties*. Geoscience Report of Shimane University, 1999, 18, 41-54.

3. Tamrakar, N.K., Yokota, S., and Shrestha, S.D. Relationships among mechanical, physical and petrographic properties of Siwalik sandstones, Central Nepal Sub-Himalayas. *Engineering Geology*, 90, 2007, 105-123.

4. Kaplan, M.F. Flexural and compressive strength of concrete as affected by the properties of coarse aggregates. *Journal of American Concrete Institute*, 30(11), 1959, 1193-1208.

5. Kaplan, M.F. The effects of properties of coarse aggregates on the workability of concrete. *Magazine of Concrete Research*, 10(29), 1958, 63-74.

6. United States Geological Survey (USGS). "USGS Minerals Information: Crushed Stone". http://minerals.usgs.gov/minerals/pubs/commodity/stone_crushed/mcs-2014-stonc.pdf Retrieved 2014-8-11.

7. Guimaraes, M.S., Valdes, J.R., Palomino, A.M., and Santamarina, J.C. Aggregate production: fines generation during rock crushing. *International Journal of Mineral Processing*, 81(4), 2007, 237-247.

8. Mahmoud, E., and Masad, E. Experimental methods for the evaluation of aggregate resistance to polishing, abrasion, and breakage. *Journal of Materials in Civil Engineering*, 19(11), 2007, 977-985.

9. Wang, L., Druta, C., and Lane, D. S. *Methods for assessing the polishing characteristics of coarse aggregates for use in pavement surface layers*. VTRC 10-CR7 final report, 2010.

Conclusions

6.1 Summary of Conclusions

Concrete materials consist of aggregates, binders, and pores with the size varying at multiple spatial scales. Deformations of concrete materials are complicated processes under external loadings, such as external force, temperature change, and other environmental factors. Mechanical failures originate from breakage of atomic bonds by separating atoms from their neighboring atoms in weak zones, especially on the interface between aggregates and binders. As a result, larger defects form and further propagate into macroscale cracks, leading to mechanical failures. Aggregate morphological characteristics have a great influence on the interlocking effect between aggregates and also on the binding effects between aggregates and binders. To better understand mechanical failures, it is essential to accurately quantify aggregate morphological characteristics at multiple scales. In this regard, the following conclusions can be drawn from this study.

(*i*) Aggregate morphological characteristics have a great influence on mechanical performances of stone-based materials, such as unbounded granular layers, hot mixed asphalt concrete, hydrated cement concrete, etc. In the third chapter, Fourier Transform Interferometry (FTI) system is presented to quantify aggregate morphological characteristics from multiple scales, including shape, angularity and surface texture. The FTI system consists of a charged-coupled device (CCD) camera, a fringe source, an angled mirror, a particle tray, and MATLAB

programs. It is capable of generating 3D coordinates of aggregates from digital snapshot images, with aggregate size ranging from 1-inch (25.4 mm) to No. 50 (300 μm). Resolutions of the acquired images in the FTI system are 35.4 μm/pixel in both *x*-axis and *y*-axis, and up to 20 μm in *z*-axis.

There are seven types of coarse aggregates passing through the 1-inch sieve and retaining on the ¾-inch sieve that were analyzed in the FTI system to quantify morphological characteristics using two-dimensional Fourier transform (FFT2) method, including blast furnace slag, copper ore, dolomite, crushed glacial gravel, rounded glacial gravel, iron ore, and limestone. FTI measurement results of shape, angularity, and texture are compared with those obtained by manual measurements and two other aggregate imaging techniques, the second generation of Aggregate Image Measurement System (AIMS II) and University of Illinois Aggregate Image Analyzer (UIAIA). Statistical analysis results demonstrate that the FTI system is capable of objectively quantifying aggregate morphological characteristics. Quantitative rankings of shape, angularity, and texture from the FTI system are generally consistent to those from AIMS II and UIAIA. Blast furnace slag and crushed glacial gravel have greater angularity values than the other aggregates, followed by iron ore and copper ore.

On the one hand, further evaluations of the FTI system should be conducted on aggregates from various sources with different colors and morphological characteristics to validate the robustness of the FTI system. Moreover, it is necessary to test the validity and repeatability of the FFT2 analysis method. On the other hand, further improvements should be conducted to enhance the

automaticity of the system and to promote potential applications to pavement engineering in the field.

(*ii*) Prevalent aggregate image techniques for aggregate morphological characterization can be discretized into two categories: dynamic digital imaging methods and static digital imaging methods. These imaging methods are compared with each other from the following aspects: equipment cost, analysis speed, accuracy, ease of use, repeatability, aggregate size range, and number of cameras, as well as morphological parameters, etc. These imaging techniques adopt different instrumental setups and use morphological parameters that are defined differently and computed using different algorithms. As a result, the morphological descriptors acquired from different imaging techniques are sometime incomparable to each other.

The fourth chapter discusses three major aggregate imaging techniques: AIMS II, UIAIA, and the FTI system. Seven types of aggregates passing through ¾-inch sieve and retaining on ½-inch sieve are analyzed in three aggregate imaging systems, with validation by manual measurements and visual rankings. ANOVA tests of shape characteristics using aggregate imaging techniques and those using manual measurements indicate that both AISM II and FTI can accurately and consistently quantify sphericity of limestone aggregates. These results match the sphericity values obtained manually. Also, both UIAIA and FTI quantify the flatness-elongation (FE) ratio of rounded glacial gravel aggregates with more consistent results than AIMS II. ANOVA tests of angularity and texture results show that the three aggregate imaging systems are capable of analyzing ½-inch aggregates with reasonable angularity and texture rankings. Blast furnace slag aggregates have greater values of angularity and texture than the other aggregates, followed by

limestone and iron ore; both dolomite and rounded glacial gravel aggregates have extremely smooth surface textures.

On the other hand, there are some differences in results obtained from the three imaging systems. For example, coarse glacial gravel aggregates are determined as aggregates with somewhat smooth texture by both AIMS II and FTI, but they are determined as aggregates with the roughest surface texture by UIAIA. Conversely, both AIMS II and UIAIA rank dolomite aggregates as the second-least angular aggregates, but the FTI system ranks them as the least angular ones. That is to say, when angularity and texture of aggregates are significantly different, the three aggregate image techniques can be sensitive enough to differentiate them; however, when angularity and texture of aggregates are not significantly different from each other, these three techniques may rank them differently. Consequently, further research should be carried out on the standardization of both definitions of morphological descriptors and computational algorithms.

(*iii*) Aggregate morphological characteristics are related to inherent properties of aggregates, such as mineral compositions, inherent defects and voids, crushing, and abrasion/polishing processes. Investigations are conducted on roughness analysis at the atomic-scale of five crystal structures (including α-quartz, dolomite, calcite, hematite, and magnetite) as dominant minerals of four typical aggregates, i.e., granite/aplite/quartzite/glacial, dolomite, limestone and iron ore. At the atomic-scale, root-mean-square (RMS) roughness ranking from rough to smooth is as follows: calcite (limestone), dolomite (dolomite), α-quartz (granite/aplite/quartzite/glacial), hematite and magnetite (iron ore). At the macroscale, FTI texture ranking from rough to smooth

is as follows: iron ore, limestone, dolomite, and rounded glacial gravel; AIMS II texture ranking from rough to smooth is as follows: limestone, dolomite, iron ore, and rounded glacial gravel. Different roughness rankings by the FTI and AIMS II systems indicate that these two systems is sensitive enough to differentiate aggregates that are significantly different in angularity and texture; conversely, these two systems may rank roughness differently while analyzing aggregates that are not significantly different in angularity and texture. Possible reasons for the differentiation between atomic-scale roughness ranking and macroscale roughness ranking are because of neglecting the following aspects: actual complicated mineral compositions, inherent defects and voids, crushing effect, and abrasion/polishing effect.

For glacial gravel aggregates, crushing process indeed has a significant influence on aggregate morphological characteristics. Compared with both rounded glacial gravel aggregates, crushed glacial gravel are more cubical, flatter and more elongated aggregates with more angular and rougher textured surfaces. On the other hand, abrasion/polishing will also alter aggregate morphological characteristics throughout the micro-deval test. After the micro-deval test, the angularity and texture show increases and decreases for different types of aggregates at different durations. Both Maymead granite and Strasburg limestone show decreases in angularity and texture values throughout the 90 minutes of micro-deval tests, indicating loss of asperity and surface texture. On the other hand, Salem dolomite shows an increase in angularity and a decrease in texture, indicating breakages of surface asperity and losses of texture; Broadway dolomite shows an increase at initial 45 minutes and then a decrease at the second 45 minutes in angularity, as well as significant increases in texture throughout the 90 minutes of micro-deval test.

6.2 CONTRIBUTIONS AND IMPLICATIONS

Aggregates are a substantial part of concrete up to 70%~80% by volume. Morphological characteristics of aggregates influence the workability and segregation resistance stiffness, creep, permeability and durability of concrete. Morphological characterization of aggregates at multiple scales offer us insights into the mechanical behaviors of concrete materials, especially their effects on local stress distributions during deformations and mechanical failures. Therefore, it is very important to quantify aggregate morphological characteristics and to evaluate the influences of aggregate morphological characteristics on mechanical performances.

In this dissertation, aggregate morphological characteristics are quantified from three scales: shape, angularity and texture using two-dimensional Fourier transform (FFT2) method with the FTI system. It is found that the FTI system is capable to rapidly capture digital images of aggregates and accurately quantify aggregate morphological characteristics based on three-dimensional coordinates determined from digital images. The FFT2 method is used to measure the morphological characteristics of aggregates at different scales, and there are six morphological descriptors, including sphericity, flatness ratio, elongation ratio, flatness & elongation (FE) ratio, angularity and texture. The FFT2 method is reliable and accurate with very good correlation to measurements obtained using manual measurements and the AIMS II and UIAIA system.

All these contributions provide a unique method named the FFT2 method in quantifying morphological characteristics of both fine and coarse aggregates from digital images. The

analysis speed of the current FTI system is limited by dimensions of aggregate particle tray where aggregates lie on, imaging speed of the CCD camera, and image analysis speed of the FTI software package. The followings are proposed for future improvements: (*i*) refining the system for better automation, (*ii*) improving both speed of capturing images and digital image resolution by using better CCD cameras, (*iii*) improving computational algorithms of the FTI software, (*iv*) developing measurement of the system in motion for its application to pavement performance evaluation, and (*v*) establishing the relationship between aggregate morphological characteristics and mechanical performances of asphalt concrete and cement concrete with specific criteria for aggregate acceptance, mix blending, quality assurance, and quality control for industry applications.

With all the aforementioned improvements, the updated FTI system with a new CCD camera can be installed on the side of a conveyor along a production line of aggregates, and then further implemented for quality assurance and quality control (QA/QC) of aggregates in aggregate plant and concrete plant. On the other hand, the update FTI system can also be implemented in the analysis of surface roughness of pavement by attaching the FTI system on vehicles. Based on digital images of pavement surfaces, it can also be used to quantify the change of surface roughness of pavement surface layer due to aggregate polishing, and to investigate pavement distresses, such as rutting depth, crack types and densities, pavement deformation, etc. Other than aggregate industry, the FTI system can be used for manufacturing of other particle products to monitor the morphological characteristics and assure the shape quality of particle products in production. For instance, pharmaceutical tablets should have less angular shapes with smooth

surfaces so that tablets can smoothly go through a hooper in the drug production line without any stuck at the very bottom of the hooper and easily be swallowed into a human stomach.

To further evaluate the influence of mineral composition, crushing, and abrasion/polishing on aggregate morphological characteristics, surface roughness at the atomic-scale is analyzed using root-mean-square (RMS) roughness for five crystal structures, including α-quartz, calcite, dolomite, hematite and magnetite. The roughness ranking of aggregates at the macroscale is compared with the roughness ranking at the atomic-scale of five dominant minerals within those four types of aggregates to evaluate the mineral effect on aggregate morphological characteristics. After that, morphological characteristics measured by the FTI system are compared for natural and crushed glacial gravel aggregates from Michigan State to quantify the influence of crushing on morphological characteristics. Micro-deval abrasion/polishing test is performed on four types of aggregates, and the morphological characteristics of these four types of aggregates are measured before and after the micro-deval test to evaluate the influence of abrasion on morphological characteristics. It is found that mineral compositions in aggregates have a great influence on morphological characteristics at the macroscale, and that crushing and abrasion/polishing will significantly alter morphological characteristics of aggregates. All these findings provide an insight into the inherent relationship between mineral compositions and aggregate surface roughness at the atomic-scale and macroscale. It can help engineers in the selection of aggregates for design concrete mixture with desired engineering properties.

6.3 RECOMMENDATIONS ON FUTURE RESEARCH

This research elucidates the importance to investigate morphological characteristics of aggregates at multiple scales. A unique aggregate imaging system named the FTI system is presented to quantify morphological characteristics of both coarse and fine aggregates (including shape, angularity and texture), with detailed descriptions of system components and computational algorithms of the FFT2 method. Further research should be carried out on the following aspects for improvements of the FTI system.

(*i*) Further evaluations should be performed for the repeatability and robustness of the FTI system and FFT2 computational algorithm on both coarse and fine aggregates from various sources.

(*ii*) Further improvements should be conducted on the automatic operation of the FTI system on digital image analysis, as the FTI system requires user's judgments to select a threshold value for image processing. The updated FTI system that can significantly reduce analysis time with automatic recognitions of the threshold value for image processes is under development.

(*iii*) National joint efforts should be carried out to develop a consensus on definitions and computational algorithms of morphological characteristics that are widely accepted, considering that incomparable definitions and computational algorithms of morphological characteristics in different aggregate imaging techniques would impede scientific development on aggregate imaging systems for quantification of morphological characteristics.

(*iv*) Once such national consensus on a set of morphological parameters has been established, a national database can be built on morphological characteristics using the FTI system for both

coarse and fine aggregates of all typical aggregates used in infrastructures, such as pavements, bridges, buildings and dams, etc.

(*v*) Quantitative relationships between aggregate morphological characteristics and mechanical performance of aggregate assembly or concrete (including HPC and HMA) should be established.

(*vi*) Further research on measurement accuracy for the FTI system in motion can be developed, so that pavement surface roughness and pavement distresses of surface courses can be investigated based on digital images of pavement surface captured by the FTI system attached on a slow moving vehicle.

(*vii*) Further modifications on the allocation of cameras and computational algorithm for digital image analysis in the FTI system can be performed to calculate 3D aggregate surface, including both top and bottom surfaces and to calculate surface area and volume of each aggregate, as the current FTI system only captures top surface of aggregates and morphological characteristics analysis is based on 3D coordinates of aggregate top surfaces.

(*viii*) Further research should be conducted on the roughness analysis at the atomic-scale based on more representative crystal structures of different types of aggregates to investigate atomic-scale roughness more accurately, by considering the following aspects: actual mineral compositions, content of different minerals, inherent defects in crystal structures, crushing, abrasion/polishing, etc.

References

Al-Rousan, T., Masad, E., Tutumluer, E., and Pan, T. Evaluation of image analysis techniques for quantifying aggregate shape characteristics. *Construction and Building Materials*, 2006, 21, 978-990.

ASTM D3398. Standard Test Method for Index of Aggregate Particle Shape and Texture. ASTM International, West Conshohocken, PA, 2006, DOI: 10.1520/D3398-00R06.

ASTM D4791. Standard Test Method for Flat Particles, Elongated Particles, or Flat and Elongated Particles in Coarse Aggregate. ASTM International, West Conshohocken, PA, 2010, DOI: 10.1520/D4791-10.

ASTM D5821. Standard Test Method for Determining the Percentage of Fractured Particles in Coarse Aggregate. ASTM International, West Conshohocken, PA, 2006, DOI: 10.1520/D5821-01R06.

Barksdale, R. D., Kemp, M. A., Sheffield, W. J., and Hubbard, J. L. Measurement of aggregate shape, surface area, and roughness. *Transportation Research Record: Journal of the Transportation Research Board*, 1301, 1991, 107-116.

Garboczi, E.J. Three-dimensional mathematical analysis of particle shape using X-ray tomography and spherical harmonics: application to aggregates used in concrete. Cement and Concrete Research, 32(10), 2002, 1621-1638.

Haas, C. T., Rauch, A. F., Kim, H., and Browne, C. *Automation of aggregate characterization using laser profiling and digital image analysis*. International Center for Aggregates Research (ICAR) 503-3 Report, Aggregate Foundation for Technology, Research, and Education, Washington, D.C., 2002.

Jahn, D. Evaluation of aggregate particle shapes through multiple ratio analysis. *Proceeding of the 8th annual symposium of the international center for aggregate research (ICAR)*, Denvor, CO, 2000.

Kim H., Haas, C. T., Rauch, A.F., and Browne, C. Wavelet-based three-dimensional descriptors of aggregate particles. *Transportation Research Record: Journal of the Transportation Research Board*, 1787, 2003, 109-116.

Lynn, T., James, R.S., Wu, P.Y., and Jared, D.M. Effect of aggregate degradation on volumetric properties of Georgia's hot-mix asphalt. *Transportation Research Record: Journal of the Transportation Research Board*, 1998, 2007, 123-131.

Mahmond, E., and Ortiz, E. *Implementation of AIMS in measuring aggregate resistance to polishing, abrasion, and breakage*. FHWA-ICT-14-014, 2014.

Masad, E., and Button, J. Unified imaging approach for measuring aggregate angularity and texture. *Journal of Computer-Aided Civil and Infrastructure Engineering*, 15(4), 2000, 173-280.

Masad, E. Review of imaging techniques for characterizing the shape of aggregates used in asphalt mixes. *Proceeding of the 9th annual symposium of the international center for aggregate research (ICAR)*, 2001, Austin, TX.

Masad E., Olcott, D., White, T., Tashman, L. Correlation of fine aggregate imaging shape indices with asphalt mixture performance. *Transportation Research Record: Journal of the Transportation Research Board*, 1757, 2001, 148-156.

Masad, E., Al-Rousan, T., Button, J., Little, D., and Tutumler, E. *Test methods for characterizing aggregate shape, texture, and angularity*. NCHRP 4-30A final report, 2005.

Masad, E., Saadeh, S., Al-Rousan, T., Garboczl, E., and Little, D. Computations of particle surface characteristics using optical and X-Ray CT images. *Journal of Computation Materials Science*, 34, 2005, 406-424.

Masad, E., Rezaei, A., Chowdhury, A., and Harris, P. *Predicting asphalt mixture skid resistance based on aggregate characteristics*. FHWA/TX-09/0-5627-1, 2009.

Ortiz, E., and Mahmond, E. Experimental procedure for evaluation of coarse aggregate polishing resistance. *Transportation Geotechnics*, 1, 2014, 106-118.

Pintner, R.M., Vinson, T.S., and Johnson. E.G. Nature of fines produced in aggregate processing. *ASCE Journal of Cold Regions Engineering*, 1(1), 1987, 10-12.

Prowell, B. D., and Brown, E. R. *Aggregate properties and the performance of superpave-designed hot mix asphalt*. National Cooperative Highway Research Program (NCHRP) report 539, 2005, Transportation Research Board, Washington, D.C.

Rao C., Tutumluer, E., and Kim, I. T. Quantification of coarse aggregate angularity based on image analysis. *Transportation Research Record: Journal of the Transportation Research Board*, 1787, 2002, 117-124.

Raunch, A. F., Haas, C. T., Browne, C., and Kim, H. *Rapid test to estimate grading of unbounded aggregate products: An evaluation of automated devices to replace and augment manual sieve analyses in determining aggregate gradation*. International Center for Aggregates Research (ICAR) 503-2 Report, 2002, Aggregate Foundation for Technology, Research, and Education, Washington, D.C.

Retsch Technology – Camsizer official website. http://www.retsch-technology.com/rt/products/digital-image-processing/camsizer, 2011.

Tutumluer, E., Rao, C., and Stefanski, J. *Video image analysis of aggregates*. Final Project Report, FHWA-IL-UI-278, Civil Engineering Studies UILU-ENG-2000-2015, 2000, University of Illinois Urbana-Champaign, Urbana, IL.

Tyler, W.S. *Particle size and shape analyzer (CPA)*, Product brochure, Mentor, OH, 2001.

Wang, L., Lai, J.S., Frost, J.D. Fourier morphological descriptors of aggregate profiles. *2nd International Conference on Image Technology Application in Civil Engineering*, 76-85, 1997, Sweden.

Wang, L. B., Frost, J. D., Lai, J. S. Characterization of air void distribution in asphalt mixes using X-Ray CT. *Journal of Materials in Civil Engineering*, 14(2), 2004, 122-129.

Wang, L., Wang, X., Mohammad, L, Abadie, C. Unified method to quantify aggregate shape, angularity and texture using Fourier analysis. *Journal of Materials in Civil Engineering*, 17(5), 2005, 498-504.

Wang, L. B., Lane, D. S., Lu, Y., and Druta, C. *Portable image analysis system for characterizing aggregate morphology*. Final contract report VTRC08-CR11, 2008, Virginia Transportation Research Council (VTRC).

Wang, L., Lane, D. S., Lu, Y., and Druta, C. Portable image analysis system for characterizing aggregate morphology. *Transportation Research Record: Journal of the Transportation Research Board*, 2104, 2009, 3-11.

Wang, L., Druta, C., and Lane, S. *Methods for assessing the polishing characteristics of coarse aggregates for use in pavement surface layers*. FHWA/VTRC 10-CR7, 2010.

Weingart, R. L., and Prowell, B. D. Specification development using the VDG-40 Videograder for shape classification of aggregates. *Proceeding of the 7th Annual Symposium of the*

International Center for Aggregate Research (ICAR), 1999, University of Texas, Austin, TX.

Wilson, J.D., and Klotz, L.D. Quantitative analysis of aggregates based on Hough transform. *Transportation Research Record: Journal of the Transportation Research Board*, 1530, 1996, 111-115.

Appendices

APPENDIX A COPYRIGHT PERMISSION

Barber, Phyllis <PBARBER@nas.edu> Thu, Apr 24, 2014 at 1:54 PM
To: Wenjuan Sun <sunwjhere@gmail.com>

Dear Mr. Sun:

The Transportation Research Board grants permission to use your paper, "Image Analysis Technique for Aggregate Morphology Analysis with Two-Dimensional Fourier Transform Method," coauthored with L. Wang, and E. Tutumluer; and your paper, "Evaluation of Aggregate Imaging Techniques for Quantification of Morphological Characteristics," coauthored with L. Wang, E. Tutumluer, and C. Druta, in your dissertation, as identified in your request of April 21, 2014, subject to the following conditions:

1. Please cite appropriately the portions that were published in *Transportation Research Record: Journal of the Transportation Research Board, No. 2267*, pp. 3-13, Washington, D.C., 2012; and in *Transportation Research Record: Journal of the Transportation Research Board, No. 2335*, pp. 39-49, Washington, D.C., 2013.
2. Please acknowledge that the material is reproduced with permission of the Transportation Research Board.
3. None of this material may be presented to imply endorsement by TRB of a product, method, practice, or policy.

Every success with your dissertation. Please let me know if you have any questions.

Sincerely,

Javy Awan
Director of Publications
Transportation Research Board

Phyllis Barber
Transportation Research Board
Publications Office
202 334-2972 phone
202 334-3495 fax
pbarber@nas.edu

APPENDIX B PUBLICATION LIST

Journal Papers

[1] **Wenjuan Sun**, Linbing Wang, and Erol Tutumluer. Image analysis technique for aggregate morphology analysis with two-dimensional Fourier Transform method. *Transportation Research Record: Journal of the Transportation Research Board*, 2012, 2267, 3-13.

[2] Yufeng Liu, **Wenjuan Sun**, Harikrishnan Nair, D. Stephen Lane, Linbing Wang. Quantification of aggregate morphologic characteristics using the updated Fourier Transform Interferometry (FTI) system with two-dimensional Fourier Transform method. Submitted to *Transportation Research Record: Journal of the Transportation Research Board* (under review).

[3] Linbing Wang**, Wenjuan Sun**, Erol Tutumluer, and Cristian Druta. Evaluation of aggregate imaging techniques for the quantification of morphological characteristics. Transportation *Research Record: Journal of the Transportation Research Board*, 2013, No. 2335, 39-49.

[4] Solomon Tafesse, Joanne Fernlund, **Wenjuan Sun,** and Fredrik Bergholm. Evaluation of image analysis methods used for quantification of particle angularity. *Sedimentology*, 2012, DOI 10.1111/j.1365-3091.2012.01367.x.

[5] Rui He, Shuanfa Chen, **Wenjuan Sun**, and Rui Gong. Deformation behavior of high performance fiber reinforced cementitious composite prepared with asphalt emulsion. *Journal of Central South University*, 2014, 21, 811-816.

[6] Shuilong Shen, Zhifeng Wang, **Wenjuan Sun**, Linbing Wang, and S. Horpibulsuk. A field trial of horizontal jet grouting using the composite-pipe method in the soft deposit of Shanghai. *Tunnelling and Underground Space Technology*, 2013, 35, 142-151.

[7] Huaina Wu, Runqiu Huang, **Wenjuan Sun**, Shuilong Shen, and Yeshuang Xu. Leaking behaviour of shield tunnels under the Huangpu River of Shanghai with induced hazards. *Nature Hazards*, 2013, DOI 10.1007/s11069-013-0863-z.

[8] Yue Hou, Linbing Wang, Pengtao Yue, and **Wenjuan Sun**. Fracture failure in crack interaction of asphalt binder by using a phase field approach. *Materials and Structures*, 2014, DOI: 10.1617/s11527-014-0372-x.

[9] Yue Hou, Linbing Wang, Troy Pauli, and **Wenjuan Sun**. Investigation of the asphalt self-healing mechanism using a phase-field model. *Journal of Materials in Civil Engineering*, 2014, CID: 04014118.

[10] Yue Hou, Pengtao Yue, Linbing Wang, **Wenjuan Sun**, and Troy Pauli. Fracture failure of asphalt binder in mixed mode (Mode I & Mode II) by using phase field model. *Road Materials and Pavement Design*, 2014, 15(1), 167-181.

[11] Yue Hou, Pengtao Yue, Linbing Wang, **Wenjuan Sun**, and Troy Pauli. Cracking failure (Mode I) in asphalt binder by using a non-conserved Phase Field model. *Journal of Materials in Civil Engineering*, 2013, DOI 10.1061/(ASCE)MT.1943-5533.0000874.

[12] Lei Ma, Yeshuang Xu, Shuilong Shen, and **Wenjuan Sun**. Evaluation of the hydraulic conductivity of aquifers with piles. *Hydrogeology Journal*, 2013, DOI 10.1007/s10040-013-1068-y.

[13] Yeshuang Xu, Lei Ma, Shuilong Shen, and **Wenjuan Sun**. Evaluation of land subsidence by considering underground structures that penetrate the aquifers of Shanghai, China. *Hydrogeology Journal*, 2012, DOI 10.1007/s10040-012-0892-9.

[14] Yang Sun, Yeshuang Xu, Shuilong Shen, and **Wenjuan Sun**. Field performance of underground structures during shield tunnel construction. *Tunnelling and Underground Space Technology*, 2012, 28, 272-277.

[15] Dong Wang, Linbing Wang, Cristian Druta, Wenjing Xue, Haocheng Xiong, and **Wenjuan Sun**. Experimental evaluation of a visco-elastic contact model. *Journal of Nanomechanics and Micromechanics*, 2013, DOI 10.1061/(ASCE)NM.2153-5477.0000064.

Conference Papers

[1] **Wenjuan Sun**, Y. Wei, Dong Wang, and Linbing Wang. Review of multiscale characterization techniques and multiscale modeling methods for cement concrete: From atomistic to continuum. *Multi-Scale Modeling and Characterization of Infrastructure Materials*, 2013, RILEM Book Series Vol. 8, 325-341.

[2] **Wenjuan Sun**, Dong Wang, and Linbing Wang. Molecular dynamic simulation of failure of ettringite. *Journal of Physics: Conference Series*, 2012, Vol. 419, 012011.

[3] **Wenjuan Sun**, Ying Li, Dong Wang, and Linbing Wang. Multiscale modelling of crack propagation in hydraulic cement concrete using finite element method and molecular dynamics method. *Proceeding of Mechanics of Nano, Micro, and Macro Composite Structures*, 2012, Politecnico di Torino.

[4] **Wenjuan Sun**, Shuilong Shen, Linbing Wang, and Yeshuang Xu. Numerical evaluation on the cutoff behaviour of retaining structures on groundwater seepage. *14th Asian Regional Conference on Soil Mechanics and Geotechnical Engineering*, 2011, Hong Kong.

[5] **Wenjuan Sun**, Shuilong Shen, and Yeshuang Xu. An innovative technology to control groundwater during excavation over confined aquifer. *GeoFrontiers 2011: Advances in Geotechnical Engineering*, ASCE Geotechnical Special Publication, 3040-3049.

[6] **Wenjuan Sun**, Shuilong Shen, Linbing Wang, and Yeshuang Xu. Numerical evaluation on cutoff behaviour of retaining structures on seepage. *Geo-Frontiers 2011: Advances in Geotechnical Engineering*, 2011, ASCE Geotechnical Special Publication.

[7] Zhifeng Wang, **Wenjuan Sun**, Shuilong Shen, Yeshuang Xu and Y.-H. Kim. Quick-gelling of soft soil with jet-grouting using two binders. *International Conference on Ground Improvement and Ground Control: Transportation Development and Natural Hazards Mitigation*, 2012, Wollongong, New South Wales, Australia, 1201-1206.

[8] Shuilong Shen, Yongxia Wu, **Wenjuan Sun**, and Zhenyu Yin. Groundwater control for a deep excavation pit in gravel aquifer of Hangzhou, China. *International Conference on Ground Improvement and Ground Control: Transportation Development and Natural Hazards Mitigation*, 2012, Wollongong, New South Wales, Australia, 1735-1745.

[9] Yeshuang Xu, Shuilong Shen, **Wenjuan Sun**, and Lei Ma. Laboratory investigation on the cutoff behaviour of retaining structure on groundwater seepage in aquifer. *Geo-Frontiers 2011: Advances in Geotechnical Engineering*, ASCE Geotechnical Special Publication.

[10] Evan Lally, Anbo Wang, **Wenjuan Sun**, Linbing Wang, Cristian Druta, and Erol Tutumluer. Interferometric profilometry for 3D analysis of aggregate particles. *90th Annual Meeting of Transportation Research Board, Compendium of papers*, 2011, Compendium of papers, CD-ROM.

[11] Yongxia Wu, Shuilong Shen, Yeshuang Xu, and **Wenjuan Sun**. Groundwater control during deep excavation in the soft deposit of China: an overview. *International Conference on Ground Improvement and Ground Control: Transportation Development and Natural Hazards Mitigation*, 2012, Wollongong, New South Wales, Australia, 1415-1422.

Technical Report and Book Chapter

[1] Linbing Wang, **Wenjuan Sun**, Evan Lally, Anbo Wang, Cristian Druta, and Erol Tutumluer. *Application of LADAR in the analysis of aggregate characteristics*. National Cooperative Highway Research Program (NCHRP) Report 724, Transportation Research Board, Washington, D. C., 2012.

[2] Shuilong Shen, and **Wenjuan Sun**. *Chapter 8 Analysis of groundwater seepage*. In Handbook of Excavation Engineering, China Architecture and Building Press, Beijing, 2009 (in Chinese).